

A DETAILED GEOLOGICAL, GEOCHEMICAL AND
MINERALOGICAL STUDY OF THE KOORAE PROSPECT
AND THE HOST ROCKS OF THE TOPSAILS INTRUSIVE
SUITE, HINDS LAKE AREA, NEWFOUNDLAND

DEAN CHARLES COURAGE

**A Detailed Geological, Geochemical and Mineralogical Study of the
Koorae Prospect and the host rocks of the Topsails Intrusive Suite,
Hinds Lake area, Newfoundland**

by

© Dean Charles Courage, B.Sc. (Hons)

A thesis submitted to
The School of Graduate Studies
in partial fulfillment of the requirements for the degree of

Master of Science
Department of Earth Sciences
Memorial University of Newfoundland

March 2013
St. John's
Newfoundland and Labrador

ABSTRACT

The Topsails Intrusive Suite (TIS) and Springdale Group comprise widespread, Silurian, post-orogenic A-type intrusive and volcanic rocks in west-central Newfoundland. Magmatic-hydrothermal Cu-Mo-Ag-Au and intrusion related U-rare earth element (REE) mineralization occur locally in these rocks near Hinds Lake. A peralkaline, amphibole-clinopyroxene granite and hydrothermal-volcanic breccia host chalcopyrite, bornite, covellite, pyrite, molybdenite and chalcocite. Magmatic-hydrothermal quartz, copper sulfides, magnetite, Fe-Ti oxides and calcic clinopyroxene replace primary amphibole and pyroxene. Common accessory minerals are hematite, zircon, fluorite and monazite. Uranium-Pb zircon ages of host amphibole-clinopyroxene granite and rhyolite yield ages of 430 ± 1.4 Ma and 428 ± 1.6 Ma, respectively, suggesting that Cu-Mo-Ag-Au mineralization is associated with early TIS peralkaline granite magmatism and equivalent volcanic rocks of the Springdale Group. Uranium and REE are hosted in late stage felsic dykes, present in accessory monazite- (Ce, La), zircon, allanite- (Ce), pyrochlore, and thorite. Felsic dykes are among the youngest and most fractionated rocks of the TIS (likely younger than ~ 427 Ma).

ACKNOWLEDGEMENTS

I would like to thank my supervisor Dr. Stephen Piercey whose guidance in scientific research and writing was of great inspiration. I would like to thank Altius Resources Corp. and JNR Resources for inviting me to join their field exploration team, especially Mr. Dale O'Reilly, Dr. Lawrence Winter and Dr. Irvine R. Annesley who provided logistical support and expertise. I would like to thank Dr. Greg Dunning and Ms. Sherri Furey for their help in the geochronology lab; Ms. Pam King for her assistance preparing samples for XRF and geochronology; Dr. Michael Shaffer for his assistance with the SEM and zircon imaging; and Dr. Derek Wilton and Dr. John Hanchar for their professional help and advice. I thank my family for giving me everything I've ever needed and facilitating many long nights at school. I thank Janine Hickey who gave me the love and encouragement to move forward during much of this program. Colleagues Stefanie Brueckner, Conor McKinley and Matthew Minnett, among many others are thanked for their thoughtful advice and friendship. This thesis was funded by an NSERC Discovery Grant and the NSERC-Altius Industrial Research Chair to Stephen Piercey sponsored by NSERC, Altius Resources Ltd., and the Research and Development Corporation of Newfoundland and Labrador (RDCNL).

TABLE OF CONTENTS

ABSTRACT	II
ACKNOWLEDGEMENTS.....	III
TABLE OF CONTENTS	IV
LIST OF TABLES	VII
LIST OF FIGURES	IX
LIST OF ABBREVIATIONS	XVIII
CHAPTER 1: AN INTRODUCTION TO THE GEOLOGY AND GEOCHEMISTRY OF TOPSAILS INTRUSIVE SUITE AND ASSOCIATED MINERALIZATION.....	1
1.1 INTRODUCTION	1
1.2 GEOLOGICAL OVERVIEW	4
1.2.1 Tectonic Setting – The Notre Dame Subzone	5
1.2.2 Topsails Intrusive Suite.....	7
1.2.3 The Springdale Group.....	9
1.3 GEOCHEMISTRY	10
1.4 MINERAL OCCURRENCES	11
1.5 OBJECTIVES.....	14
1.6 METHODOLOGY	15
1.6.1 Geological Mapping and Sampling	15
1.6.2 Lithogeochemistry.....	16
1.7 THESIS PRESENTATION	16
CHAPTER 2: GEOLOGY, LITHOGEOCHEMISTRY AND METALLOGENY OF THE TOPSAILS INTRUSIVE SUITE AND SPRINGDALE GROUP, HINDS LAKE AREA, NEWFOUNDLAND, CANADA	21
2.1 ABSTRACT	21
2.2 INTRODUCTION	22
2.3 TECTONIC SETTING	24
2.4 GEOLOGY AND STRATIGRAPHY	25
2.5 PETROGRAPHY: PRIMARY AND ALTERATION MINERALS	28
2.5.1 Marginal Amphibole-Clinopyroxene Granite.....	29
2.5.2 Quartz- Feldspar Porphyry Intrusions.....	30

2.5.3 Springdale Group Volcanic Rocks	30
2.5.4 Late Aplite to Pegmatitic Dykes	32
2.6 MINERALIZATION: THE KOORAE CU-MO-AG-AU PROSPECT – GEOLOGY, ALTERATION AND MINERALIZATION	32
2.6.1 Stratigraphy	32
2.6.2 Host Rock Mineralogy and Alteration	34
2.6.2.1 Marginal Amphibole-clinopyroxene Granite	34
2.6.2.2 The Springdale Group Volcanic Rocks	35
2.6.3 Cu-Mo-Ag-Au Mineralization	36
2.6.3.1 Marginal Amphibole-clinopyroxene Granite	36
2.6.3.2 Springdale Group Volcanic Rocks	37
2.7 MINERALIZATION: URANIUM AND REE – GEOLOGY, ALTERATION AND MINERALIZATION.....	38
2.7.1 Stratigraphy	38
2.7.2 Host Rock Mineralogy and Alteration	38
2.7.3 Uranium and REE Mineralization	39
2.8 GEOCHEMISTRY	41
2.8.1 Sampling and Analytical Methods	41
2.8.2 Major Element Geochemistry.....	42
2.8.3 Trace Element Geochemistry	45
2.8.3.1 Marginal Phase Granite.....	46
2.8.3.2 Springdale Group Volcanic Rocks	46
2.8.3.3 Quartz-Feldspar Porphyry	47
2.8.3.4 Late Aplitic to Pegmatitic Dykes.....	48
2.8.3.5 Mafic Rocks	49
2.9 GEOCHRONOLOGY.....	49
2.9.1 U-Pb Geochronology Sampling and Analytical Techniques.....	49
2.9.2 Zircon Characteristics and Results.....	52
2.9.3 Interpretation.....	53
2.10 DISCUSSION	54
2.11 EXPLORATION IMPLICATIONS	58
2.12 CONCLUSIONS	60
CHAPTER 3: SUMMARY AND DIRECTION FOR FUTURE RESEARCH	94

3.1 KEY CONCLUSIONS.....	94
3.2 POTENTIAL DIRECTIONS FOR FUTURE RESEARCH	96
REFERENCES	99
APPENDIX A : LITHOGEOCHEMICAL ANALYTICAL METHODS, QUALITY CONTROL AND QUALITY ASSURANCE	105
A.1 INTRODUCTION.....	105
A.2 PRECISION.....	106
A.3 ACCURACY	108
APPENDIX B : LITHOGEOCHEMISTRY OF THE TOPSAILS INTRUSIVE SUITE	129

LIST OF TABLES

Table 2.1	Summary of the U-Pb zircon age, stratigraphy, mineralogy, alteration and mineralization of the main lithological units of the TIS. Mineral abbreviations are given on page xv. Alteration textures and mineralogy are provided for: 1) magmatic hydrothermal alteration and: 2) secondary magmatic hydrothermal alteration.....	65
Table 2.2	Paragenetic sequence of alteration and mineralization and comparison between regional and ore related amphibole-clinopyroxene granite. The thicknesses of lines correspond to increasing mineral occurrence. Minerals marked with an X are not typically found in the mineral assemblage. The shaded field highlights the magmatic-hydrothermal alteration assemblage. Mineral abbreviations are seen on page xv.	68
Table 2.3	Summary of U, Th, REE and Zr concentrations in mineralized felsic dykes and granite. Prospects are labeled accordingly.	81
Table 2.4	A summary of the isotope data collected from two sets of zircons using thermal ionization mass spectrometry (TIMS).	89
Table 2.5	Ore deposit models analogous to Cu-Mo-Ag-Au and U-REE mineralization in the TIS and Springdale group describing the resource, tectonic setting, geology, geochemistry, alteration, and mineralization style for IOCG and peralkaline U-REE deposits. Source of information for IOCG is from Groves and Vielreicher (2001), Williams et al. (2005) and McPhie et al. (2011) while those for peralkaline U-REE are from Schonenberger et al. (2008).	93
Table A.1	Precision and accuracy results for standard reference materials analyzed by ICP-MS at OGL.	109
Table A.2	Precision and accuracy results using standard reference materials analysed by ICP-OES for total digestion at the SRC.	113

Table A.3	Precision and accuracy results using standard reference materials analyzed by ICP-OES for whole rock and partial digestion at the SRC.	117
Table A.4	Precision and accuracy results using standard reference materials for analysis by pressed pellet XRF at MUN.....	121
Table B.1	Geochemical results for the TIS samples providing the sample type details and location. Easting and northing are Nad 27 specific.	130

LIST OF FIGURES

- Figure 1.1** Geological map of Newfoundland highlighting the tectonostratigraphic zones of Newfoundland and the location of the TIS in the Notre Dame subzone of the Dunnage Zone. Solid black lines bounding the Notre Dame subzone include the BVL to the west and RIL to the east. An insert map of Canada highlights the location of Newfoundland in the northeasternmost extent of the Appalachians in North America. Geology from Williams et al. (1988) and Williams (2004)..... 18
- Figure 1.2** Tectonic model for the Salinic orogeny culminating with collision of the Laurentian and Gondwanan (Ganderia) plate margins followed by post-orogenic collapse and slab breakoff. The Notre Dame arc and other oceanic and volcanic rocks are accreted to the Laurentian plate margin forming the Notre Dame subzone. Major crustal sutures including the BVOT and RIL separate the zone from Precambrian Laurentian basement rocks to the west and the composite Ganderia plate margin to the east. Asthenosphere-derived mafic magmas interacted to create both subcontinental lithospheric mantle (SCLM)- derived A-type magmas and VAG-like crustal partial melts that intrude the overriding Notre Dame subzone following orogenesis. Model from Whalen et al. (1996) and van Staal (2007). 19
- Figure 1.3** Geological map of the Hinds Lake area showing the location and abundance of Silurian igneous and volcanic rocks in relation to Ordovician and older rocks. The location of the Koorae Prospect, U-REE occurrences and major structures are indicated. The documented ages for the TIS are provided for the identified units. Modified from Whalen and Currie (1988b). 20
- Figure 2.1** Regional geological map of Newfoundland and tectonostratigraphic zonations including the location of the Notre Dame Subzone and TIS. The red box outlines the study area near Hinds Lake and the map

location of Figure 2.2. The black lines bounding the coloured area are the BVBL in the west and RIL to the east. Modified after Williams (1979) and Williams et al. (1988)..... 62

Figure 2.2 Geological map of the Hinds Lake region showing the location of mineral occurrences in relation to roof zone lithologies and geological structures. The approximate coverage area for each lithology is plotted against age and encompasses an area extending to the northeast beyond this map. Peralkaline amphibole-clinopyroxene granite is identified from other non-peralkaline marginal granite. Mafic basal occurrences are also highlighted from the larger Springdale Group. Coordinates are provided as easting and northing in NAD 27. Modified after Whalen and Currie (1988b)..... 63

Figure 2.3 Representative hand samples (bar = 1 cm) for the major lithologies of the TIS, including (a) spherulitic rhyolite with lithophysae hosted quartz sericite alteration, (b) coarse grained, amphibole granite, (c) marginal phase amphibole-clinopyroxene granite with hematized feldspar, quartz cavities and fracture hosted chlorite alteration, (d) quartz-feldspar porphyry showing hematized subhedral K-feldspar phenocrysts and hematized, very fine-grained matrix, (e) mixed mafic and felsic marginal granite sampled near agmatite zone, (f) mineralized pegmatitic dyke showing strong quartz carbonate alteration and relict amphibole grains replaced by chlorite, carbonate and calcic-pyroxene..... 66

Figure 2.4 Thin section photomicrographs of regional alteration and mineralogy from dominant lithologies of the TIS. (a) Amphibole-clinopyroxene granite displays aegirine-augite grains with rims of hornblende and prismatic arfvedsonite overgrowths. Magnetite and hematite filled cavities contain marginal inclusions of zircon, rutile, monazite, fluorite and arfvedsonite (plane polarized light). (b) Granophyric groundmass of quartz and alkali-feldspar in amphibole-clinopyroxene granite.

Interstitial richterite and replaced by hematite and associated with arfvedsonite, magnetite, rutile and monazite (cross-polarized light). **(c)** Green amphibole occur in the quartz-feldspar porphyry as poikilitic to subhedral masses and disseminated, fine-grained acicular crystals throughout the groundmass. Alkali feldspar phenocrysts are perthitic and show variable hematite dusting (plane polarized light). **(d)** A fabric is defined in the groundmass of a quartz-feldspar porphyry by aligned crystals that wrap around quartz phenocrysts. A xenocryst in the right of the image is preferentially altered to sericite, carbonate and hematite. Biotite filled fractures parallel the fabric (cross-polarized light). **(e)** Flow banded rhyolite showing clusters of magnetite, chlorite and clay parallel to banding and local biotite, sericite and hematite altered perlitic fractures (plane polarized light). **(f)** Strongly granophyric, mineralized felsic dyke with green interstitial hedenbergite that hosts local carbonate, Fe-Ti oxides, monazite and fluorite (cross-polarized light)..... 70

Figure 2.5 Geological map of the Koorae Prospect. Intrusive contacts of the amphibole-clinopyroxene granite are marked with heavy dashed lines, whereas the fault zone is marked by a light dashed line. The stratigraphic column is a schematic representation from point A to B highlighted by the grey transparent line. 71

Figure 2.6 Outcrop photos from the Koorae Prospect. **(a)** Host marginal amphibole-clinopyroxene granite porphyry of the Koorae Prospect showing dextral faulting along the white dashed line offsetting the volcanic stratigraphy. Black dashed lines represent the contact between granite, tuff and basalt. **(b)** Conformable contact between the flow-banded rhyolite and tuff in the eastern end of the trench. **(c)** Chilled margin of the granite intrusion against a lapilli tuff with hand sample images showing the

change in texture. **(d)** Mafic dykes intrude the granite porphyry isolating local blocks of granite..... 72

Figure 2.7 Hand specimens of mineralized units from the Koorae Prospect. Scale bar is 1 cm. **(a)** Spherulitic rhyolite showing chalcopyrite hosted in quartz-filled perlitic fractures, banding and around spherulites. **(b)** Strongly hematized amphibole-clinopyroxene granite porphyry with chalcopyrite hosted in miarolitic quartz cavities. **(c)** Brecciated amphibole-clinopyroxene granite near a fault zone showing alteration by chlorite, carbonate and quartz with minor chalcopyrite disseminated and in veinlets. **(d)** Brecciated tuff with abundant copper sulfides hosted in chloritic breccias. **(e)** Deformed and altered granodiorite of the Hungry Mountain Complex sampled from a fault zone. Sericite alteration is parallel to the deformation and hosts minor chalcopyrite. **(f)** Strongly hematized and potassic-altered rhyolite margin hosting abundant disseminated chalcopyrite..... 74

Figure 2.8 Hand sample and photomicrographs representing the paragenetic sequence of Cu-Mo-Ag-Au hosted amphibole-clinopyroxene granite between outcrops distal to mineralization (a, a1 and a2), mineralized outcrops (b, b1 and b2), and secondary syn- to post-mineralization (c, c1 and c2). **(a)** Hand sample of non-mineralized granite showing weakly porphyritic texture and more common amphibole. **(a1)** Deuteric replacement of arfvedonite and aegirine-augite by magnetite, riebeckite, ilmenite, hematite, rutile and titanite. **(a2)** Complete replacement of amphiboles and increased interstitial quartz and Fe-Ti oxides. **(b)** Mineralized porphyritic granite with interstitial to miarolitic copper sulfides and Fe-Ti oxides. **(b1)** Miarolitic cavity hosting chalcopyrite with hematite rims, among clinopyroxene and plagioclase. **(b2)** Interstitial quartz hosting euhedral zircon crystals among fluorite, clinopyroxene, chalcopyrite and hematite. **(c)** Brecciated host granite

showing increased magnetite, hematite and chlorite alteration associated with copper sulfides and crosscut by white quartz-carbonate veins. **(c1)** Quartz-carbonate veins hosting minor chalcopyrite. **(c2)** Magnetite- and hematite-filled fractures and microbreccias..... 75

Figure 2.9 Thin section photomicrographs of volcanic host rocks from the Koorae Prospect showing typical alteration associated with Cu-Mo-Ag-Au mineralization. **(a)** Rhyolite flow hosting quartz, chlorite, arfvedsonite in synvolcanic cavities and biotite and pyrite in perlitic fractures. **(b)** Strongly hematized rhyolite flow margins with interstitial chalcopyrite, chlorite, quartz and fluorite to radiating aegirine-augite crystals. **(c)** Mineralized tuff breccia hosting chalcopyrite in quartz, chlorite, fluorite veins and disseminations in alkali feldspar. **(d)** Mineralized lapilli tuff with bornite, albite and alkali-feldspar in perlitic cavities. 77

Figure 2.10 Reflected light and scanning electron microscope (SEM) images of mineralized host rocks from the Koorae Prospect. **(a)** Sulfides in the amphibole-clinopyroxene granite show covellite replacement of bornite and minor chalcopyrite associated with secondary malachite. **(b)** Secondary monazite and hematite replace aegirine-augite and titanite in fractures and cavities of amphibole-clinopyroxene granite. Fractured pyrite grain margins also host secondary xenotime. **(c)** Chalcopyrite mineralization in hematized rhyolite flow margins show secondary covellite, pyrite and hematite on rims and fractures. **(d)** Chlorite alteration in rhyolite hosts chalcopyrite and rounded zircon inclusions. **(e)** Distinct sulfide exsolution texture of chalcopyrite in bornite with covellite rims. The sulfide assemblage occurs in the matrix of a hydrothermal breccia in lapilli tuff. **(f)** SEM image of chalcopyrite containing clausthalite and hessite inclusions as well as fibrous molybdenite in fractures. The sulfide assemblage occurs in the matrix of a hydrothermal breccia in lapilli tuff. 79

Figure 2.11 Mineralogy and alteration associated with U and REE mineralization in felsic dykes and granite. **(a)** Uranium-bearing marginal granite hosting poikilitic, light-green aegirine augite with inclusions of calcite, titanite, quartz, fluorite and zircon as well as secondary fine-grained, brown hedenbergite. **(b)** Interstitial calcite, uanpyrochlore, fluorite zircon and titanite hosted in uranium bearing amphibole granite. **(c)** Mineralized granitic dyke hosting allanite and monazite in interstitial quartz cavities associated with magnetite and ilmenite. **(d)** Strongly altered U-REE bearing pegmatitic dyke hosting monazite and zircon in an alteration assemblage of chlorite, calcite, ilmenite and quartz. Fine grained aegirine-augite grains show rims of monazite. 80

Figure 2.12 Major element discrimination diagrams for the TIS, Springdale Group volcanic rocks and mafic to intermediate rocks. Samples from The Koorae Prospect and mineralized felsic dykes (filled symbols) are differentiated from regional samples (open symbols). **(a)** AI-CCPI alteration box plot diagram for least altered samples of the TIS region (Large et al., 2001). **(b)** $\text{Al}_2\text{O}_3/\text{Na}_2\text{O}-\text{Na}_2\text{O}$ plot showing alteration causing Na-loss outside the field of least altered samples. **(c)** $\text{K}_2\text{O}-\text{Na}_2\text{O}$ plot from Middlemost (1975) classifying the TIS as K-series, alkalic magmas. **(d)** K_2O vs Rb shows the positive correlation between increased K_2O and Rb from K-feldspar-sericite alteration. Unaltered granites in the middle of the diagram display increasing Rb, with decreasing K_2O suggesting fractionation of feldspar. **(e)** Total alkali vs silica (TAS) diagram (LeBas et al., 1986) classifying the majority of the TIS and Springdale Group volcanic rocks as high silica, weakly alkaline to sub-alkaline rhyolites. Samples of the Hungry Mountain Complex show the most heterogeneity from basaltic-andesite to rhyolite. The dividing line between alkaline and sub-alkaline magma series is from Miyashiro (1978). 83

Figure 2.13 Trace element discrimination diagrams for the TIS, Springdale Group and mafic to intermediate rocks using the same symbol key as the previous diagram. **(a)** The Shand's index uses the aigpatic index [$AI = \text{molecular Al}/(\text{molecular Na} + \text{K})$] and alumina saturation index [$ASI = \text{molecular Al}/(\text{molecular Ca} + \text{Na} + \text{K})$] to classify the TIS and associated rocks as peralkaline to weakly metaluminous and peraluminous (Frost et al., 2001). **(b)** A revised Winchester and Floyd (1977; Pearce 1996) diagram uses Nb/Y vs. Zr/TiO₂ to classify the TIS and associated rocks as mostly alkali rhyolite to subalkaline rhyolite/dacite. **(c)** Immobile element pairs Th vs. Yb show the correlation of TIS and associated rocks samples in the calc-alkaline field (Th/Yb > 0.65). **(d)** Immobile element pairs Zr vs. Y correlate between samples of the TIS and associated rocks in the calc-alkaline field. **(e)** The Y vs. Nb plot (Pearce et al., 1984) classify the TIS and Springdale Group volcanic rocks as within plate granite (WPG), whereas the Hungry Mountain Complex plots in the volcanic arc (VAG) and syn-collisional granite (COLG) field. **(f)** Ga/Al against Zr can discriminate A-type granites from other I- and S-type granites (Whalen et al., 1987)..... 85

Figure 2.14 Primitive mantle normalized multi-element plots compare regional signatures of TIS granitic rocks (shaded) to **(a)** mineralized samples from The Koorae Prospect and a U mineralized amphibole granite from the Railway showing and **(b)** mineralized felsic dykes. Two types of mineralized felsic dykes show different patterns but similar enrichments in Th, U, Nb and Ta. Negative anomalies in Ba, K, Sr, P and Ti are marked by dashed lines and are common in most felsic samples. **(c)** Chondrite normalized REE plots (Sun and McDonough, 1989) compare the range of signatures seen in amphibole-clinopyroxene granite, quartz-feldspar porphyries and the Springdale Group rhyolite. All units are marked by strong negative Eu anomalies. Positive Ce anomalies are associated with decreased HREE in host amphibole-clinopyroxene

granite at the Koorae Prospect while negative Ce anomalies in some rhyolite show enriched HREE. The rhyolite samples show a broad range of LREE to MREE signatures resulting from alteration. Quartz-feldspar porphyry samples show slightly elevated LREE compared to amphibole-clinopyroxene granite. **(d)** Chondrite-normalized REE patterns (Sun and McDonough, 1989) for late felsic dykes showing strong REE enrichments in mineralized samples compared to non mineralized samples. All samples show slight negative sloping patterns and negative Eu anomalies. 86

Figure 2.15 Zircons separated from mineralized rhyolite, imaged using cathode luminescence (CL; a,b) and backscatter (c,d) from SEM. The scale provided corresponds to all images. 87

Figure 2.16 Zircons separated from mineralized granite, imaged using cathode luminescence (CL; a,b) and petrographic microscope using transmitted light (c) and reflected light (d). The scale provided corresponds to all images. 88

Figure 2.17 Concordia plots for zircons analyzed from the Koorae Prospect rhyolite (left) and mineralized amphibole-clinopyroxene granite (right). Three zircon fractions were analyzed by TIMS for each rock type and are shown in Figs. 2.15 and 2.16. Samples provide a concordant age of 428 ± 1.6 Ma and 430 ± 1.4 Ma for rhyolite and granite, respectively. The ages are also highlighted on each plot. 90

Figure 2.18 Regional map of the Notre Dame subzone highlighting the age of Silurian non-arc magmatism. Ages of the TIS are highlighted in red (Whalen et al., 1987b, 2006) and blue (this report). The map area under investigation in this manuscript is highlighted in the red box. An outline of Newfoundland is seen as a semi-transparent grey line. Modified from van Staal (2005) and Whalen et al. (2006). 91

Figure 2.19 A schematic diagram illustrating the principal geological components and environments of the TIS in the Hinds Lake area. **(1)** The Koorae prospect Cu-Mo-Ag-Au mineralization hosted in a sill-like amphibole-clinopyroxene granite intruding the Springdale Group near a faulted unconformity with the Hungry Mountain Complex. **(2)** U-REE hosted pegmatite to aplite dykes (LRMa and LRMb) and veins that crosscut the youngest units of the TIS. **(3)** Uranium hosted in local peralkaline granite (Railway) near the margins of the intrusions..... 92

List of Abbreviations

Silicates

Ab	–	albite
Aeg	–	aegirine
Afs	–	alkali feldspar
Aln	–	allanite
Arf	–	arfvedsonite
Agt	–	aegirine-augite
Bt	–	biotite
Chl	–	chlorite
Ep	–	epidote
Hbl	–	hornblende
Hd	–	hedenbergite
Kfs	–	potassium feldspar

Oxides

Ap	–	apatite
Cal	–	calcite
Cb	–	carbonate
Hem	–	hematite
Ilm	–	ilmenite
Mag	–	magnetite
Mal	–	malachite
Pcl	–	pyrochlore
Rt	–	rutile
Xtm	–	xenotime

Mnz	–	monazite
Qtz	–	quartz
Pl/Plag	–	plagioclase
Prh	–	prehnite
Px	–	pyroxene
Rit	–	ritcherite
Ser	–	sericite
Th	–	thorite
Ttn	–	titanite
Zr/Zrn	–	zircon

Sulfides

Bn	–	bornite
Cc	–	chalcocite
Ccp	–	chalcopyrite
Cov	–	covellite
Mo	–	molybdenite
Py	–	pyrite
Stn	–	stannite

Others

Fl/F	–	fluorite
Hes	–	hessite
Cl	–	clausthalite

Chapter 1: An Introduction to the Geology and Geochemistry of Topsails Intrusive Suite and associated Mineralization

1.1 INTRODUCTION

The Topsails Intrusive Suite (TIS) and coeval Springdale Group of west-central Newfoundland are a Silurian, post-orogenic suite of felsic dominated plutonic and volcanic rocks. The TIS has been the focus of much academic research, but until recently has not been considered as a potentially fertile environment for mineral deposits. This study provides the first documentation of magmatic-hydrothermal Cu-Mo-Ag-Au, and intrusion-related U-REE mineralization hosted in the TIS and equivalent Springdale Group. It investigates the relationship between mineralization and the geological framework of the region. The TIS and Springdale Group are located in the northeastern part of the North American Appalachians, and represent a widespread plutonic event that followed closure of the Paleozoic Iapetus ocean (Strong, 1978; Williams, 1979; Whalen et al., 1996, 2006; van Staal, 2007). The Notre Dame subzone, which hosts the TIS, includes Cambrian to Ordovician ophiolite, submarine volcanic rocks, and volcanic arc sequences accreted to the Laurentian margin (Fig 1.1). The TIS, and equivalent volcanic rocks of the Springdale Group, intrude and overlie these rocks and are associated with periods of extension and transcurrent faulting (Taylor et al., 1980; Whalen et al., 1996, 2006).

The TIS crops out over $> 2200 \text{ km}^2$ (Whalen, 1989; Whalen et al., 1996, 2006) and is a suite of peralkaline dominated, A-type granites. The main intrusive phase is a coarse-grained, peralkaline aegirine-arfvedsonite granite. Contemporaneous finer-grained granite and hypabyssal intrusions exposed in the Hinds Lake area are more variable in

nature and geochemistry. Peralkaline rocks commonly host distinct alkali amphibole and sodic-pyroxene while non-peralkaline rocks are biotite-bearing and amphibole-poor. Chemically they are distinguished using the Shand's index (Maniar and Piccoli, 1989) and the molar ratio of $\text{Al}_2\text{O}_3 / \text{Na}_2\text{O} + \text{K}_2\text{O}$ and $\text{Al}_2\text{O}_3 / \text{CaO} + \text{Na}_2\text{O} + \text{K}_2\text{O}$. Similar to A-type complexes these rocks have high $\text{Na}_2\text{O} + \text{K}_2\text{O}$ and highly-charged cations including Zr, Nb, Y, REE (except Eu) and Ga compared to I-type granites (Loiselle and Wones, 1979; Collins et al., 1982).

The TIS and associated Springdale Group volcanic rocks host recently discovered magmatic-hydrothermal Cu-Mo-Ag-Au mineralization (ie. Koorae Prospect) as well as other U and REE occurrences near Hinds lake (Fig. 2.2). The setting, style and control of mineralization require further investigation. The TIS has a complex petrogenetic history involving fractionation, volatile fluxing, and mixing with mafic magmas (Taylor et al., 1980; Whalen et al., 1996, 2006); however, it is poorly understood how these processes might affect mineralization. It is also uncertain whether or not fluorine has a role in the transport of Cu-Mo-Ag-Au and U-REE in these occurrences as it has been identified to affect the REE compositions of certain fluids (Collins et al., 1982; Taylor et al., 1981; Linnen and Cuney, 2005). Furthermore, there are poor age constraints on TIS granite magmatism and there is no accurate age for marginal phase granite. Published ages of the TIS main amphibole granite, quartz-feldspar porphyry, and Springdale Group rhyolite overlap in uncertainty and thus are considered to be coeval (Fig. 1.3; Whalen et al., 1987b, 2005).

The earliest exploration of the Hinds Lake area was conducted by a variety of mineral exploration companies, including Abitibi, Noranda, and Teck, during the early to late 1980s for gold and copper (NL Geological Survey, Assessment file, Nfld/1320). During this time copper sulfide mineralization, hosted by quartz-carbonate-chlorite veins within a basalt flow of the larger Springdale Group volcanic rocks, was discovered near Hinds Lake (Case and Zagorevski, 2009). No further base and precious metal discoveries were made until recently when Altius Resources Corp. and JNR Resources Inc. discovered the Koorae Prospect in 2009 (JNR news release, Nov, 30 2009). The Koorae Prospect is a Cu-Mo-Ag-Au sulphide occurrence hosted predominantly in miarolitic cavities of a peralkaline, marginal phase amphibole-clinopyroxene granite of the TIS, as well as rhyolite flows and felsic volcanic breccias of the Springdale Group (Fig 1.3). Elsewhere, numerous U and REE occurrences hosted in fractionated and evolved granitic dykes and veins were also discovered proximal to marginal granite intrusions (Fig 1.3). The TIS shares geological similarities to the many peralkaline/ subaerial volcanic ore-hosting environments (e.g., southwest US; Dilles and Gans, 1995), as well as iron oxide copper-gold (IOCG)-type Cu-Mo-Ag-Au, U and REE mineralization (Hitzman et al., 1992; Barton and Johnson, 1996).

This chapter provides an introduction to the regional geology and geochemistry of the TIS and the Springdale Group, highlights the objectives of the research, describes the methods used in data collection, and elucidates the format of the thesis. Chapter 2 provides a manuscript that integrates fieldwork, geochemistry, petrography and U-Pb

geochronology to explain the relationships and controls on Cu-Mo-Ag-Au, U and REE mineralization within the TIS and Springdale Group.

1.2 GEOLOGICAL OVERVIEW

The TIS and coeval Springdale Group volcanic rocks were emplaced during post-orogenic extension following the closure of the Iapetus Ocean and represent one of the largest magmatic events within the Appalachian Orogen (Taylor, 1979; Williams, 1979; Whalen et al., 1996, 2006; van Staal, 2007). Previous studies of the TIS have identified the presence of two granitoid suites of distinct geochemical affinity, each with equivalent volcanic to sub-volcanic expressions in the Springdale Group (Taylor et al., 1980, 1981; Whalen et al., 1995). The peralkaline suite consists of a main amphibole granite and similar marginal phase amphibole-clinopyroxene granite, quartz-feldspar porphyry, rhyolite flows and ignimbrites. These contain elevated concentrations of high field strength elements (HFSE), including Zr, Nb, Y, and Th, REE (except Eu), and U (Taylor et al., 1981; Whalen et al., 1996). The non-peralkaline rocks are a variety of fine-grained marginal phase granite including subsolvus to hypersolvus biotite and biotite-amphibole granite as well as equivalent quartz-feldspar porphyry, rhyolite flows and volcanoclastics. Formation of the A-type TIS and Springdale Group involved the interplay of numerous crustal and igneous processes including basaltic underplating, crustal melting, magma mixing, crystal fractionation as well as volatile fluxing and subsequent metasomatism (Taylor et al., 1981; Whalen and Currie, 1984, 1990; Whalen et al., 1995, 2006). The following discussion of the TIS and Springdale Group explains the current understanding of the tectonic setting within the Notre Dame subzone, the regional geology and

geochemistry of the TIS and Springdale Group, and the recently discovered mineral occurrences.

1.2.1 Tectonic Setting – The Notre Dame Subzone

The Appalachian Orogen in Newfoundland comprises several tectonostratigraphic zones that record the opening and closure of the Iapetus ocean complete with accretion of various geological terranes to both the Laurentian and Gondwanan plate margins (Fig 1.2). The TIS and Springdale Group are located within the Notre Dame subzone, a tectonostratigraphic zone with a complex history of subduction and accretion to the Laurentian continental margin that culminated in the Silurian Salinic Orogeny (Fig 1.2; Williams, 1979; van Staal, 2007). The Notre Dame subzone is bounded on the west by the Baie Verte-Brompton Line (BVBL) and to the east by the Red Indian Line (RIL) (Fig 1.1). These crustal sutures are marked by highly deformed ophiolitic rocks and mélanges (Williams et al., 1988; van Staal, 2007). The Notre Dame subzone hosts a number of Cambrian to Ordovician (510-460 Ma) oceanic to ophiolite sequences including the Lushes Bight Oceanic Tract (LBOT), the Baie Verte Oceanic Tract (BVOT), and the Annieopsquotch Accretionary Tract (AAT; Fig 1.2; van Staal, 2007). These highly deformed rocks are stitched together by the extensive Ordovician to Early Silurian (488-435 Ma) plutons of the Notre Dame arc which formed from multiple subduction events beneath the Laurentian margin which ultimately led to the collision and amalgamation of Ganderia with the composite Laurentian margin (Fig 1.2; Williams, 1988; Dunning et al., 1990; van Staal, 2007). Generation of the widespread, Silurian TIS magma could be explained by a tectonic model involving crustal thickening-related anatexis, slab break

off, lithospheric delamination and convective lithospheric erosion (Fig 1.2; Whalen et al., 1995, 2006).

The age of plutonic rocks throughout the Notre Dame Subzone indicate a rapid progression from arc-type to non-arc-type mafic magmatism, and contemporaneous volcanic arc granite (VAG) to within plate granite (WPG) intrusion (Whalen et al., 1995, 2006). The Rainy Lake Complex (see below) is the oldest component of the TIS and likely reflects the end of VAG magmatism before the onset of widespread WPG magmatism (Whalen, 1989; Whalen et al., 1995). The TIS thus marks an important transition from long-lived volcanic arc magmatism to widespread rapid, post-orogenic Silurian granitic magmatism (Taylor et al., 1979; Whalen and Currie, 1984, 1990; Whalen et al., 1996, 2005). Near Hinds Lake, the TIS intrude and overlie deformed diorite to granodiorite of the Hungry Mountain Complex (HMC) and to a lesser extent, the Hinds Brook Granite plutons (Fig 1.3; 460-467 Ma; Whalen, 1989). The HMC and Hinds Brook Granite are among the oldest igneous rocks in the southern Notre Dame subzone and are in fault contact with oceanic to arc-type supracrustal rocks of the Buchans and Glover Groups (Fig 1.3; 473 ± 2 Ma; Dunning, 1987; Whalen, 1989). Several faults have been inferred from regional mapping (Fig 1.3; Whalen and Currie, 1988b), most notably; a northwest-trending fault that follows the western shore of Hinds Lake, and a northeast-trending fault that corresponds with the orientation of TIS agmatite zones and associated mafic dykes (Fig 1.3). The age and association of these structures with the TIS is poorly constrained and there is limited outcrop exposure.

1.2.2 Topsails Intrusive Suite

The oldest unit in the TIS is the 435 ± 1 Ma Rainy Lake Complex (Whalen et al., 2006), which consists of volcanic arc-related gabbro and younger dioritic to granitic phases (Whalen, 1989). Other alkaline igneous rocks of the TIS intrude bimodal volcanic rocks of the Springdale Group (Fig 1.3; 429 ± 4 Ma; Whalen et al. 1987b) and are discussed in detail below. A suite of monzodiorite to quartz syenite and granite form small intrusive bodies that predate the majority of the TIS and are not discussed herein given their low abundance in the study area (Fig 1.3). Narrow agmatite zones with diverse mafic fragments in variously hybridized granite post-date the Rainy Lake Complex and appear to grade into granitic rocks (Fig 1.3; Whalen, 1989). The formation of agmatite zones provide evidence of a coexisting mafic magma that mingled with felsic magma to produce hybrid compositions (Whalen and Currie, 1984, 1990). The most voluminous granite of the TIS is a *ca.* 427 ± 1 Ma peralkaline, aegirine-arfvedsonite granite (aka amphibole granite) with an outcrop area of 868 km^2 (Whalen et al., 1987b, 2006; Whalen and Currie, 1990). This coarse-grained, amphibole granite has been considered the precursor to a number of finer-grained and more diverse bodies of marginal phase granites that dominate the Hinds Lake region (Fig 1.3). However, new U-Pb results provided in this thesis illustrate that some marginal granites pre-date the amphibole granite, and therefore extend the age of A-type magmatism in the TIS.

Marginal phase granites commonly fringes the coarse-grained amphibole granite or occur as isolated and sometimes linear intrusions surrounded by Springdale Group volcanic rocks (Fig 1.3). Marginal phase granites are subdivided into peralkaline and non-

peralkaline varieties (Whalen and Currie, 1990; Whalen et al., 1996) each with a distinct mineral assemblage and chemistry. Non-peralkaline phases may reflect mixing of an originally peralkaline magma with mafic magma or contamination via assimilation of wall rock such as the HMC through which the TIS was emplaced (Whalen and Currie, 1990). Peralkaline marginal phase granite includes a hypersolvus, arfvedsonite-aegirine-bearing granite (termed amphibole-clinopyroxene granite) and is host to Cu-Mo-Ag-Au mineralization at the Koorae Prospect (Fig 1.3). The non-peralkaline granites are generally amphibole-poor and subsolvus to hypersolvus (Whalen et al., 1996). They include biotite-amphibole granite and amphibole-biotite granite to biotite granite (Whalen and Currie, 1988b, 1990; Whalen et al., 1996). Overall the marginal granites show weak, low-temperature alteration to chlorite, sericite, hematite, carbonate and epidote. Alteration often replaces mafic minerals, overprint alkali feldspar or form in late brittle fractures.

The hypabyssal quartz-feldspar porphyry (427 ± 3 Ma; Whalen et al., 1987b) and late mafic to felsic dykes intrude the marginal phase granites and are considered the youngest intrusive event in the TIS. These high-level, sub-volcanic plutons are variably porphyritic to glassy and can be inter-layered and/or grade into rhyolite (Whalen and Currie, 1990). The mineralogy is similar to the peralkaline amphibole granite and marginal amphibole-clinopyroxene granite, containing arfvedsonite and aegirine as late, fine-grained clusters surrounding phenocrysts of quartz and alkali feldspar. Granite to pegmatite dykes are not abundant in the TIS and there is minimal documentation of their occurrence. They crosscut quartz-feldspar porphyry intrusions indicating that they are the

youngest unit observed in the TIS. Similar peralkaline porphyry dykes and composite basalt-rhyolite dykes intrude the coarse grained amphibole granite and quartz-feldspar porphyry (Whalen and Currie, 1982). Late granitic to pegmatitic dykes (< 1 m wide) are locally mineralized with U-REE, and contain abundant accessory minerals and quartz. They appear structurally controlled along intrusive margins and parallel to major joints.

1.2.3 The Springdale Group

The Springdale Group volcanic rocks constitute one of a number of Silurian subaerial, volcanic-plutonic suites in the Notre Dame subzone (Coyle and Strong, 1987). The Springdale Group near Hinds Lake is composed of widespread flow-banded rhyolite, ash flow tuff and subaerial vesicular basalt that form screens above younger intrusive rocks of the TIS. A sample of flow-banded rhyolite yielded a U-Pb zircon age of 429 ± 4 Ma (Whalen et al., 1987), equivalent to the TIS amphibole granite. The volcanic setting provides evidence of a collapse caldera from apparent ring dykes (Taylor et al., 1981; Coyle and Strong, 1987) and mixed rhyolite-basalt dykes (Whalen and Currie, 1982). The Springdale Group sits unconformably on Lower Ordovician submarine volcanic rocks and ophiolite rocks of the HMC and Buchans Group (Fig 1.3; Coyle and Strong, 1987).

The Springdale Group rhyolite is highly siliceous, brick red and often flow-banded. Phenocrysts of quartz and euhedral potassium feldspar are often present in a matrix of intergrown microperthitic feldspar and quartz with accessory zircon, fluorite and topaz. Spherulites with intricate quench textures are remarkably preserved and range in diameter from 2-3 mm to 2-3 cm. Mafic minerals are concentrated in siliceous flow bands or disseminated and normally altered to fine-grained chlorite, sericite, titanite and

opaque minerals (Whalen, 1989). Ash flow tuff units are also abundant and contain lithic rich-zones, welded pumice fragments, and flattened grey dacitic fragments in a rhyolitic matrix (Whalen, 1989). Reddened basalt flows exhibit frothy vesicular tops and amygdules altered by chlorite and carbonate (Whalen 1989). In general, the Springdale Group volcanics are the most strongly altered and fractured unit. They host hydrothermal quartz and carbonate veins with variable chlorite, sericite, hematite, carbonate and fluorite alteration.

1.3 GEOCHEMISTRY

The TIS and its composed units have major and trace element chemistries similar to most A-type granites. Compared to I-type granite, they have elevated SiO_2 , $\text{K}_2\text{O}+\text{Na}_2\text{O}$, $\text{Fe}_2\text{O}_3/\text{MgO}$ ratio and low CaO and Al_2O_3 (White and Chappell, 1983). A-type granite are also enriched in REE (except Eu) Zr, Y, Nb, Ga, are depleted in Sr, Ba and transition metals, and have high Ga/Al ratios (*cf.* Collins et al., 1982; White and Chappell, 1983; Whalen et al., 1987a; 1996; Eby, 1990; Whalen & Currie, 1990). Despite a preponderance of A-type signatures, the TIS ranges from peralkaline to metaluminous or slightly peraluminous in composition (Whalen et al., 1996). The distinctive chemical features of the TIS become less pronounced in marginal phase granites that transition into peraluminous compositions (Whalen and Currie, 1990). As described in Chapter 2, this may be related to the intrusive setting and hydrothermal alteration.

The TIS mafic to intermediate lithologies include the Rainy Lake Complex mafic igneous rocks, mafic to gabbroic dykes, and the Springdale Group basalt. The Rainy Lake Complex consists of basaltic to dioritic lithologies with calc-alkaline compositions and

incompatible element patterns similar to calc-alkaline arc basalts (Whalen, 1989; Whalen et al., 1996). The TIS mafic igneous rocks and Springdale Group basalts are basaltic to basaltic andesites and considered transitional, plotting across tholeiitic to calc-alkaline and alkaline and subalkaline fields (Whalen, 1989). Immobile element discrimination diagrams suggest that these Silurian mafic rocks are within plate basalts though there is some overlap with the field of arc-type basalt (Whalen, 1989; Whalen et al., 1996).

The Springdale Group bimodal volcanic rocks are more calc-alkaline but may reflect hybridization of tholeiitic magma and crustal-derived felsic melts (Whalen, 1989). Rhyolites of the Springdale Group can be subdivided into high-silica and low-silica rhyolites by a noticeable gap in silica content (Coyle and Strong, 1986, 1987). The high silica rhyolites exhibit elevated Nb, Y, Zr, Rb contents and low Sr (Coyle and Strong, 1986, 1987), and are most comparable to rhyolites in the Hinds Lake region (Whalen, 1989). Whalen (1989) suggested that within the Hinds Lake region K-feldspar porphyritic rhyolites might also be stratigraphically younger than equivalent flow-banded rhyolites, are comparatively less altered, exhibit lower silica and higher TiO_2 , FeO, Ba, Sr, Sc and V and lower Nb, and Ga/Al. Regardless of trace element composition, the TIS and Springdale group plot as subalkaline on an alkali-silica diagram, though extensive scatter occurs with increasing silica likely resulting from magmatic-hydrothermal quartz and associated alteration.

1.4 MINERAL OCCURRENCES

Exploration of the TIS in the Hinds Lake area was performed following identification of several uranium anomalies in lake sediment and till samples. Upon

evaluation of the geological characteristics of the TIS and Springdale Group, the area was considered prospective for volcanic-hosted uranium deposits such as the Streltsovka deposit in Russia and McDermitt caldera in Nevada (JNR news release, 2007).

Currently there are two general types of mineral occurrences in the TIS including: 1) intrusion-related U-REE; and 2) magmatic-hydrothermal Cu-Mo-Ag-Au. The U-REE occurrences are hosted in peralkaline granite, pegmatitic dykes and hematized rhyolite, suggesting that mineralization is associated both spatially and genetically with igneous and volcanic rocks in a hypabyssal setting. The investigated U-REE settings include: (1) the Railway prospect, hosted in an amphibole granite outside of the map area, which returned assay values up to 0.62% U_3O_8 and anomalous Pb, Zn, Ni, As, and Cu; (2) the Long Range Mountain prospect A (Fig. 1.3), hosted in vein-dykes within a quartz-feldspar porphyry, that has yielded assays up to 1.40% total rare earth oxides (TREO), 0.35% Y, 1.24% Zr, 0.28% Nb, 0.023% U and 0.154% Th; and (3) the Long Range Mountain prospect B (Fig 1.3) hosted in an aplite dyke within a region where numerous igneous-volcanic grab samples provide up to 3.11% TREO, 0.50% Y, 2.38% Zr, 0.18% Nb, 0.019% U and 0.144% Th (JNR news release, 2007).

Copper-Mo-Ag-Au mineralization is exemplified by the Koorae Prospect, discovered in 2009 in an area previously recognised by base metal mineralization in boulders. In 1998 Geotech Surveys discovered chalcopyrite mineralization in felsic volcanic rocks and intense silica, sericite and pyrite alteration of boulders similar in appearance to footwall alteration observed in volcanogenic massive sulfide deposits (Geotech Surveys Inc. assessment report, 1999). At the Koorae Prospect, strongly altered

felsic tuff boulders returned assays of up to 3.7% Cu, 0.1% Mo, 53.3 g/t Ag and 0.24 g/t Au (JNR news release, 2009). In 2010 further excavation, detailed mapping and sampling was carried out over an area of approximately 200 by 25 meters and exposed pervasively disseminated Cu mineralization hosted in a porphyritic, amphibole-clinopyroxene granite, lapilli tuff, and rhyolite. Of twenty-three grab samples randomly collected from the granite porphyry, twenty-one returned anomalous values of up to 0.87% Cu, with an average of 0.15% Cu. Felsic lapilli tuff returned a best in-situ result of 0.39% Cu, 0.04% Mo and 0.9 g/t Ag, and a rhyolite returned 0.67% Cu, 0.03% Mo and 7.4 g/t Ag. The volcanic sequence consists of inter-bedded green, welded lapilli tuff, flow-banded and spherulitic rhyolite flows and basalt, which are intruded by the amphibole-clinopyroxene granite. Sub-parallel trending diabase dikes crosscut all units, and are weakly deformed, locally pyritic, and non-mineralized. Drilling was performed by Geotech Surveys in 1998 (Geotech Surveys Inc. assessment report, 1999) targeting the Cu showing at The Koorae Prospect and a coincident induced polarization anomaly. Drill holes ended at 100 and 180 meters depths, plunging 45° north to the showing. Unfortunately no drill core has been preserved; however, the logs indicate that one hole intersected strongly sheared and fractured basalt intruded by multiple granitic dykes with associated hematization, epidote and calcite veining (Geotech Surveys Inc. assessment report, 1999). The other hole intersected a biotite granite with localized shearing and strong hematite, sericite, epidote and calcite alteration. No chalcopyrite or volcanoclastic rocks were intersected and the property was abandoned.

1.5 OBJECTIVES

The TIS and Springdale Group have been the foci for detailed regional mapping and geochemical studies in the past; however, no detailed study integrating mineral occurrences within this regional geological framework exists. In order to provide a framework for the newly identified styles of mineralization in the TIS, it is the focus of this study to:

1) use completed geological mapping to compare and contrast the field relationships and petrologies of intrusive and volcanic rocks including the coarse grained amphibole granite, marginal amphibole-clinopyroxene granite, quartz-feldspar porphyry and Springdale Group rhyolite, tuff and basalt;

2) document the alteration, mineralization and geochemical signatures of the host rocks and alteration assemblages;

3) describe and document the geological, mineralogical, and lithogeochemical differences between mineralized and unmineralized rocks; identify the controls of Cu-Mo-Ag-Au and U-REE mineralization; and provide a paragenetic sequence for the alteration and mineralization; and

4) provide U-Pb age constraints on the host rocks and mineralization at the Koorae Prospect and discuss the implications of the results for regional mineralization and exploration.

1.6 METHODOLOGY

1.6.1 Geological Mapping and Sampling

Field mapping and sampling were conducted during the summers of 2009 and 2010 in conjunction with a joint venture exploration program by Altius Resources Corp. and JNR Resources Inc.. The field area is at Hinds Lake in central Newfoundland approximately 18 kilometres northwest of Buchans. The property is in the southwest of the Long Range Mountains and is easily accessible by numerous gravel roads that lead southward from Howley. The elevation is undulating from 300 meters at Hinds Lake to 500 meters near the centre of the property. The nearest airport is at Deer Lake, approximately 50 km to the northwest.

Outcrop exposure is excellent in topographically high areas where vegetation is limited to low lying shrubs and extensive bogs. Valleys are more densely covered by glacial till and spruce forest with sporadic outcrop. Extensive glacial activity is suggested by sculpted hills and till cover. Ice flow indicators suggest a dominant westward to northwestward glacial event in the Hinds Lake area (Batterson and Taylor, 1990).

Regional geological mapping was conducted on 1:50,000 and 1:25,000 scales (Fig. 1.3), whereas trench maps were produced at scales of both 1:50 and 1:100. Rock chip samples were taken from 129 outcrops including the HMC, TIS and Springdale Group lithologies. They include dioritic gneiss, amphibole granite, marginal amphibole-clinopyroxene granite, non peralkaline marginal granite, quartz-feldspar porphyry, felsic and mafic dykes, basalt, rhyolite and volcanoclastic rocks. Mineralized samples were collected primarily from the Koorae Prospect and several smaller U-REE occurrences.

Samples chosen for U-Pb geochronology include the porphyritic, amphibole-clinopyroxene (marginal) granite and rhyolite from the Koorae Prospect.

1.6.2 Lithogeochemistry

All of the 129 samples collected were analyzed for major and trace element geochemistry, including both whole rock geochemistry and assays. Major, minor, and trace elements were determined by inductively coupled plasma optical emission spectroscopy (ICP-OES; 46 partial digestion and 16 total digestion) at the Saskatchewan Research Council (SRC). A similar trace element suite including REE were obtained through closed vessel, multi-acid digestion and analysis via inductively coupled plasma mass spectroscopy (ICP-MS) at the Ontario Geosciences Laboratories (Sudbury, Ontario). Many samples had concentrations that exceeded the upper limit of detection for HFSE and REE, and so additional analysis by X-ray fluorescence (XRF) was performed at MUN on pressed powder pellets. Gold was determined by standard fire assay, dissolution of the bead in aqua regia and then analyzed by ICP-OES and/or atomic absorption spectrometry (AAS) at the SRC.

1.7 THESIS PRESENTATION

Following the introductory chapter there is a chapter including a research manuscript intended for publication in a scientific journal (Chapter 2). Chapter 3 provides a brief summary of the key results of this thesis and implications for further research. Appendix A includes an assessment of quality assurance and quality control of laboratory geochemical data. Appendix B provides all the geochemical data used for each sample and a list of sample lithology and locality.

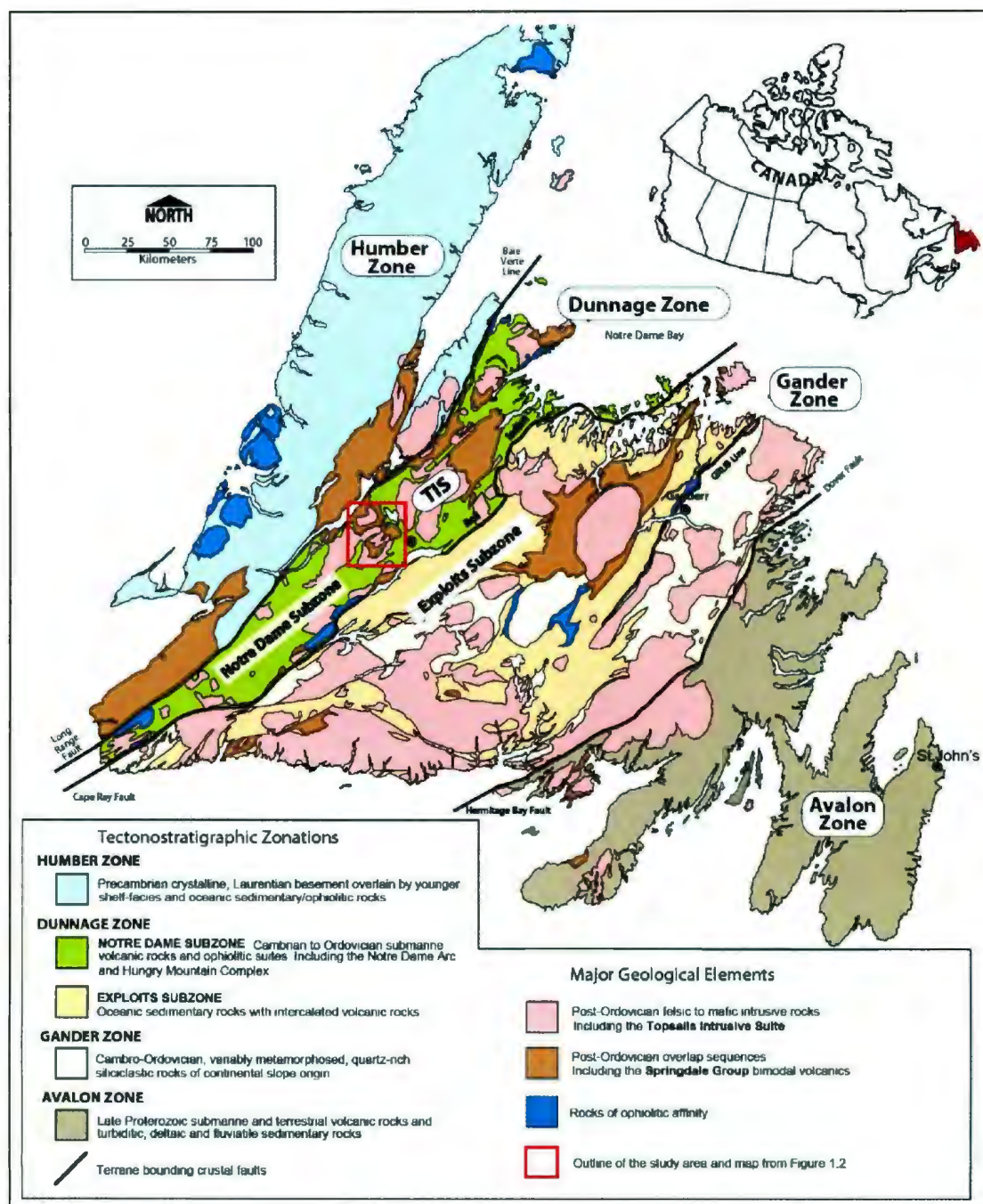


Figure 1.1: Geological map of Newfoundland highlighting the tectonostratigraphic zones of Newfoundland and the location of the TIS in the Notre Dame subzone of the Dunnage Zone. Solid black lines bounding the Notre Dame subzone include the BVL to the west and RIL to the east. An insert map of Canada highlights the location of Newfoundland in the northeasternmost extent of the Appalachians in North America. Geology from Williams et al. (1988) and Williams (2004).

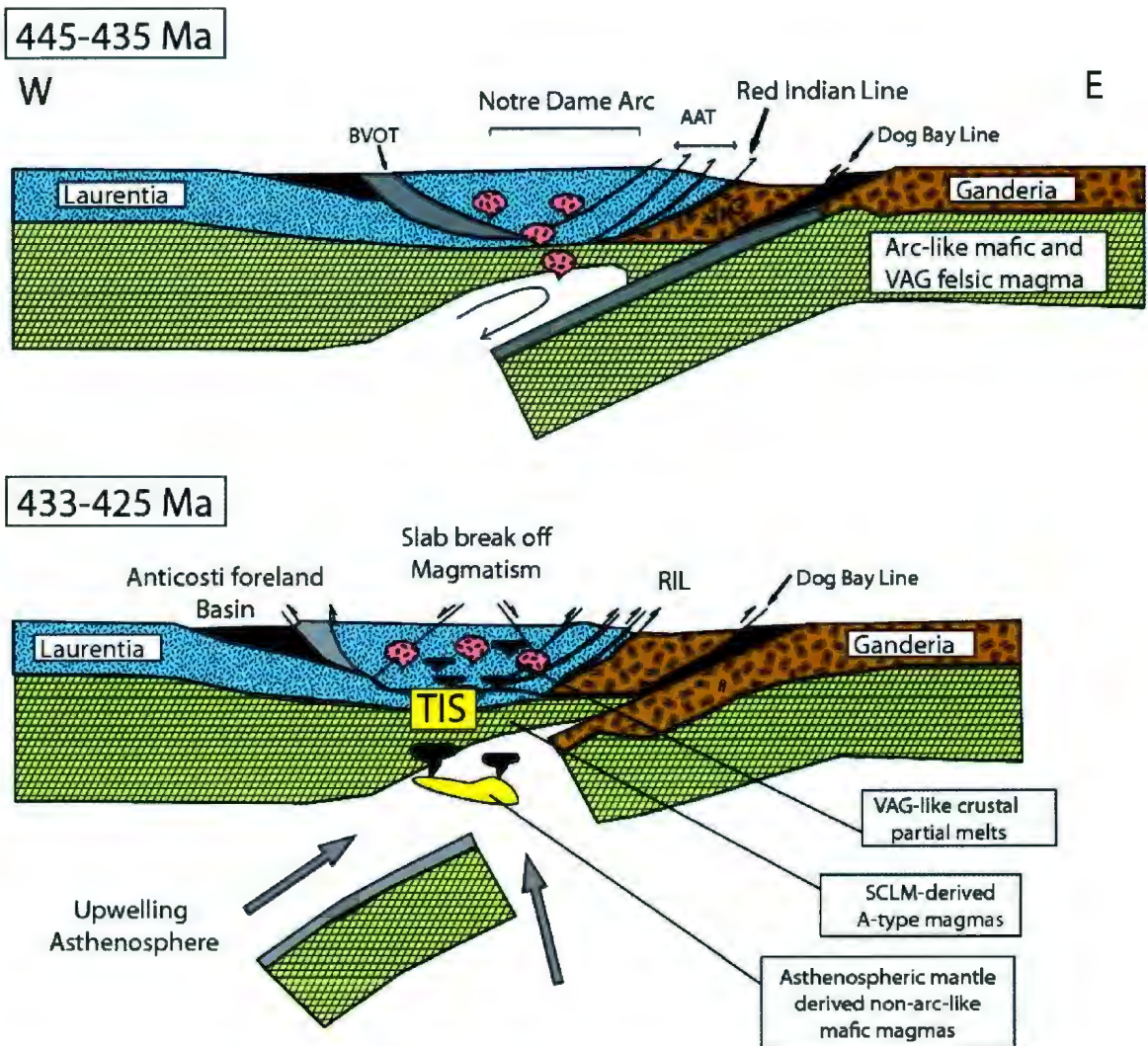


Figure 1.2: Tectonic model for the Salinic orogeny culminating with collision of the Laurentian and Gondwanan (Ganderia) plate margins followed by post-orogenic collapse and slab breakoff. The Notre Dame arc and other oceanic and volcanic rocks are accreted to the Laurentian plate margin forming the Notre Dame subzone. Major crustal sutures including the BVOT and RIL separate the zone from Precambrian Laurentian basement rocks to the west and the composite Ganderia plate margin to the east. Asthenosphere-derived mafic magmas interacted to create both subcontinental lithospheric mantle (SCLM)- derived A-type magmas and VAG-like crustal partial melts that intrude the overriding Notre Dame subzone following orogenesis. Model from Whalen et al. (1996) and van Staal (2007).

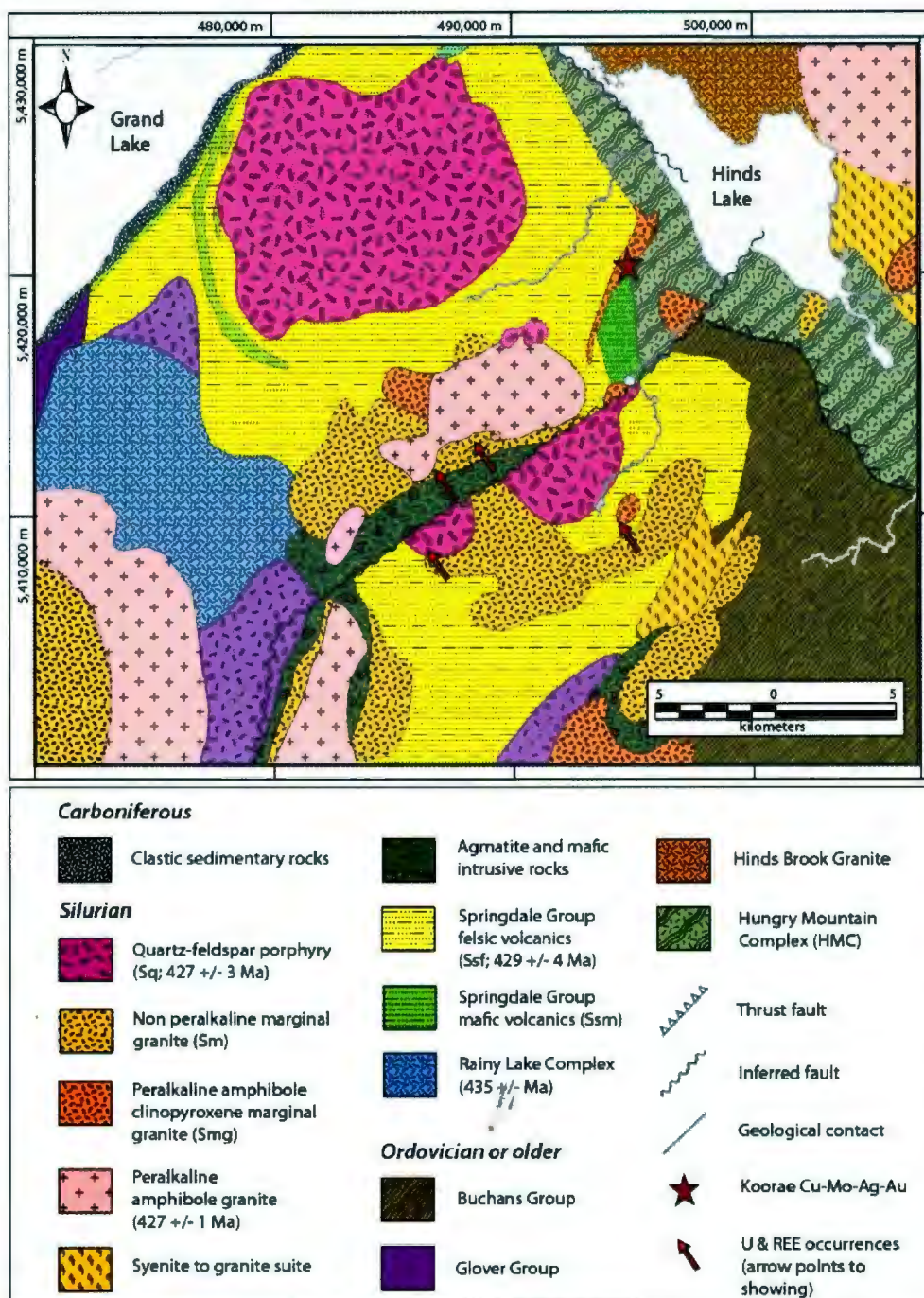


Figure 1.3: Geological map of the Hinds Lake area showing the location and abundance of Silurian igneous and volcanic rocks in relation to Ordovician and older rocks. The location of the Koorae Prospect, U-REE occurrences and major structures are indicated. The documented ages for the TIS are provided for the identified units. Modified from Whalen and Currie (1988b).

Chapter 2: A Detailed Geological, Geochemical and Mineralogical Study of the Koorae Prospect and the host rocks of the Topsails Intrusive Suite, Hinds Lake area, Newfoundland, Canada

2.1 ABSTRACT

The Topsails Intrusive Suite (TIS) and Springdale Group comprise voluminous, Silurian, post-orogenic, plutonic and volcanic rocks that host magmatic-hydrothermal Cu-Mo-Ag-Au and intrusion-related U-rare-earth element (REE) mineralization. The Hinds Lake region of west-central Newfoundland contains numerous granitic rocks and sub-volcanic intrusions of the TIS that intrude bimodal volcanic rocks of the Springdale Group. The Koorae Prospect is a magmatic-hydrothermal Cu-Mo-Ag-Au occurrence hosted in peralkaline, amphibole-clinopyroxene granite and equivalent volcanic rocks that has features similar to iron oxide copper-gold (IOCG)-type deposits. Similarities include structurally controlled mineralization, low-S copper sulfide assemblages, association with magnetite-hematite, fluorite and sodic-calcic alteration, a lack of quartz veins, and enrichments in REE (particularly LREE) P, F, U and Th. Late stage felsic dykes contain U-REE mineralization associated with monazite- (Ce, La), zircon, allanite- (Ce), uranpyrochlore, and thorite within quartz, carbonate, calcic clinopyroxene and Fe-Ti oxides. Uranium-Pb zircon ages of host rocks, including the amphibole-clinopyroxene granite (430 ± 1.4 Ma), and volcanic rocks (428 ± 1.6 Ma) are similar to some of the oldest members of the TIS and Springdale Group, suggesting that Cu-Mo-Ag-Au is associated with the initial stages of TIS development. Uranium- and REE-bearing felsic dykes crosscut some of the youngest members of the TIS and are at least 427 Ma or younger, and represent one of the latest phases of TIS evolution.

The magmatic-hydrothermal Cu-Mo-Ag-Au is hosted in miarolitic cavities of the granite and local volcanic breccias, and consists of a sulfide assemblage of chalcopyrite, bornite, covellite and chalcocite, associated magnetite-hematite, and calcic clinopyroxene. Mineralization is directly associated with hematite, fluorite, zircon and monazite, providing evidence for mobilization of high field strength elements (HFSE) and REE in magmatic-hydrothermal fluids. It is envisioned that the Cu-Mo-Ag-Au mineralization formed via the exsolution of these fluids from the earliest F-rich peralkaline melts within the TIS. Uranium and REE mineralization in felsic dykes are hosted in monazite- (Ce, La), zircon, allanite- (Ce), thorite and uranpyrochlore. These rocks are strongly enriched in REE and HFSE, and their genesis is attributed to magmatic to magmatic-hydrothermal fractionation from highly evolved peralkaline felsic melts during the latter stages of TIS development.

2.2 INTRODUCTION

The Topsails Intrusive Suite (TIS) and Springdale Group volcanic rocks in the west-central Newfoundland Appalachians, Canada, represent a widespread Silurian (435-427 Ma) volcanic-plutonic complex that has been the focus of previous academic research (e.g., Whalen et al., 2006); however, until recently has not been considered as a potentially fertile environment for mineral deposits. This study is the first documentation of Cu-Mo-Ag-Au, U and REE mineralization hosted in the TIS and Springdale Group links mineralization to Silurian magmatism and tectonics in west-central Newfoundland. The TIS and Springdale Group represent widespread, post-orogenic, A-type magmatism emplaced during extension, transcurrent faulting, and caldera collapse (Taylor et al. 1980;

Coyle and Strong, 1987; Whalen et al., 1996, 2006). The Hinds Lake area represents high-level volcanic-plutonic rocks of the TIS and Springdale Group and the latter lie in unconformable contact with Ordovician oceanic and island arc-type volcanic rocks near Hinds Lake (Fig 2.2).

The geology of Hinds Lake contains peralkaline granite and hypabyssal quartz-feldspar porphyry intrusions of the TIS, and bimodal volcanic rocks of the Springdale Group (Fig. 2.2). Recent mineral discoveries, including Cu-Mo-Ag-Au at the Koorae Prospect and other U and REE occurrences (Fig. 2.2), are hosted in peralkaline granite and bimodal volcanic rocks, and peralkaline felsic dykes, respectively. The relationship of the mineralization to the geological, temporal, and metallogenic evolution of the TIS and Springdale Group remain poorly known. In addition, the TIS and Springdale Group have many geological similarities to other peralkalic/subaerial volcanic ore-hosting environments (e.g., southwest US; Coyle and Strong, 1987), but only recently have they been considered a potential environment to host iron oxide copper-gold (IOCG)-type and U-REE mineralization. This paper documents the two distinct styles of mineralization, their geological setting, and their interpreted genesis. In addition, this study provides relative age constraints and U-Pb geochronology to constraint the temporal and geological evolution of the TIS, Springdale Group, and associated mineralization. The final aim of this paper is to provide geological, geochemical, and temporal constraints on the setting and genesis of magmatic Cu-Mo-Ag-Au and U-REE mineralization in the TIS and Springdale Groups, such as to provide potential exploration criteria for finding future mineralization in this area and the Appalachians.

2.3 TECTONIC SETTING

The TIS and Springdale group are within the Notre Dame subzone of the Dunnage Zone in the Newfoundland Appalachians. The Dunnage Zone contains a record of Cambrian-Ordovician arc and back-arc magmatism and deformation (e.g., Taconic orogeny) associated with the closure of the Iapetus Ocean (Fig. 2.1; Williams, 1979; Williams et al., 1988; van Staal, 2007, and references therein). The Notre Dame subzone is bounded by two major terrane bounding crustal faults resulting from subduction beneath both the Laurentian and Gondwanan plate margins (Fig 2.1). Obduction of peri-Laurentian elements onto the Humber Zone led to the formation of the Baie Verte-Brompton Line (BVBL) to the west. Collision of the peri-Laurentian margin with peri-Gondwanan elements resulted in the formation of the Red Indian Line (RIL) to the east during the Taconic Orogeny (Fig 2.1; Williams et al., 1988; van Staal, 2007).

The TIS and Springdale Groups in the Hinds Lake area were built upon rocks of the Notre Dame arc (488-435 Ma), which includes an accreted Cambrian to Ordovician magmatic arc terrain (Whalen et al., 1996; 2006; van Staal et al., 2007). The Hungry Mountain Complex (HMC) is the most widespread unit of Notre Dame arc in the Hinds Lake area and is basement to the Silurian volcanic-plutonic rocks. The HMC consists of gabbroic to diorite and granite to granodiorite rocks that are unconformably overlain by the Springdale Group and intruded by the TIS (Whalen and Currie, 1988b).

The TIS and Springdale Groups in central Newfoundland represent a voluminous Silurian magmatic event and one of the larger A-type, peralkaline volcanic-plutonic complexes in the world. These Silurian igneous rocks (435 - 427 Ma) have been

modelled as a sheet-like mass of approximately 5 km thickness and covering an area of roughly 2200 km² (Whalen and Currie, 1983, 1984, 1990; Whalen et al., 1987b). Large volumes of bimodal, peralkaline intrusive and extrusive rocks are interpreted to have formed via crustal melting associated with crustal thickening, slab break off, lithospheric delamination and convective lithospheric erosion (Taylor et al., 1980; Whalen, 1989; Whalen et al., 2006; van Staal et al., 2007). The presence of large volumes of mafic rocks beneath the TIS and Springdale Group is indicated by gravity and aeromagnetic data (Kornik et al., 1987) and is highlighted by mixed agmatite zones and widespread mafic dykes (Fig 2.2; Whalen and Currie, 1988b).

2.4 GEOLOGY AND STRATIGRAPHY

The Hinds Lake area is dominated by numerous bodies of fine grained to porphyritic marginal phase granite, hypabyssal quartz-feldspar porphyry and bimodal volcanic rocks of the Springdale Group (Fig. 2.2). The area is interpreted to be a roof zone to a coarse grained, peralkaline amphibole granite that is widespread elsewhere in the region (Whalen and Currie, 1988b; Whalen et al., 2006). The main lithologies, stratigraphy, mineralogy, alteration, mineralization and age relationships are presented in Table 2.1.

The oldest component of the TIS is the Rainy Lake Complex (435 ± 1 Ma; Whalen et al., 2006), which consists predominantly of volcanic-arc related gabbroic rocks formed prior to the onset of non-arc related magmatism (Whalen, 1989). A later suite of monzodiorite to quartz syenite and granite form small intrusive bodies that predate the majority of the TIS and are not discussed herein given their low abundance in the study

area. The most voluminous phase of the TIS is a coarse grained, peralkaline, aegirine-arfvedsonite granite or amphibole granite (427 ± 1 Ma; Fig. 2.3b; Whalen et al., 2006). These voluminous, coarse grained, peralkaline granites are relatively homogenous and are interpreted to be the magmatic root to higher level, marginal phase granites. Marginal phase granites range from fine grained to sometimes porphyritic textured peralkaline amphibole-clinopyroxene granite to peraluminous biotite granite (Whalen et al., 1987b). Recent U-Pb zircon ages of a marginal phase amphibole-clinopyroxene granite (430 ± 1 Ma; this study) suggest that older peralkaline magmatism exists. The marginal granites form small isolated intrusions, and local sill-like bodies (e.g., Koorae Prospect) that commonly intrude the Springdale Group volcanics.

The bimodal Springdale Group (429 ± 4 Ma; Whalen et al., 1987b) includes widespread flow banded rhyolite, subordinate vesicular basalt and rhyolitic ash flow tuff. High silica rhyolites from the Springdale Group are interpreted to have formed from a large layered silicic magma chamber within an epicontinental caldera (Coyle and Strong, 1987). The rhyolites are commonly red, hematized, massive to flow banded and weakly porphyritic with spherulites, lithophysae (Fig. 2.3a) and auto-breccias. Rhyolite flows and breccias contain variable lithic fragments (< 30 cm) of rhyolite, basalt, diorite and granite. Mixed rhyolite-basalt flows and dykes have been mapped surrounding larger quartz-feldspar porphyry intrusions. Rhyolites are variably altered resulting in partial to patchy replacement of the primary mineralogy and structures typically by hematite, quartz, chlorite, sericite, epidote and fluorite. Felsic tuffs are dark grey to green and mostly ash, but contain variable lithic-rich zones and flattened pumice fragments. Subaerial, vesicular

basalt occur locally in the western and eastern margins of the volcanic package (Fig. 2.2), and have been documented with frothy vesicular tops (Whalen, 1989). Pillow basalts have been mapped locally in the northeast of the field area and suggest a change between subaqueous and subaerial extrusion. In general, the Springdale Group volcanic rocks are the most strongly altered rocks in the region. This is particularly true near intrusive contacts with the TIS and unconformities with Ordovician or older rocks west of Hinds Lake (Fig 2.2).

Quartz-feldspar porphyries (427 ± 3 Ma; Whalen et al., 1987b) are the youngest dated unit of the TIS and intrude other igneous and volcanic rocks of the TIS and Springdale Group. They are commonly red, massive, quartz-K-feldspar porphyritic intrusions (Fig. 2.3d). In the northern part of the map area (Fig 2.2) the porphyries occur both as flows and porphyritic dykes, suggesting they are high level subvolcanic intrusions to cyptoflows (i.e., partially intrusive to extrusive). Basalt and mixed rhyolite-basalt dykes have been mapped locally (Fig 2.2) and suggest possible emplacement in a collapse caldera-type setting (Coyle and Strong, 1987; Whalen, 1989). In the quartz-feldspar porphyry, alkali amphibole forms fine-grained clusters that are disseminated in a reddened groundmass among euhedral K-feldspar and bipyramidal quartz phenocrysts. The unit is mostly weakly altered, and often siliceous with local quartz veining.

Mafic magmatism was contemporaneous with the evolution of the TIS and is reflected by the presence of mixed mafic and felsic rocks near intrusive margins or in agmatite zones (Fig. 2.3e), as well as widespread mafic dyke swarms (Taylor et al., 1980; Whalen and Currie, 1984; Whalen, 1989). Agmatite zones south of Hinds Lake form

along the fringes of amphibole granite intrusions and follow a northeast trending fault that transects the area (Fig. 2.2)(Whalen and Currie, 1982). Mafic dykes crosscut all units of the TIS and Springdale group, except the later granitic/pegmatitic dykes. They often have a steeply dipping orientation, are between 1 to 3 meters thick and trend northeast to northwest, corresponding generally with regional fractures and joints within the igneous and volcanic units.

Late granitic (to pegmatitic) dykes are not voluminous in the TIS and intrude all other units including the quartz-feldspar porphyry, making them the youngest intrusive event in the region. These fine grained to pegmatitic dykes occur in or near the contacts of marginal granite, quartz-feldspar porphyry and/or conformable to rhyolite flows. Dyke orientations are generally northeast to northwest and steeply dipping, and occur as thin (< 10 cm) granitic veins, to granitic and aplitic dykes (< 1 m thick).

Multiple inferred faults intersect the Hinds Lake region including a northwest trending normal fault along the western shore of Hinds Lake that is proximal to the unconformity between the Springdale Group and HMC (Fig 2.2). This is crosscut by a younger, northeast trending normal fault that correlates with mafic dykes and agmatite zones in the TIS (Fig 2.2). Despite faulting, the majority of igneous rocks are weakly deformed, hosting brittle joints and fracture sets, with local narrow shear zones.

2.5 PETROGRAPHY: PRIMARY AND ALTERATION MINERALS

The peralkaline nature of the TIS is exemplified by distinct alkali-amphibole, sodic pyroxene, and enrichment in HFSE-REE-rich accessory minerals including zircon, titanite, monazite and allanite. The Springdale Group volcanic rocks and TIS hypabyssal

intrusions have similar mineral assemblages, though less distinct given their fine grained nature. Table 2.1 provides a summary of the mineralogy and alteration assemblages associated with the main units of the TIS. Table 2.2 provides a paragenetic sequence of primary and secondary minerals in the peralkaline amphibole sodic-pyroxene granite regionally compared to mineralized granite at the Koorae Prospect. Outlined below are the petrographic characteristics of both primary and secondary minerals within the various units in the Hinds Lake area.

2.5.1 Marginal Amphibole-Clinopyroxene Granite

Non-mineralized amphibole-clinopyroxene granite is pink to reddish, medium grained to weakly K-feldspar porphyritic. Perthitic feldspar phenocrysts are hosted in a holocrystalline groundmass of quartz and microperthite that is locally granophyric (Fig. 2.4b). Albite is very fine-grained, and form local rims around K-feldspar phenocrysts. Interstitial to subophitic grains of light green aegirine-augite and blue-green arfvedsonite are variably replaced by fine-grained richterite and hematite along cleavage planes (Fig. 2.4b) with overgrowths of acicular arfvedsonite. Fine-grained, subhedral accessory minerals including magnetite, ilmenite, titanite, monazite, zircon, allanite and fluorite form inclusions in these mafic minerals (Fig. 2.4a), as well as in interstitial quartz and along grain boundaries. Amphibole can be entirely replaced by richterite, hematite, Fe-Ti oxides and sericite. Weak to moderate brittle fractures overprint the primary textures and contain quartz, chlorite, hematite, sericite and fluorite.

2.5.2 Quartz- Feldspar Porphyry Intrusions

Quartz-feldspar porphyry intrusions are distinct from other units given their porphyritic texture of feldspars phenocrysts set in a maroon to grey-green glassy groundmass. They are among the least altered rocks in the Hinds Lake area. Phenocrysts of pink to orange K-feldspar are subhedral to euhedral, and have perthitic textures with local zoning of albite and dusty hematite (Fig. 2.4c). Bipyramidal quartz phenocrysts are equicrystalline and less abundant than feldspar. The groundmass locally displays an anastomosing fabric defined by quartz, microperthite and oriented quartz phenocrysts (Fig. 2.4d). Arfvedsonite to riebeckite and aegirine-augite form fine-grained masses, poikilitic clusters and disseminated fine-grained prismatic crystals in a matrix of quartz and feldspar (Fig. 2.4c). Amphibole grains contain minor inclusions of stubby, subhedral titanite, rutile, zircon, monazite, apatite, and fluorite. Fine-grained magnetite crystals are disseminated throughout a variably hematized matrix. Hydrothermal alteration is hosted in fractures, veins and breccias and includes quartz, sericite, chlorite, biotite, hematite, carbonate and minor monazite, fluorite and zircon. Trace amounts of chalcopyrite and pyrite are present locally in biotite-filled fractures (Fig. 2.4d).

2.5.3 Springdale Group Volcanic Rocks

Rhyolitic rocks of the Springdale Group contain well preserved volcanic textures including spherulites, lithophysae, breccias and flow banding. These rocks are more strongly altered and deformed than intrusive rocks of the TIS. Fresh rhyolites are red, massive to K-feldspar porphyritic with flow banding defined by alternating siliceous, micropoikilitic textured layers and Fe-oxide layers (Fig. 2.4e). Arfvedsonite and

hedenbergite form fine-grained, disseminated prismatic to acicular grains associated with interstitial quartz and albitized feldspar. Accessory minerals including magnetite, ilmenite, pyrite, titanite, apatite and fluorite, which are disseminated in the groundmass of quartz and alkali feldspar. Perlitic fractures, microbreccias and cleavage planes often host hydrothermal quartz, hematite, sericite, chlorite and biotite. Fine-grained titanite, monazite and fluorite are associated with quartz-hematite-sericite veins and fractures and in some cases contain trace amounts of pyrite.

Felsic tuffs and ignimbrites range from weakly altered welded and lapilli tuff to moderately altered volcanic breccias. Fine ash is typically grey to green and weakly altered to quartz, chlorite and sericite with minor carbonate veining. Lapilli are sub-angular (1-10 cm), poorly sorted, and polymictic ranging from plagioclase-phyric mafic rocks to strongly hematized rhyolite and granite. Hornblende and pyroxene grains occur in minor amounts and are commonly altered to epidote and chlorite. Accessory minerals include stubby titanite and zircon crystals disseminated in alkali feldspar. Late quartz-carbonate veining and alteration postdate early silica and albite alteration of the tuffs.

Basalts are green to maroon, amygdaloidal and commonly massive to plagioclase phyric. They contain fine-grained intergranular plagioclase and pyroxene with abundant disseminated magnetite and titanite grains. Amygdules are commonly well preserved and filled with quartz, chlorite and epidote. In rare cases amygdules contain traces of chalcopyrite and pyrite. Basalt is variably altered from weak to locally intense, most commonly by epidote, chlorite, carbonate, hematite and trace pyrite that fill amygdules and local microbreccias.

2.5.4 Late Aplite to Pegmatitic Dykes

Aplitic to pegmatitic dykes include amphibole-clinopyroxene-bearing granitic dykes, aplite dykes and pegmatitic veins. They are often quartz- and alkali feldspar-rich with granophyric intergrowths of quartz and perthitic feldspar (Fig. 2.4f). Unaltered aplite and granitic dykes contain distinct crystals of green hedenbergite (Fig. 2.4f) to aegirine-augite, that form primary interstitial, poikilitic or prismatic grains. These sodic-calcic pyroxenes are the most common host for accessory minerals including titanite, monazite, allanite, zircon, apatite and fluorite. Quartz-carbonate altered granitic and pegmatite dykes contain abundant fine-grained, disseminated ilmenite, hematite and magnetite, and absent or entirely replaced amphibole and clinopyroxene. Fine-grained accessory minerals including titanite, zircon, allanite, monazite and fluorite are associated with Fe-Ti oxides, replaced amphibole-pyroxene sites or in quartz-carbonate alteration. Felsic dykes often show brecciated and/or assimilated margins between the wall rock and are usually altered by quartz, carbonate and sericite.

2.6 MINERALIZATION: THE KOORAE CU-MO-AG-AU PROSPECT – GEOLOGY, ALTERATION AND MINERALIZATION

2.6.1 Stratigraphy

The Koorae Prospect contains Cu-Mo-Ag-Au mineralization hosted in the TIS amphibole-clinopyroxene granite and Springdale Group bimodal volcanic rocks near an unconformity with the HMC. Detailed geology and stratigraphy of the prospect is illustrated on a map in Figure 2.5. Photos showing the stratigraphy and structure of the The Koorae Prospect outcrops are displayed in Figure 2.6a-d. Photographs of representative hand samples from the host lithologies and mineralization style are

samples selected from the Koorae Prospect represent marginal amphibole-clinopyroxene granite of the TIS and Springdale Group volcanic equivalents. Approximately 30kg of rock chip samples were collected from separate outcrops and processed by the following methods to extract zircon for thermal ionization mass spectrometry (TIMS) analysis.

Each rock sample was washed, then crushed in a jaw crusher and ground to a fine powder in a BICO disc mill. The powder was panned using a Wilfley table to produce a 100 to 200 ml heavy mineral concentrate. The concentrate was passed through heavy liquids and a Frantz magnetic separator to separate minerals according to their density and magnetic susceptibility. The least magnetic, high-density zircon fractions, which usually provide the best quality zircon, were selected for analysis.

Zircon grains were selected according to criteria of morphology and clarity, using tweezers under a microscope. In most cases, a small number of zircon grains were grouped into fractions of like morphology to allow precise measurement of all Pb masses on the mass spectrometer. At an age of ca. 410 Ma, for clear high quality zircon, this amounts to 2- 6 grains of zircon per fraction. The chemical abrasion technique (Mattinson, 2005) was used to remove radiation-damaged parts of the crystal in an attempt to minimize or eliminate Pb-loss corrections. These corroded zircon fractions were washed in distilled HNO₃, then doubly distilled H₂O, then distilled acetone, prior to weighing on a microbalance and loading in Krogh- type TEFLON dissolution bombs. A mixed ²⁰⁵Pb/²³⁵U tracer was added in proportion to the sample weight, along with ca. 15 drops distilled HF and 1 drop HNO₃, then the bomb was sealed and placed in an oven at 210°C for 5 days. Ion exchange chemistry was carried out according to the procedure of

Krogh (1973), with modified columns and reagent volumes scaled down to one tenth of those reported in 1973. The purified Pb and U were collected in a clean beaker in a single drop of ultrapure H_3PO_4 .

Lead and uranium were loaded together on outgassed single Re filaments with silica gel and dilute H_3PO_4 . Mass spectrometry was carried out using a multi-collector MAT 262. The faraday cups were calibrated with NBS 981 lead standard and the ion counting SEM detector was calibrated against a faraday cup by measuring a known lead isotopic ratio. Small amounts of Pb were measured by peak jumping on the ion counter, with measurement times weighted according to the amounts of each mass present. U was measured by peak jumping on the SEM. A series of sets of data were measured in the temperature range 1400 to 1550°C for Pb and 1550 to 1640°C for U, and the best sets combined to produce a mean value for each ratio. The measured ratios were corrected for Pb and U fractionation of 0.1% / atomic mass unit (amu) and 0.03%/amu respectively as determined from repeat measurements of NBS standards. The ratios were also corrected for laboratory procedure blanks (1-2 picograms - Pb, 0.3 picogram - U) and for common lead above the laboratory blank with lead of the composition predicted by the two-stage model of Stacey and Kramers, (1975) for the age of the sample. Ages were calculated using the decay constants recommended by Jaffey et al. (1972).

The uncertainties on the isotopic ratios and ages are calculated using an unpublished program and are reported at two sigma. Sources of uncertainty considered (at 2 sigma) include: uncertainties on the isotopic ratio measurements by mass spectrometry, assigned 80% uncertainty on the Pb and U fractionation, assigned 50% uncertainty on the

amount of the Pb and U blanks, and a 4% uncertainty on the isotopic composition of the Pb used to subtract the common lead present above laboratory blank. These uncertainties are quadratically added to arrive at final two sigma (absolute) uncertainties that are reported after the isotopic ratios in the data table. Ages are reported as the weighted averages of the $^{206}\text{Pb}/^{238}\text{U}$ ages, calculated using Isoplot (Ludwig, 2003), and are reported at the 95% confidence interval. A summary of analytical results from TIMS are provided in Table 2.5. Zircons separated from mineralized granite and rhyolite are imaged in Figures 2.15a-d and 2.16a-d, respectively.

2.9.2 Zircon Characteristics and Results

Zircon separates from the amphibole-clinopyroxene granite and rhyolite were mounted in epoxy resin, polished, carbon coated and imaged with a scanning electron microscope (SEM) using cathode luminescence (CL) and backscatter electrons. This method helped to identify detailed crystal morphology (i.e., zoning) and to analyze the composition of particular inclusions. Representative zircon images for the two rock types are shown in Figure 2.15a-d and 2.16a-d.

Zircons from the rhyolite flow are clear, euhedral prisms between 150-200 microns in length (Fig. 2.15a-d) and are more stubby than those from the granite. They lack any zoning and contain local inclusions of anhedral monazite and euhedral apatite crystals (Fig. 2.15d). Three analysis of 3 to 5 prisms were each concordant and overlapping (Fig. 2.17) with a weighted average $^{206}\text{Pb}/^{238}\text{U}$ of 428 ± 1.6 Ma at the 95% confidence interval (MSWD=0.2) calculated with Isoplot (Ludwig, 2003). This is the

interpreted age of crystallization of the rhyolite and is the best estimate for the age of associated Cu-Mo-Ag-Au mineralization.

Zircons selected from the amphibole-clinopyroxene granite (Fig. 2.16a-d) are clear, euhedral, slender prisms between 150 and 200 microns in length. They are void of hydrozircon overgrowths or zoning as is expected in water deficient, hypersolvus magmas (Pupin 1980). Inclusions of chalcopyrite, monazite and apatite are seen in some zircons (Fig. 2.16d). Three fractions of annealed prisms are concordant and overlapping (Fig. 2.17) with a weighted average $^{206}\text{Pb}/^{238}\text{U}$ age of 430 ± 1.4 Ma at the 95% confidence interval (MSWD=0.2) calculated with Isoplot (Ludwig 2003). This is interpreted as the age of crystallization of the granite and corresponding Cu-Mo-Ag-Au mineralization.

2.9.3 Interpretation

The ages provided herein place the Koorae Prospect within the temporal framework of the TIS, and regional Silurian non-arc plutons in the Notre Dame Subzone (Fig. 2.18). Field relationships indicate that the Springdale Group volcanic rocks (429 ± 4 Ma; Whalen et al., 1987b) are intruded by the TIS of which the quartz-feldspar porphyry (427 ± 3 Ma; Whalen et al., 1987b) is the youngest event. Whalen et al (2006) reported a U-Pb zircon age of the TIS peralkaline granite to be 427 ± 1 Ma, while this report documents a peralkaline granite with an age of 430 ± 1.4 Ma. It is reasonable to suggest that the TIS peralkaline magmatism may have lasted longer than was previously understood. The age of the rhyolite from the Koorae Prospect (428 ± 1.6 Ma) overlaps in

uncertainty with the age of the peralkaline granite ($430 \pm 1.4\text{Ma}$) and is considered coeval, provided that the granite intrudes the volcanic package.

The age of magmatic hydrothermal Cu-Mo-Ag-Au mineralization is interpreted to be $\sim 430\text{-}428\text{ Ma}$, correlative with the age of the host granite and rhyolite. This is suggested by the documented mineral assemblages, the style of mineralization and the presence of chalcopyrite inclusions in the zircon from the host granite. The U-REE mineralization hosted in granitic to pegmatitic dykes crosscut the quartz feldspar porphyry intrusions and is thus younger than the latest TIS magmatism, although no U-Pb zircon dates exist for felsic dykes. The geochemistry of felsic dykes also suggests they are younger because they have a very high concentration of incompatible elements likely representing a later melt fraction of the TIS. Therefore it is concluded that magmatic hydrothermal Cu-Mo-Ag-Au mineralization is associated with the oldest known peralkaline granites of the TIS, whereas U-REE mineralization is likely the youngest magmatic event.

2.10 DISCUSSION

This study provides the first documentation of magmatic-hydrothermal Cu-Mo-Ag-Au and U-REE mineralization hosted within the Topsails Igneous Suite (TIS) and Springdale Group in central Newfoundland, and one of the few occurrences of this style of mineralization within the Dunnage Zone of the Canadian Appalachians. The results herein provide key information on the type of mineralization, host rocks and assemblages, hydrothermal alteration, and the timing of mineralization. Mineralization within the TIS consists of two main types (Fig 2.19), each with distinctive host rocks, alteration, and

temporal associations: 1) magmatic-associated Cu-Mo-Ag-Au mineralization associated with intrusive and volcanic rocks; and 2) intrusion related U-REE associated solely with late stage felsic dykes. The Cu-Mo-Ag-Au mineralization is associated with the Koorae Prospect where mineralization is structurally controlled in a narrow sill-like granitic intrusion and rhyolitic rocks near a regional unconformity with basement gneiss of the HMC (Fig. 2.19). The Cu-Mo-Ag-Au mineralization in the granite occurs within miarolitic cavities and the granophyric groundmass associated with quartz, albite, calcic clinopyroxene, magnetite, hematite, zircon and fluorite (Fig. 2.8b-b2). The granite also hosts later quartz-carbonate-chalcopyrite veins that crosscut the groundmass (Fig. 2.8c). In the volcanic rocks, the mineralization is associated with breccia zones, but with similar metal assemblages. The mineralization is interpreted to be syngenetic, of likely magmatic-hydrothermal affinity, and the Cu-sulfide assemblages are associated with magnetite that is rimmed by hematite indicating deposition from Fe-bearing oxidized fluids. Furthermore, the presence of selenides (e.g., hessite) associated with the mineralization also points to a fluid with low reduced sulfur content (Fig. 2.10b). The mineralization is also closely associated with, but likely post-dates, an early phase of sodic metasomatism characterized by arfvedsonite to richterite and aegirine-augite to hedenbergite (Fig. 2.4a-b). Evidence for HFSE- and REE-enrichment in early to late stages of alteration and mineralization includes secondary fluorite, zircon, monazite and xenotime (Fig. 2.8b2 and Fig. 2.10b).

While there is clearly HFSE and REE mobility associated with the Cu-Mo-Ag-Au mineralization (Fig. 2.10b), the majority of REE- and HFSE-enrichment is associated

with late stage, crosscutting felsic dykes. The felsic dykes of the TIS are spatially associated with the contacts of the marginal granites including the amphibole-clinopyroxene granite and quartz-feldspar porphyry. Uranium-REE mineralization is hosted in dykes or multiple parallel vein-like dykes that are highly siliceous, enriched in accessory minerals (e.g., monazite, allanite, zircon, thorite, pyrochlore) and depleted in alkali feldspar. In most cases, these REE-bearing minerals are hosted in late Fe-Ti oxides, calcic clinopyroxene or strong sodic-calcic alteration (e.g., carbonate, chlorite, albite, ilmenite, hedenbergite; Fig.2.11), but unlike at the Koorae Prospect they are not associated with fluorite or hematite. Uranium and thorium are enriched in some peralkaline granites without significant REE mineralization suggesting that U and Th were enriched in TIS granites via magmatic hydrothermal processes similar to that at the Koorae Prospect. Felsic dykes are also characterized by depleted alkali elements, enriched quartz and carbonate alteration, but have a common Th/U ratio, suggesting that they were derived from a common source. They also have the highest Nb/Y, Zr/TiO₂ and Ga/Al ratios suggesting that felsic dykes are the most fractionated units in the TIS (Fig. 2.13f). All of these features support that REE-enrichment is due to late stage magmatic fractionation.

The coupling of field relationships and geochronology provide key temporal constraints on the origin of the mineralization and metallogeny of the TIS and Springdale Group. The amphibole-clinopyroxene granite at the Koorae Prospect has yielded a U-Pb age of 430 ± 1.4 Ma, whereas the rhyolite yielded an age of 428 ± 1.6 Ma. These host rocks are considered broadly coeval as the ages overlap in uncertainty, and field

relationships at the Koorae Prospect indicate that the rhyolite and tuff are intruded by the granite. The age of Cu-Mo-Ag-Au mineralization in the TIS is best estimated by the age of the host rocks. Furthermore, the host amphibole-clinopyroxene granite provides the oldest age for the TIS (e.g., Whalen et al., 2006) suggesting that magmatic Cu-Mo-Ag-Au mineralization formed during early magmatism of the TIS. By contrast, the U-REE mineralization is associated with felsic dykes that post-date the youngest events of the TIS. Granitic to pegmatitic dykes crosscut the quartz-feldspar porphyry (427 ± 3 Ma; Whalen et al., 1987b), implying that U-REE mineralization is at least 427 Ma or younger. This is consistent with their highly fractionated geochemistry implying that U-REE mineralization is associated with the youngest melts of the TIS.

The diverse host rocks, alteration, metal assemblages ranging from Cu-Mo-Ag-Au to U-REE, and tectonic environment of the TIS and its mineralization bear striking similarities to iron oxide copper-gold (IOCG) districts, globally, and the TIS represents a potential underexplored and rarely considered terrain for IOCG-type Cu-Au-U-REE mineralization (Table 2.5). In particular, the tectonic setting of the mineralization within the TIS shares a number of similarities to IOCG deposit environments, including (Table 2.5): 1) association with large scale continental, A-type magmatism; 2) proximity to crustal-scale faults or sutures; 3) coeval mafic to felsic volcanic-plutonic rocks; and 4) formation at shallow to mid crustal levels. These deposits are also associated with sodic-calcic alteration and form from oxidized fluids that are often sulfur-poor (e.g., Hitzman et al., 1992; Barton and Johnson, 1996; Williams et al., 2005; Groves et al., 2010), features that are inferred for the Koorae Prospect Cu-Mo-Ag-Au mineralization based on the

alteration assemblages and the sulfur-poor assemblages present. Other features similar to IOCG (Table 2.5) include: 1) being hosted in calc-alkaline and fractionated granite that is coarse grained to porphyritic; 2) they are dominated by low-sulfur copper minerals including chalcopyrite and bornite; 3) are associated with magnetite, hematite and potassic alteration at shallow crustal levels; 4) have a lack of quartz veins; 5) show pervasive texture destroying alteration; and 6) are enriched in REE, particularly LREE as well as P, F, U and Th. The ubiquitous presence of fluorite within the host rocks and IOCG-type mineralization also point to the importance of F-rich fluids in metal transport, features also common to IOCG-type deposits (Groves and Vileicher, 2001; Williams et al., 2005; McPhie et al., 2011).

It is currently uncertain whether the late stage U-REE present in crosscutting felsic dykes within the TIS represents a continuation of the main IOCG stage of mineralization, or a distinctly younger U-REE event. Further U-Pb dating of these felsic dykes is required to test this hypothesis. Nevertheless, the U-REE mineralization in the felsic dykes and peralkaline granite are associated with late magmatic hydrothermal alteration and share many mineralogical attributes with the Ilimaussaq deposit of Greenland (Schonenberger et al. 2008; Table 2.5), and is typical of U-REE associated with roof zones of alkaline intrusions.

2.11 EXPLORATION IMPLICATIONS

The Koorae Prospect and associated U-REE occurrences, while only showings, illustrate the mineral potential of the TIS to host IOCG-type, and peralkaline related U-

REE mineralization. Future exploration for these styles of mineralization should consider the following:

- 1) peralkaline amphibole-clinopyroxene granites and felsic volcanics are prospective host rocks, particularly near intrusive margins, regional faults, unconformable contacts with the HMC, or distinct contacts within volcanic stratigraphy (i.e., basalt-tuff);
- 2) mineral assemblages should contain abundant magnetite, hematite, and low sulfur phases (e.g., bornite) indicative of oxidized, sulfur-poor fluids;
- 3) hydrothermal alteration of the Springdale Group volcanics is often stratigraphically controlled and thus more detailed mapping of the stratigraphy is necessary;
- 4) widespread sodic to calcic metasomatism of granitic host rocks include distinct aegirine-augite, hedenbergite and arfvedsonite that show variable amounts of iron-oxide (hematite, magnetite, ilmenite) replacement near mineralized zones. Alteration is weak to moderate, generally with an early sodic event, later calcic (mineraliation) event, and even later potassic (post-mineral) event; and;
- 5) alteration geochemistry of the Springdale Group may provide an important tool for identifying magmatic-hydrothermal events provided its setting above numerous granitic phases. In general, hydrothermal alteration is associated with depleted LREE and anomalous U, Th, Sr and Ba. Positive Ce anomalies are evident in normalized REE plots and are specific to amphibole-clinopyroxene granite.

2.12 CONCLUSIONS

The Hinds Lake area of west-central Newfoundland is associated with Silurian (430-427 Ma) intrusive and volcanic rocks of the TIS and Springdale Group, respectively, and is host to two types of recently discovered styles of mineralization including; early IOCG-type, magmatic-hydrothermal Cu-Mo-Ag-Au at the Koorae Prospect (~430-428 Ma); and peralkaline-type, U-REE in late felsic dykes (<427 Ma).

At the Koorae Prospect, chalcopyrite, bornite, pyrite, covellite and chalcocite are hosted in miarolitic cavities and a granophyric groundmass of a marginal phase, amphibole-clinopyroxene granite porphyry as well as felsic volcanic-hydrothermal breccias of the Springdale Group. Mineralization is associated with early magnetite, late hematite as well as calcic clinopyroxene, fluorite and LREE-bearing accessory minerals. Uranium-Pb zircon geochronology of the host peralkaline granite provides the oldest age for A-type magmatism in the TIS (430 ± 1.3 Ma) suggesting that IOCG-type mineralization is related to early, peralkaline, amphibole-clinopyroxene granites. Mineral paragenesis of host rocks suggests that regional sodium metasomatism of peralkaline granite by fluorine bearing magmatic fluids is succeeded by a sodic-calcic and iron-rich assemblages that replace arfvedsonite, locally host Cu sulfides and hydrothermal monazite and zircon. Increased potassic hydrothermal alteration of host rocks results in non-peralkaline major element geochemical signatures, cause depletions in LREE, and anomalous Sr, Ba and Ce.

Uranium- and REE-bearing felsic dykes, in contrast, are among the youngest rocks in the TIS and are younger than 427 ± 3 Ma (Whalen et al., 1987b). They contain

abundant U-REE-bearing accessory minerals (monazite- (Ce, La), allanite- (La), zircon, thorite and uranpyrochlore) hosted in primary calcic clinopyroxene and magmatic-hydrothermal quartz, carbonate and Fe-Ti oxides. Host rocks are highly siliceous, amphibole-poor and metaluminous. Geochemically, they are the most fractionated and evolved units in the TIS with the highest Nb/Y, Zr/TiO₂ and Ga/Al ratios. Dykes and veins are often parallel to a northeast trending fault suggesting an association with regional fracture sets.

The geological setting and mineral association of newly discovered mineralization in the TIS suggest that it is a underexplored terrain for hosting potential IOCG-type Cu-Au-U-REE. Regional faults, major geological unconformities and intrusive contacts coincide with mineral occurrences and likely fostered magmatic-hydrothermal alteration. Further exploration of the TIS should focus on small intrusive bodies of amphibole-clinopyroxene granite that have evidence for sodic and calcic alteration, Fe-oxide alteration, and associated geochemical anomalies present in the host rocks.

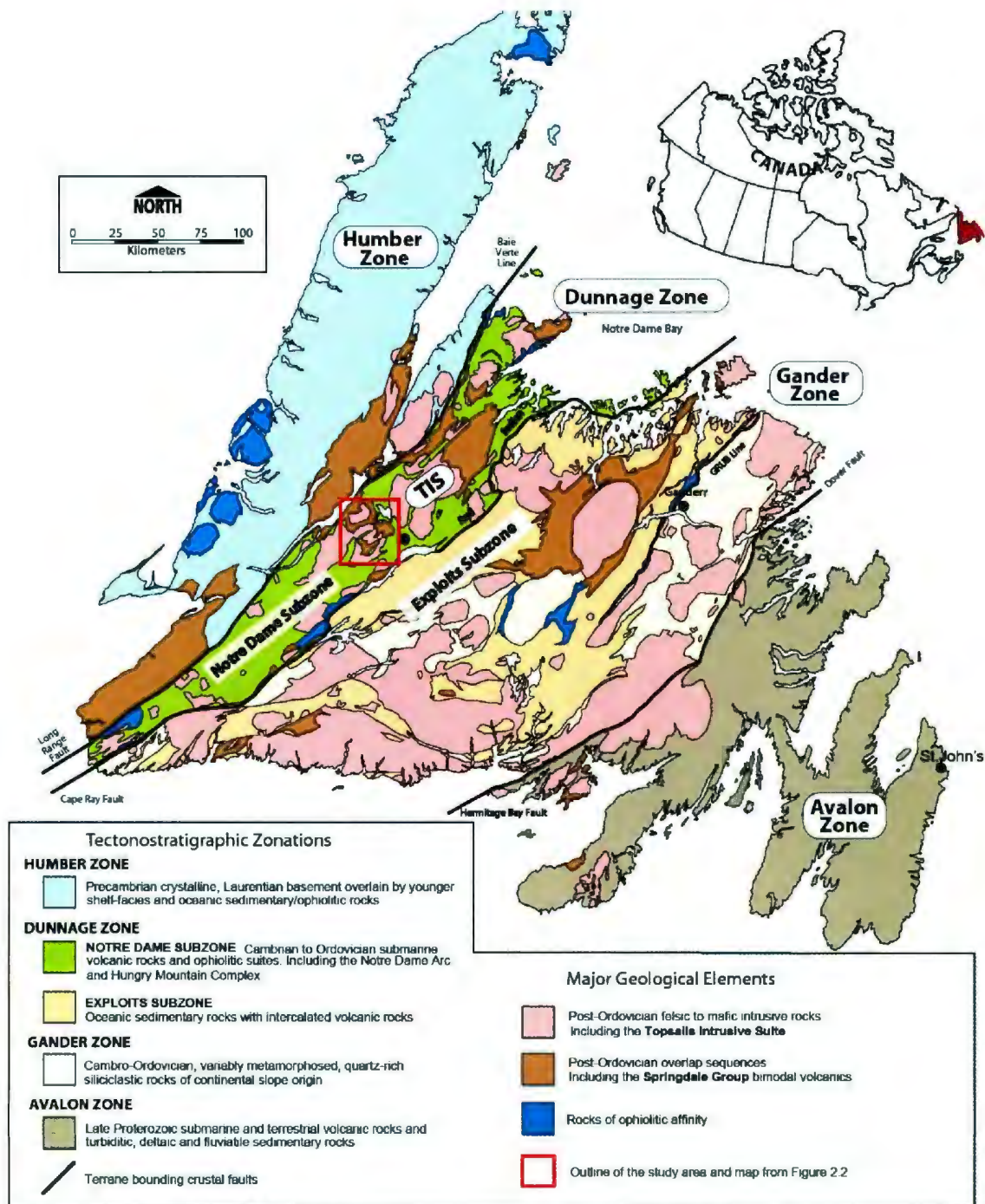


Figure 0.1: Regional geological map of Newfoundland and tectonostratigraphic zonations including the location of the Notre Dame Subzone and TIS. The red box outlines the study area near Hinds Lake and the map location of Figure 2.2. The black lines bounding the coloured area are the BVBL in the west and RIL to the east. Modified after Williams (1979) and Williams et al. (1988).

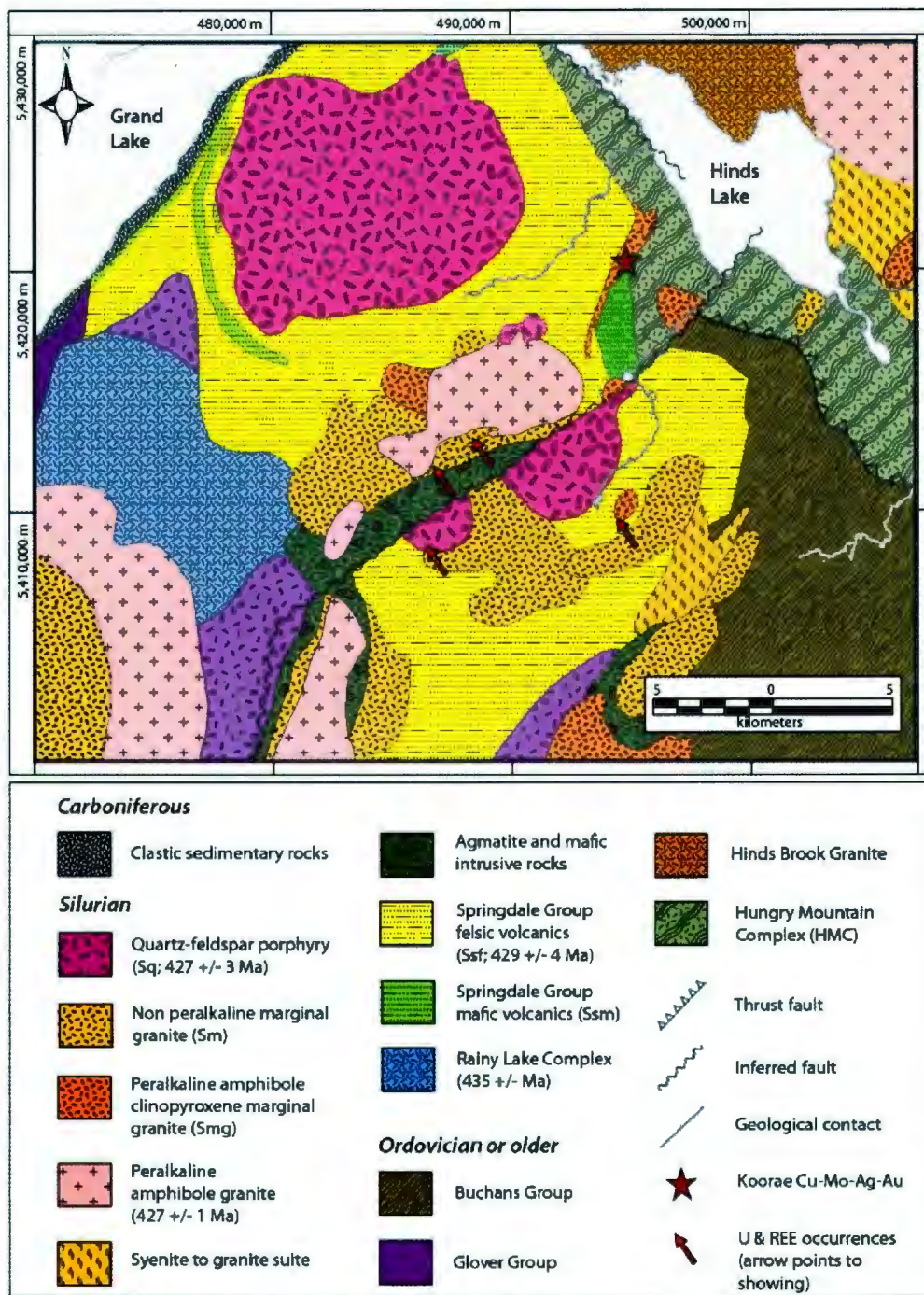


Figure 0.2: Geological map of the Hinds Lake region showing the location of mineral occurrences in relation to roof zone lithologies and geological structures. The approximate coverage area for each lithology is plotted against age and encompasses area extending to the northeast beyond this map. Peralkaline amphibole-clinopyroxene granite is identified from other non-peralkaline marginal granite. Mafic basal occurrences

are also highlighted from the larger Springdale Group. Coordinates are provided as easting and northing in NAD 27. Modified after Whalen and Currie (1988b).

Table 0.1: Summary of the U-Pb zircon age, stratigraphy, mineralogy, alteration and mineralization of the main lithological units of the TIS. Mineral abbreviations are given on page xv. Alteration textures and mineralogy are provided for: 1) magmatic hydrothermal alteration and: 2) secondary magmatic hydrothermal alteration.

TIS Unit	Granitic Dykes (Sdc)	Quartz-Feldspar Porphyry (Sq)	Marginal Amphibole Clinopyroxene Granite (Smg)	Coarse-grained Amphibole Granite (Sp)	Springdale Group Volcanics (Ssf)
Age	Syn- to post- Sq	427 +/-3 Ma ¹	430 +/- 1.4 Ma ²	427 +/- 1 Ma ³	428 +/- 1.6 Ma ² 429 +/- 4 Ma ¹
Stratigraphy	Late crosscutting, aplitic to pegmatitic veins (< 10 cm) and dykes (< 1 m). Associated with intrusive margins.	Subvolcanic plutons with intermittent porphyritic dykes and flows. May grade into rhyolite.	Marginal phase irregular to elongate intrusions. Younger than the precursor though older units exist.	Homogeneous precursor intrusions reflect deeper stratigraphy to marginal phases.	Rhyolite flows, ignimbrites and subaerial basalt show well developed stratigraphy.
Major Minerals	Qtz>Kfs>Ab>Hd>Agt	Qtz>Kfs>Ab>Arf>Agt	Qtz>Kfs>Ab>Arf>Rit>Agt>Hd>Hbl	Qtz>Kfs>Pl>Arf>Agt>Rit	Qtz>Kfs>Ab>Arf>Agt>Hd
Accessory Minerals	Ttn>Mnz>Aln>Zr>Fl>Ap>Pcl>Th>Xtm	Ttn>Rt>Zr>Mnz>Fl>Ap	Ttn>Rt>Zr>Mnz>Aln>Th>Xtm>Fl	Ttn>Zn>Aln>Fl>Mnz>Ap	Ttn>Rt>Zrn>Fl>Mnz>Ap
Alteration Textures	1.Interstitial, amphibole replaced 2.Feldspar destructive, fracture hosted	1.Matrix hosted 2.Fracture, vein, and breccia hosted	1.Interstitial/miarolitic cavities, amphibole replaced 2.Interstitial, fracture hosted	1.Interstitial, amphibole replaced 2.Feldspar destructive, fracture hosted	1.Interstitial 2.Fracture, vein and breccia hosted.
Alteration Mineralogy	1.Ab>Cb>Hd>Ilm>Mag>Hem>Aln>Mnz>Zr 2.Qtz>Chl>Hem>Pcl>Fl>Th>Xtm	1.Ab>Arf>Mag>Hem>Rit>Ilm>Zr>Fl 2.Qtz>Ser>Chl>Bt>Hem>Cb>Mnz>Fl>Zr>Py	1.Ab>Arf>Hd>Rit>Mag>Ilm>Ttn>Rt>Mnz>Zr>Aln>Fl 2.Hem>Mag>Cb>Chl>Ser>Zr>Mnz>Fl	1.Ab>Arf>Hd>Rit>Mag>Ttn>Zr>Mnz>Aln>Fl 2.Chl>Ser>Hem>Cb>Ilm>Fl>Zr	1.Ar>Agt>Hd>Ab>Mag>Ttn>Ap>Zr>Fl>Py 2.Qtz>Hem>Ser>Chl>Bt>Ttn>Mnz>Fl>Py
Mineralization	Up to 78.6 g/t U and 0.94 wt% REE	Trace pyrite and chalcopyrite	Up to 0.92 wt% Cu (avg 0.15 wt% Cu), trace Mo, Ag and Au	Up to 40.9 g/t U	Up to 3.66 wt% Cu, 0.099 wt% Mo, 53 g/t Ag and 0.24g/t Au
1. Igneous metasomatism / magmatic-hydrothermal alteration. 2. Secondary magmatic-hydrothermal alteration. 1. Whalen et al. (1987b) 2. This paper 3. Whalen et al. (2006)					

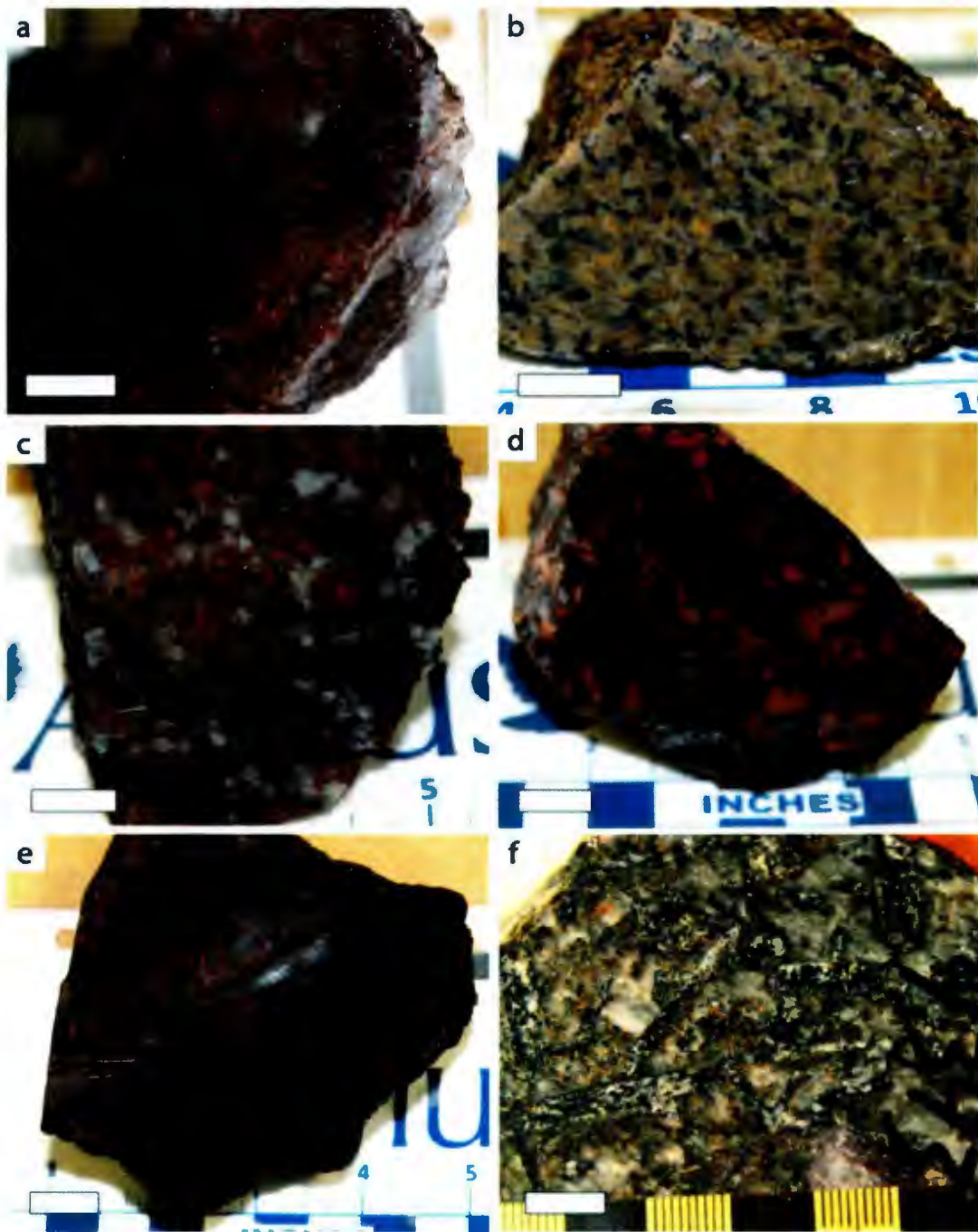




















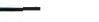











Figure 0.3: Representative hand samples (bar = 1cm) for the major lithologies of the TIS, including (a) spherulitic rhyolite with lithophysae hosted quartz sericite alteration, (b) coarse grained, amphibole granite, (c) marginal phase amphibole-clinopyroxene granite with hematized feldspar, quartz cavities and fracture hosted chlorite alteration, (d) quartz-feldspar porphyry showing hematitized subhedral K-feldspar phenocrysts and hematitized, very fine-grained matrix, (e) mixed mafic and felsic marginal granite sampled near

agmatite zone, (f) mineralized pegmatitic dyke showing strong quartz carbonate alteration and relict amphibole grains replaced by chlorite, carbonate and calcic-pyroxene.

Table 0.2: Paragenetic sequence of alteration and mineralization and comparison between regional and ore related amphibole-clinopyroxene granite. The thicknesses of lines correspond to increasing mineral occurrence. Minerals marked with an X are not typically found in the mineral assemblage. The shaded field highlights the magmatic-hydrothermal alteration assemblage. Mineral abbreviations are seen on page xv.

Amphibole Clinopyroxene Granite	Early  Late Regional	Early  Late Koorae / Ore Related
Quartz		
Arfvedsonite+Richterite		
Aegirine-Augite		
Albite+K-Feldspar		
Sericite+Chlorite		
Biotite		
Carbonate		
Ca-Pyroxene		
Magnetite		
Hematite		
Ilmenite+Titanite+Rutile		
Zircon+Monazite		
Sulphide		
Fluorite		

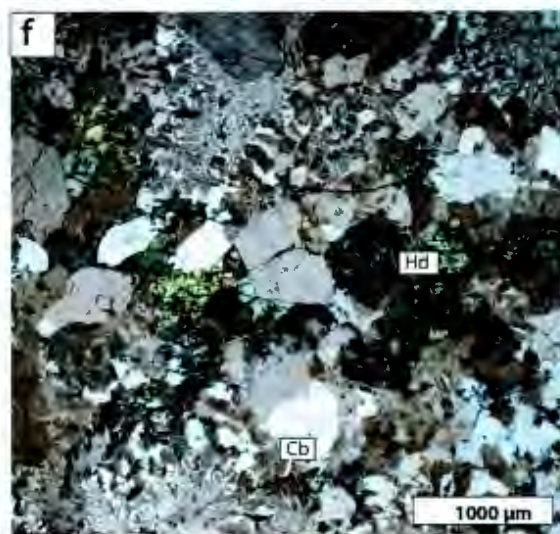
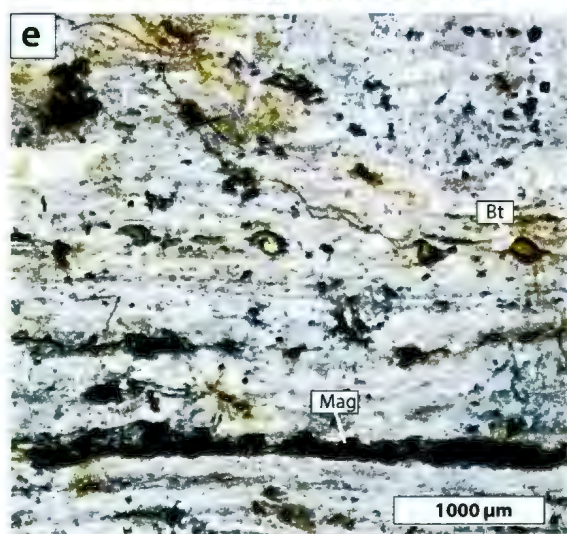
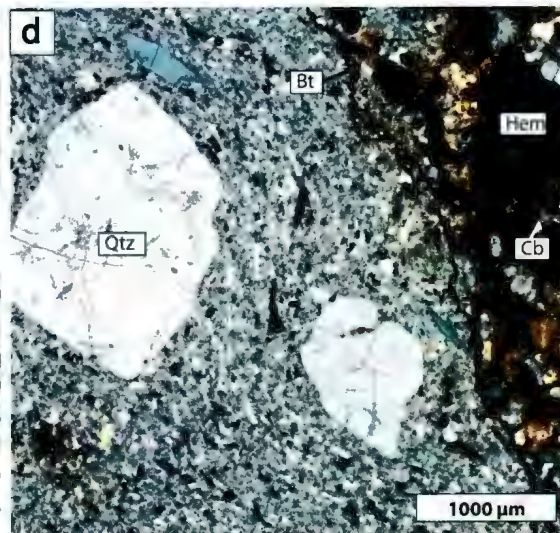
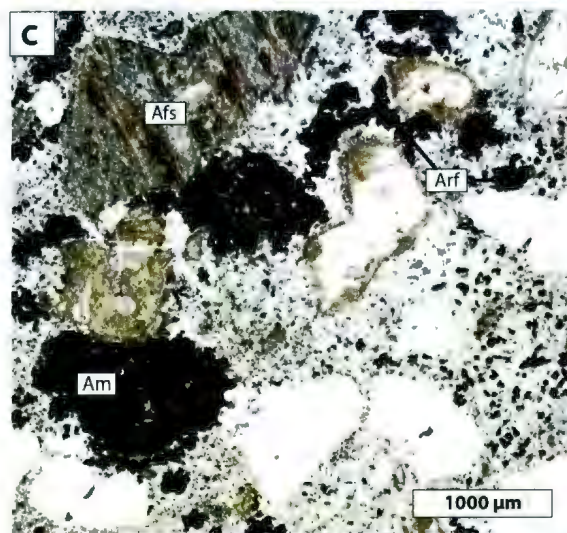
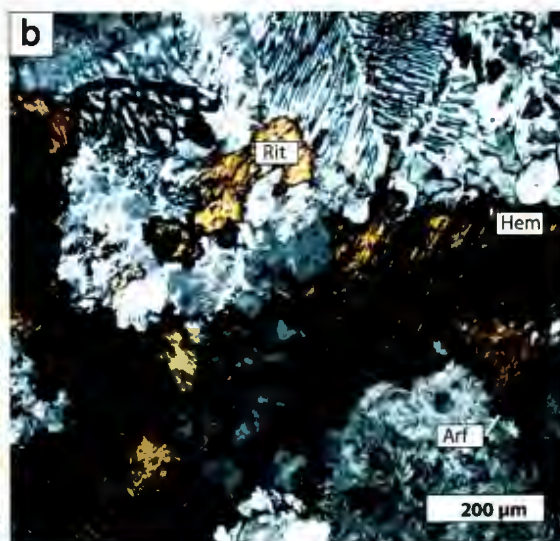
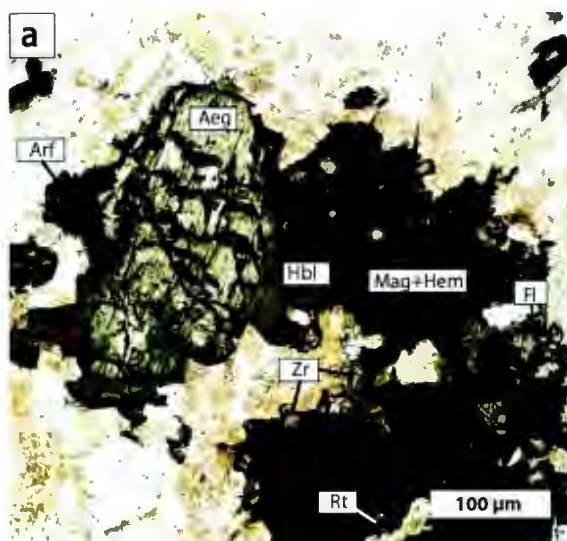


Figure 0.4: Thin section photomicrographs of regional alteration and mineralogy from dominant lithologies of the TIS. **(a)** Amphibole-clinopyroxene granite displays aegirine-augite grains with rims of hornblende and prismatic arfvedsonite overgrowths. Magnetite and hematite filled cavities contain marginal inclusions of zircon, rutile, monazite, fluorite and arfvedsonite (plane polarized light). **(b)** Granophyric groundmass of quartz and alkali-feldspar in amphibole-clinopyroxene granite. Interstitial richterite and replaced by hematite and associated with arfvedsonite, magnetite, rutile and monazite (cross-polarized light). **(c)** Green amphibole occur in the quartz-feldspar porphyry as poikilitic to subhedral masses and disseminated, fine-grained acicular crystals throughout the groundmass. Alkali feldspar phenocrysts are perthitic and show variable hematite dusting (plane polarized light). **(d)** A fabric is defined in the groundmass of a quartz-feldspar porphyry by aligned crystals that wrap around quartz phenocrysts. A xenocryst in the right of the image is preferentially altered to sericite, carbonate and hematite. Biotite filled fractures parallel the fabric (cross-polarized light). **(e)** Flow banded rhyolite showing clusters of magnetite, chlorite and clay parallel to banding and local biotite, sericite and hematite altered perlitic fractures (plane polarized light). **(f)** Strongly granophyric, mineralized felsic dyke with green interstitial hedenbergite that hosts local carbonate, Fe-Ti oxides, monazite and fluorite (cross-polarized light).

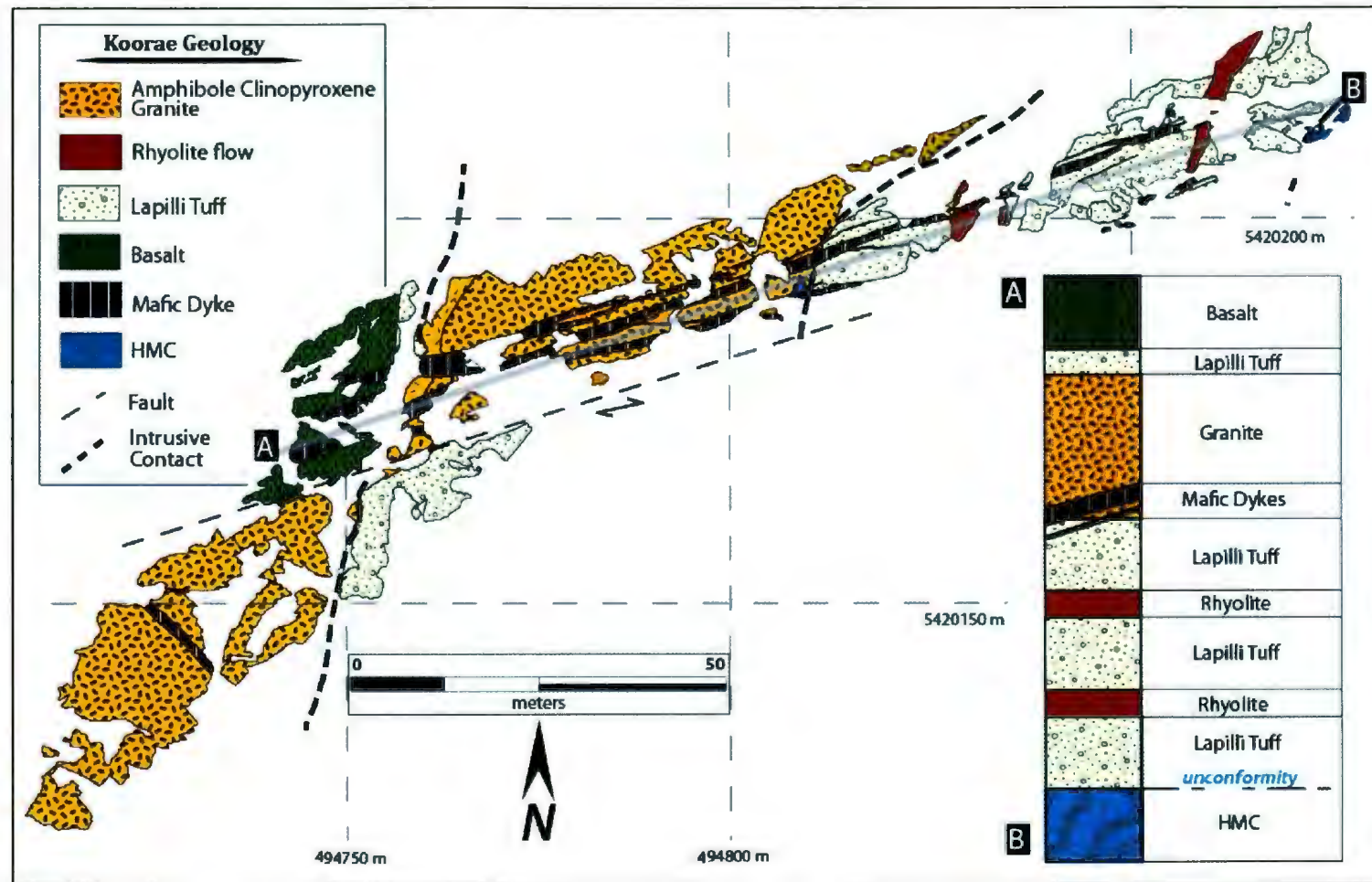


Figure 0.5: Geological map of the Koorae Prospect. Intrusive contacts of the amphibole-clinopyroxene granite are marked with heavy dashed lines, whereas the fault zone is marked by a light dashed line. The stratigraphic column is a schematic representation from point A to B highlighted by the grey transparent line.

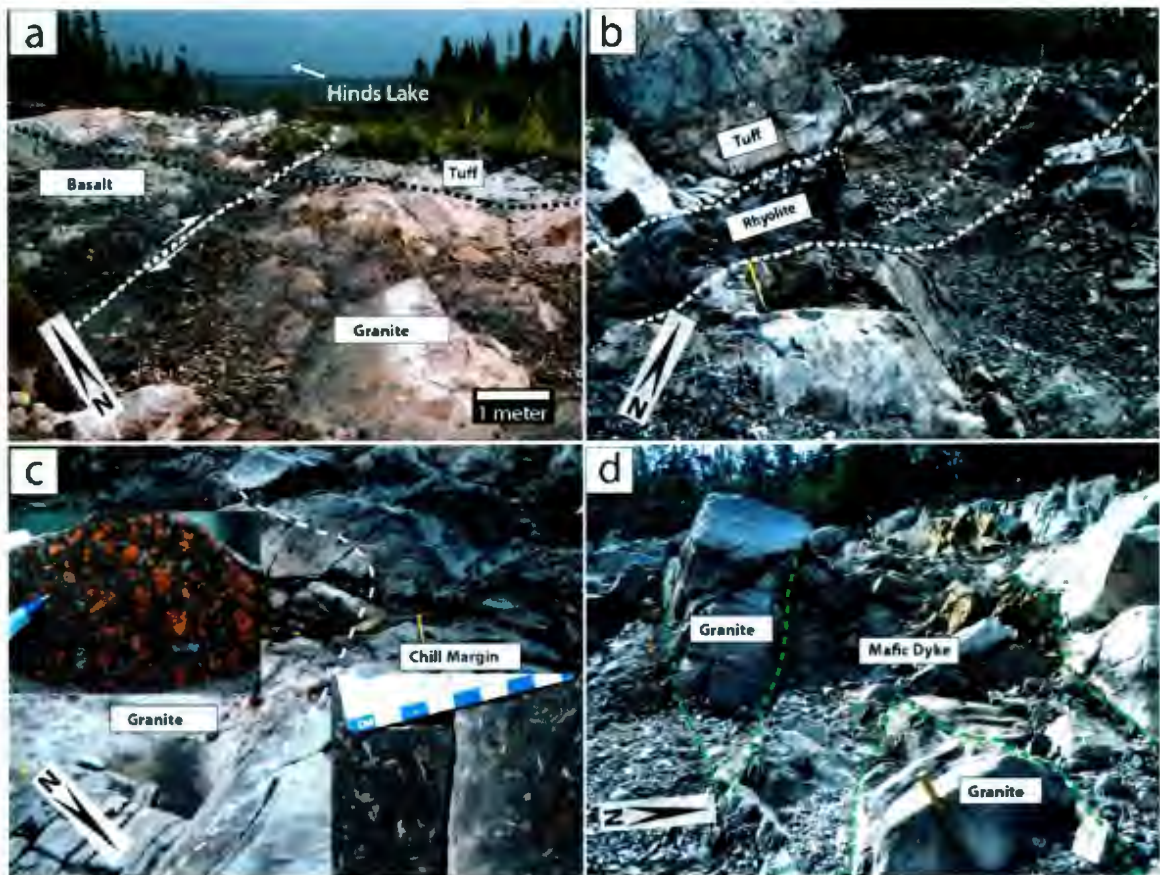


Figure 0.6: Outcrop photos from the Koorae Prospect. **(a)** Host marginal amphibole-clinopyroxene granite porphyry of the Koorae Prospect showing dextral faulting along the white dashed line offsetting the volcanic stratigraphy. Black dashed lines represent the contact between granite, tuff and basalt. **(b)** Conformable contact between the flow-banded rhyolite and tuff in the eastern end of the trench. **(c)** Chilled margin of the granite intrusion against a lapilli tuff with hand sample images showing the change in texture. **(d)** Mafic dykes intrude the granite porphyry isolating local blocks of granite.

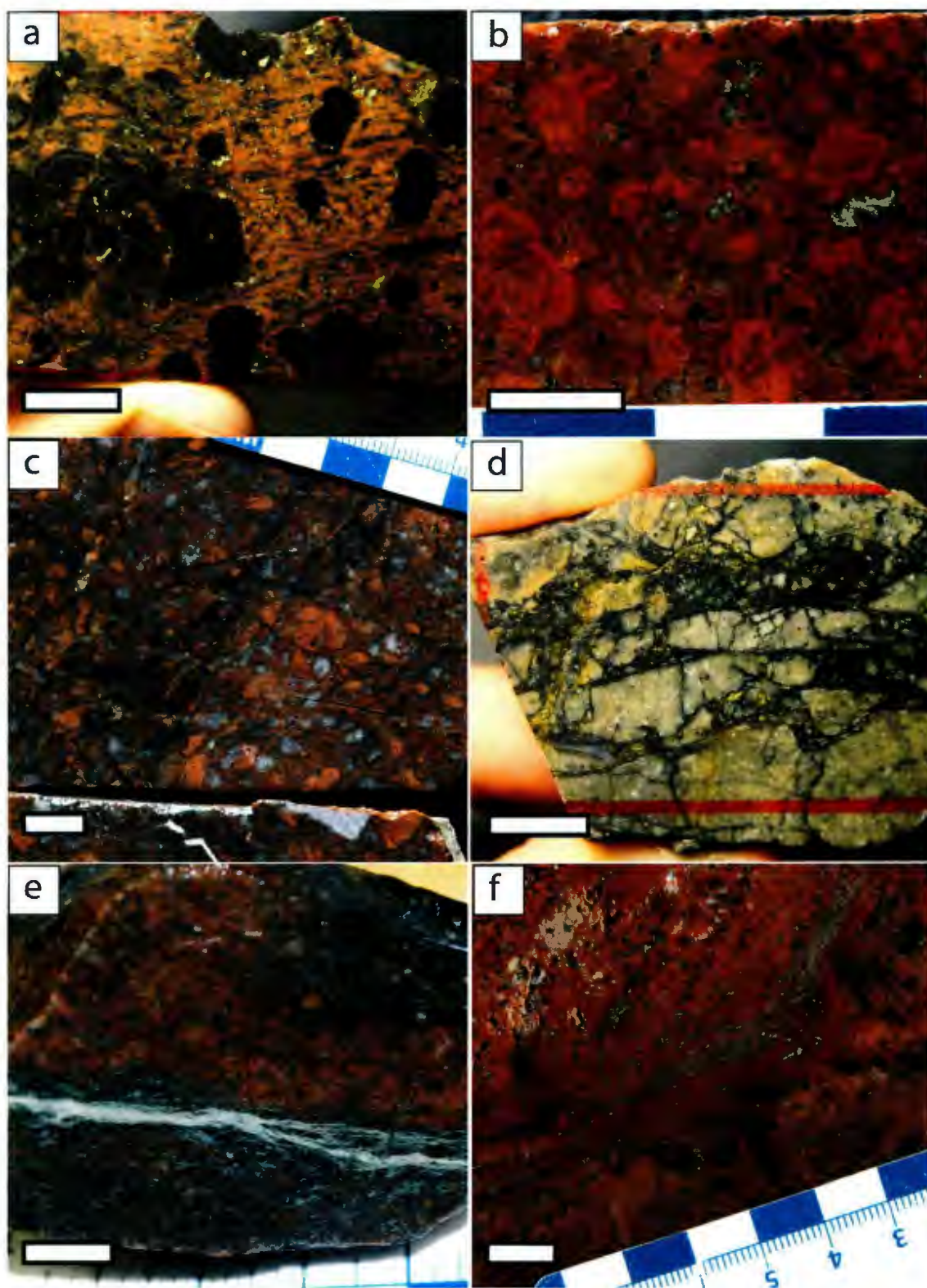


Figure 0.7: Hand specimens of mineralized units from the Koorae Prospect. Scale bar is 1 cm. **(a)** Spherulitic rhyolite showing chalcopyrite hosted in quartz-filled perlitic fractures, banding and around spherulites. **(b)** Strongly hematized amphibole-clinopyroxene granite porphyry with chalcopyrite hosted in miarolitic quartz cavities. **(c)** Brecciated amphibole-clinopyroxene granite near a fault zone showing alteration by chlorite, carbonate and quartz with minor chalcopyrite disseminated and in veinlets. **(d)** Brecciated tuff with abundant copper sulfides hosted in chloritic breccias. **(e)** Deformed and altered granodiorite of the Hungry Mountain Complex sampled from a fault zone. Sericite alteration is parallel to the deformation and hosts minor chalcopyrite. **(f)** Strongly hematized and potassic-altered rhyolite margin hosting abundant disseminated chalcopyrite.

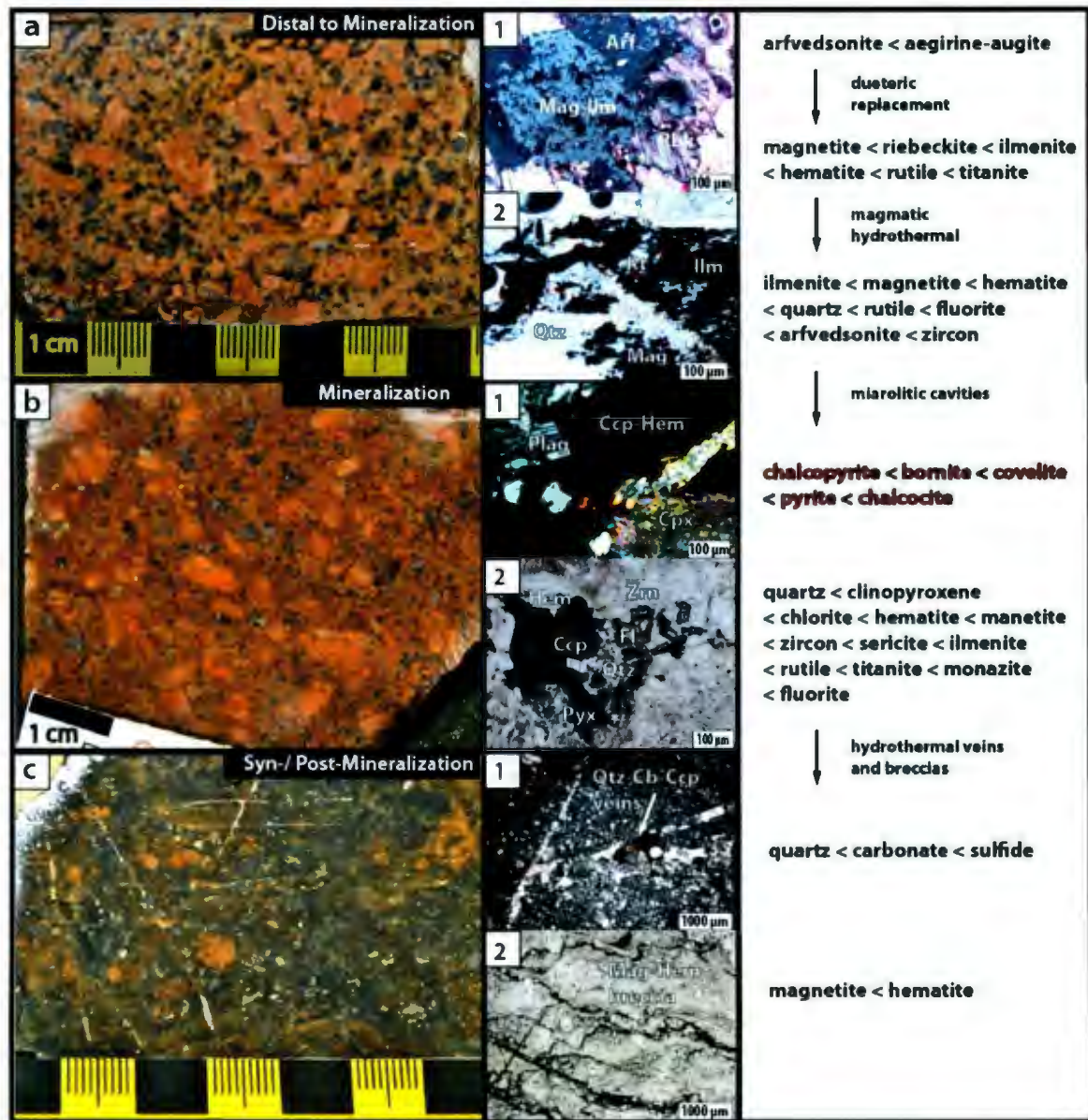


Figure 0.8: Hand sample and photomicrographs representing the paragenetic sequence of Cu-Mo-Ag-Au hosted amphibole-clinopyroxene granite between outcrops distal to mineralization (a, a1 and a2), mineralized outcrops (b, b1 and b2), and secondary syn- to post-mineralization (c, c1 and c2). **(a)** Hand sample of non-mineralized granite showing weakly porphyritic texture and more common amphibole. **(a1)** Deuteric replacement of arfvedonite and aegirine-augite by magnetite, riebeckite, ilmenite, hematite, rutile and titanite. **(a2)** Complete replacement of amphiboles and increased interstitial quartz and Fe-Ti oxides. **(b)** Mineralized porphyritic granite with interstitial to miarolitic copper sulfides and Fe-Ti oxides. **(b1)** Miarolitic cavity hosting chalcopyrite with hematite rims, among clinopyroxene and plagioclase. **(b2)** Interstitial quartz hosting euhedral zircon crystals among fluorite, clinopyroxene, chalcopyrite and hematite. **(c)** Brecciated host granite showing increased magnetite, hematite and chlorite alteration associated with

copper sulfides and crosscut by white quartz-carbonate veins. **(c1)** Quartz-carbonate veins hosting minor chalcopyrite. **(c2)** Magnetite- and hematite-filled fractures and microbreccias.

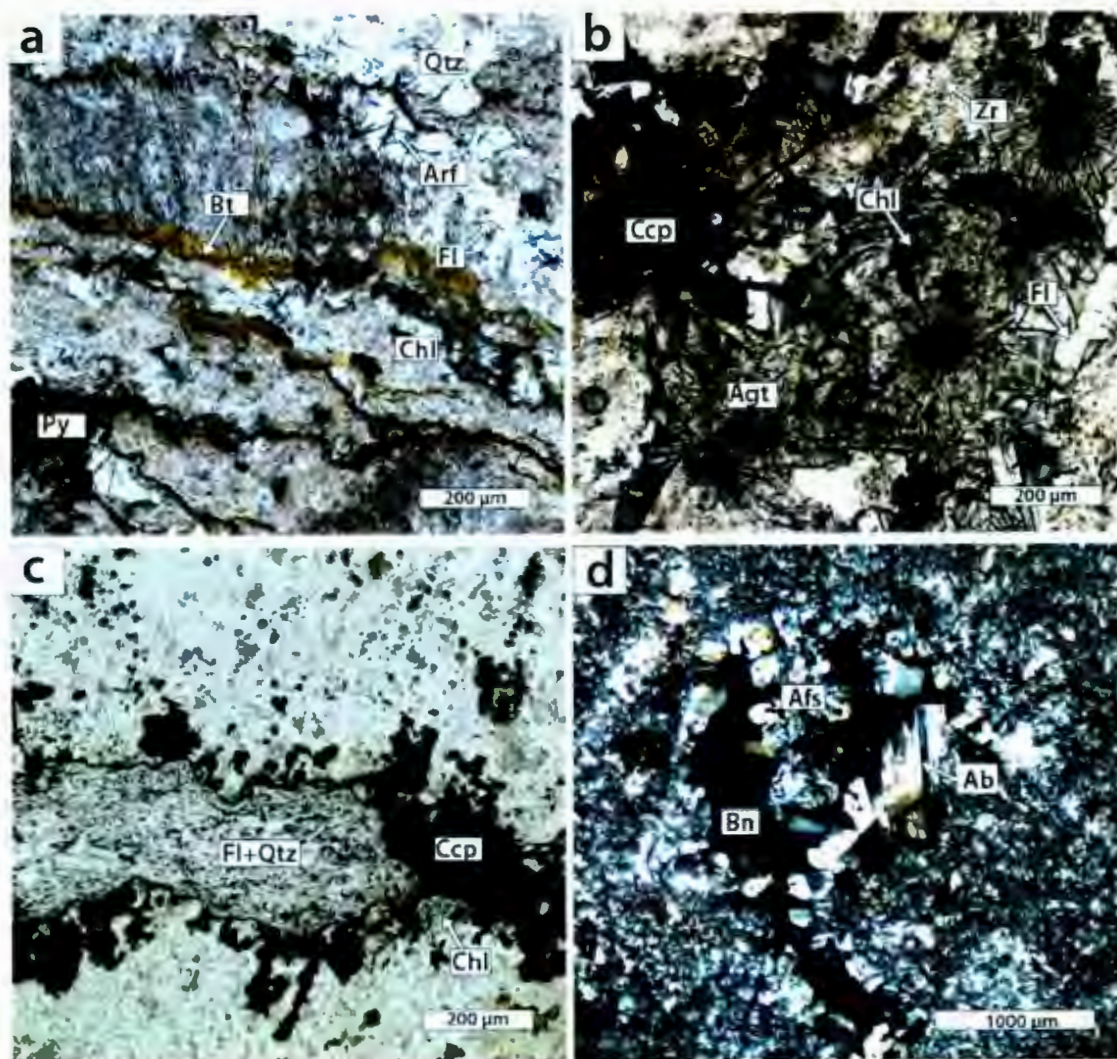


Figure 0.9: Thin section photomicrographs of volcanic host rocks from the Koorae Prospect showing typical alteration associated with Cu-Mo-Ag-Au mineralization. (a) Rhyolite flow hosting quartz, chlorite, arfvedsonite in synvolcanic cavities and biotite and pyrite in perlitic fractures. (b) Strongly hematized rhyolite flow margins with interstitial chalcopyrite, chlorite, quartz and fluorite to radiating aegirine-augite crystals. (c) Mineralized tuff breccia hosting chalcopyrite in quartz, chlorite, fluorite veins and disseminations in alkali feldspar. (d) Mineralized lapilli tuff with bornite, albite and alkali-feldspar in perlitic cavities.

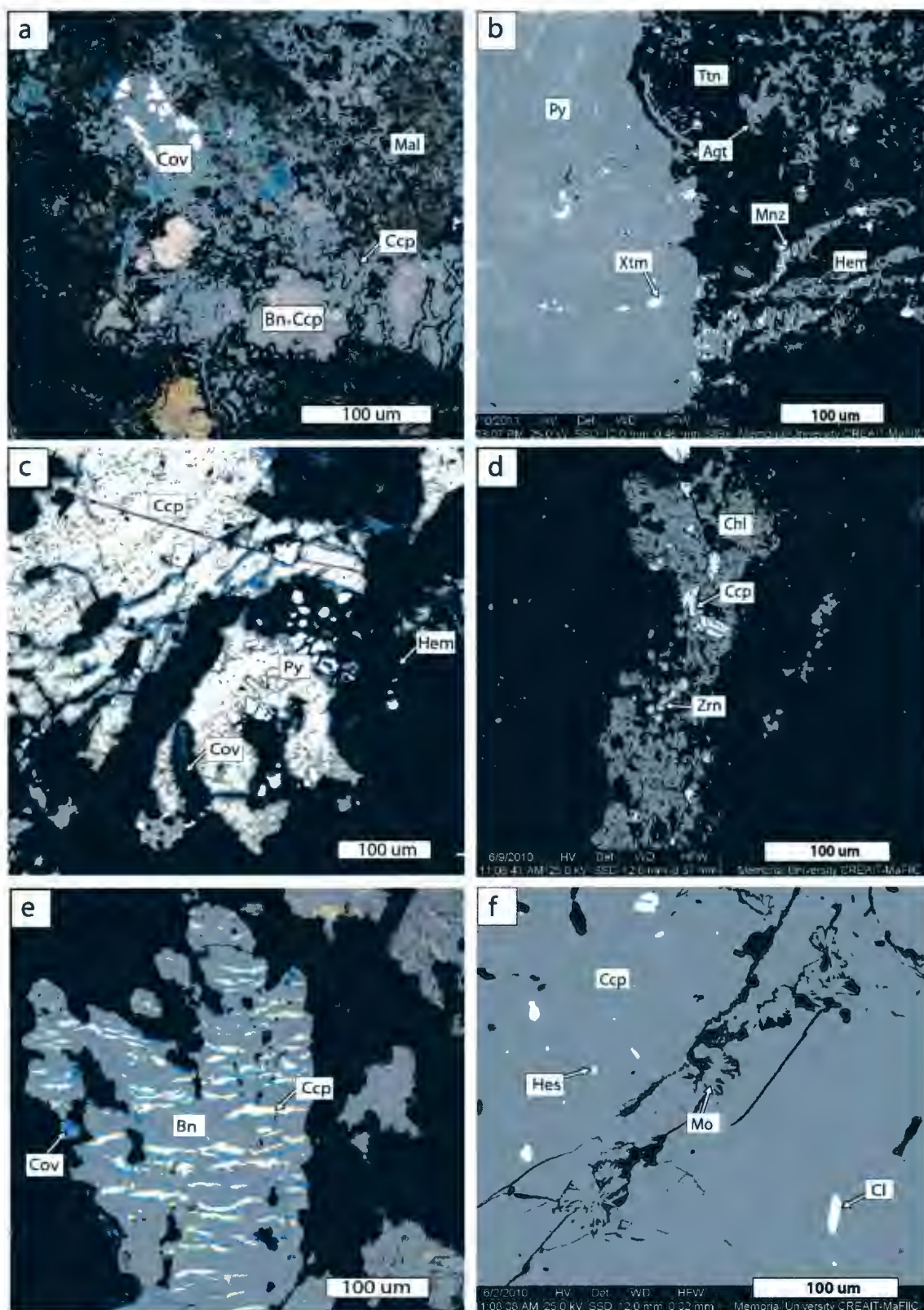


Figure 0.10: Reflected light and scanning electron microscope (SEM) images of mineralized host rocks from the Koorae Prospect. **(a)** Sulfides in the amphibole-clinopyroxene granite show covellite replacement of bornite and minor chalcopyrite associated with secondary malachite. **(b)** Secondary monazite and hematite replace aegirine-augite and titanite in fractures and cavities of amphibole-clinopyroxene granite. Fractured pyrite grain margins also host secondary xenotime. **(c)** Chalcopyrite mineralization in hematized rhyolite flow margins show secondary covellite, pyrite and hematite on rims and fractures. **(d)** Chlorite alteration in rhyolite hosts chalcopyrite and rounded zircon inclusions. **(e)** Distinct sulfide exsolution texture of chalcopyrite in bornite with covellite rims. The sulfide assemblage occurs in the matrix of a hydrothermal breccia in lapilli tuff. **(f)** SEM image of chalcopyrite containing clausthalite and hessite inclusions as well as fibrous molybdenite in fractures. The sulfide assemblage occurs in the matrix of a hydrothermal breccia in lapilli tuff.

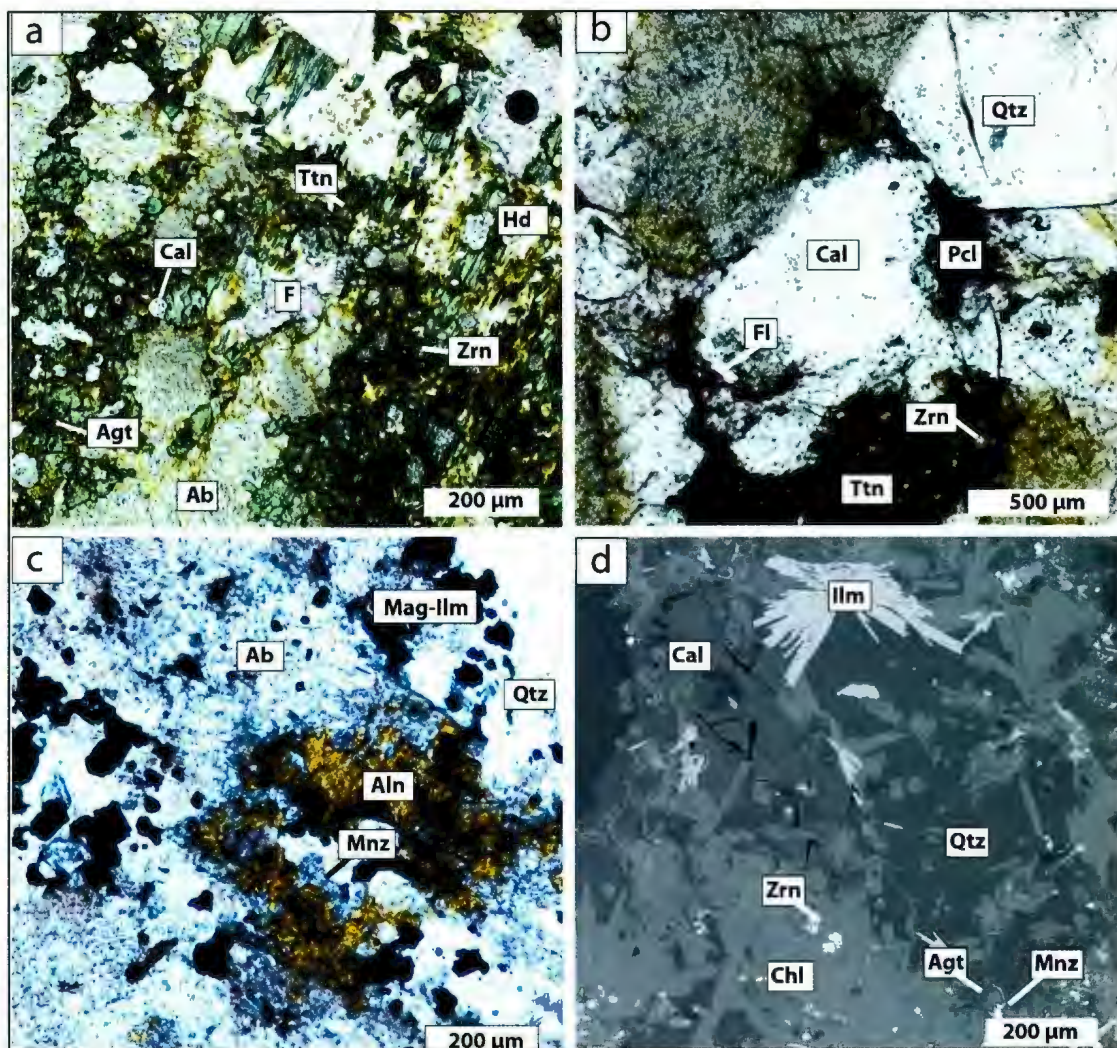


Figure 0.11: Mineralogy and alteration associated with U and REE mineralization in felsic dykes and granite. **(a)** Uranium-bearing marginal granite hosting poikilitic, light-green aegirine augite with inclusions of calcite, titanite, quartz, fluorite and zircon as well as secondary fine-grained, brown hedenbergite. **(b)** Interstitial calcite, uanpyrochlore, fluorite zircon and titanite hosted in uranium bearing amphibole granite. **(c)** Mineralized granitic dyke hosting allanite and monazite in interstitial quartz cavities associated with magnetite and ilmenite. **(d)** Strongly altered U-REE bearing pegmatitic dyke hosting monazite and zircon in an alteration assemblage of chlorite, calcite, ilmenite and quartz. Fine grained aegirine-augite grains show rims of monazite.

Table 0.3: Summary of U, Th, REE and Zr concentrations in mineralized felsic dykes and granite. Prospects are labeled accordingly.

Sample #	Lithology	U (ppm)	Th (ppm)	LREE (ppm)	HREE (ppm)	Zr (ppm)
3179	Granitic vein (LRMb)	26.00	98.00	1370.70	419.50	3241.80
3546	Granitic dyke (LRMb)	54.00	164.00	3311.00	1311.80	8879.00
4343	Pegmatitic veins (LRMa)	50.10	265.00	6545.60	2849.60	6202.20
3028	Aplitic dyke	78.60	208.00	260.80	389.80	2291.00
3234	Marginal granite	49.50	80.00	318.60	577.00	2210.10
3521	Granitic dyke	39.20	122.00	2747.50	1228.40	9012.30
3018	Amphibole granite (Railway)	40.90	12.00	127.20	125.00	703.50

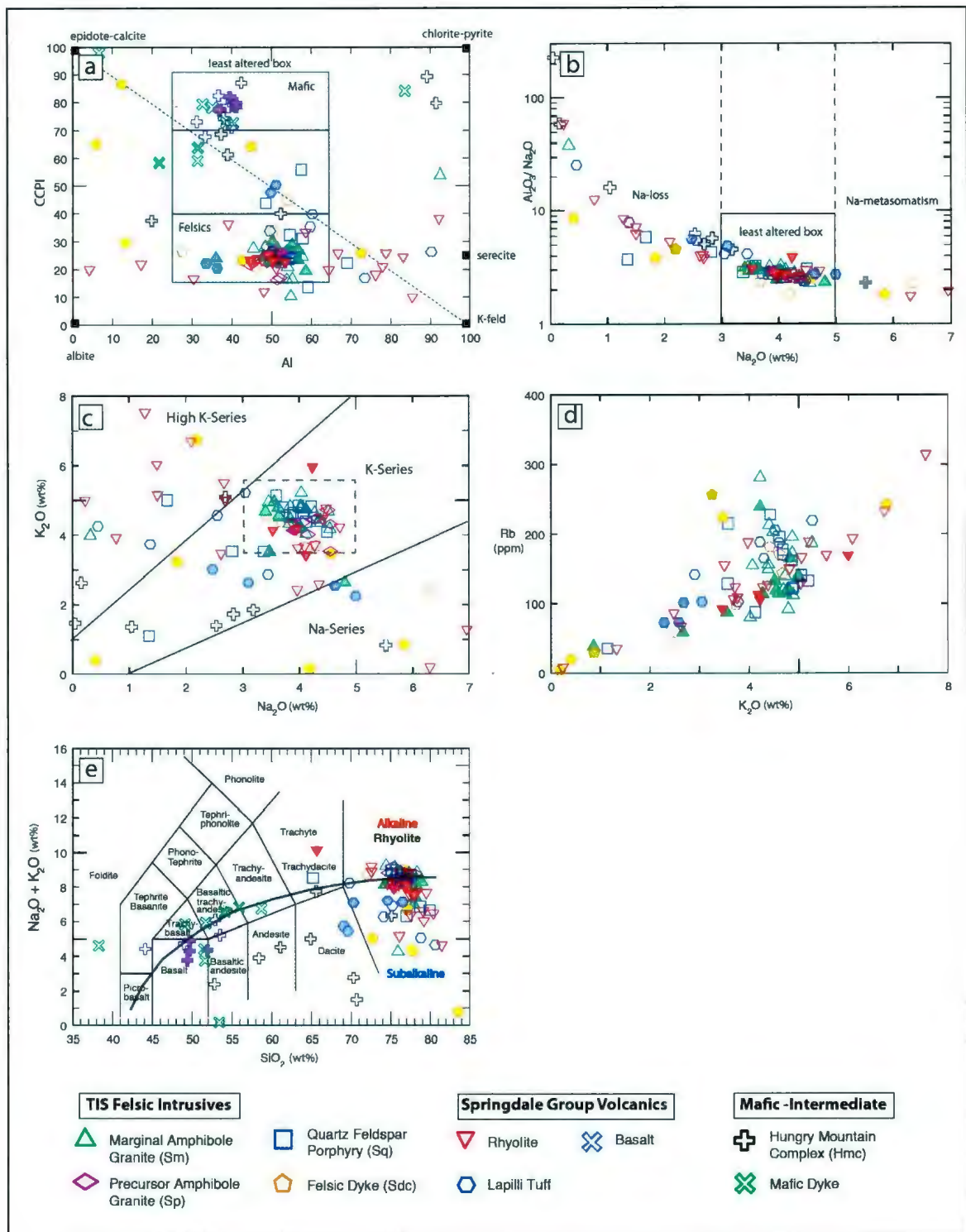


Figure 0.12: Major element discrimination diagrams for the TIS, Springdale Group volcanic rocks and mafic to intermediate rocks. Samples from The Koorae Prospect and mineralized felsic dykes (filled symbols) are differentiated from regional samples (open symbols). **(a)** AI-CCPI alteration box plot diagram for least altered samples of the TIS region (Large et al., 2001). **(b)** $\text{Al}_2\text{O}_3/\text{Na}_2\text{O}-\text{Na}_2\text{O}$ plot showing alteration causing Na-loss outside the field of least altered samples. **(c)** $\text{K}_2\text{O}-\text{Na}_2\text{O}$ plot from Middlemost (1975) classifying the TIS as K-series, alkalic magmas. **(d)** K_2O vs Rb shows the positive correlation between increased K_2O and Rb from K-feldspar-sericite alteration. Unaltered granites in the middle of the diagram display increasing Rb, with decreasing K_2O suggesting fractionation of feldspar. **(e)** Total alkali vs silica (TAS) diagram (LeBas et al., 1986) classifying the majority of the TIS and Springdale Group volcanic rocks as high silica, weakly alkaline to sub-alkaline rhyolites. Samples of the Hungry Mountain Complex show the most heterogeneity from basaltic-andesite to rhyolite. The dividing line between alkaline and sub-alkaline magma series is from Miyashiro (1978).

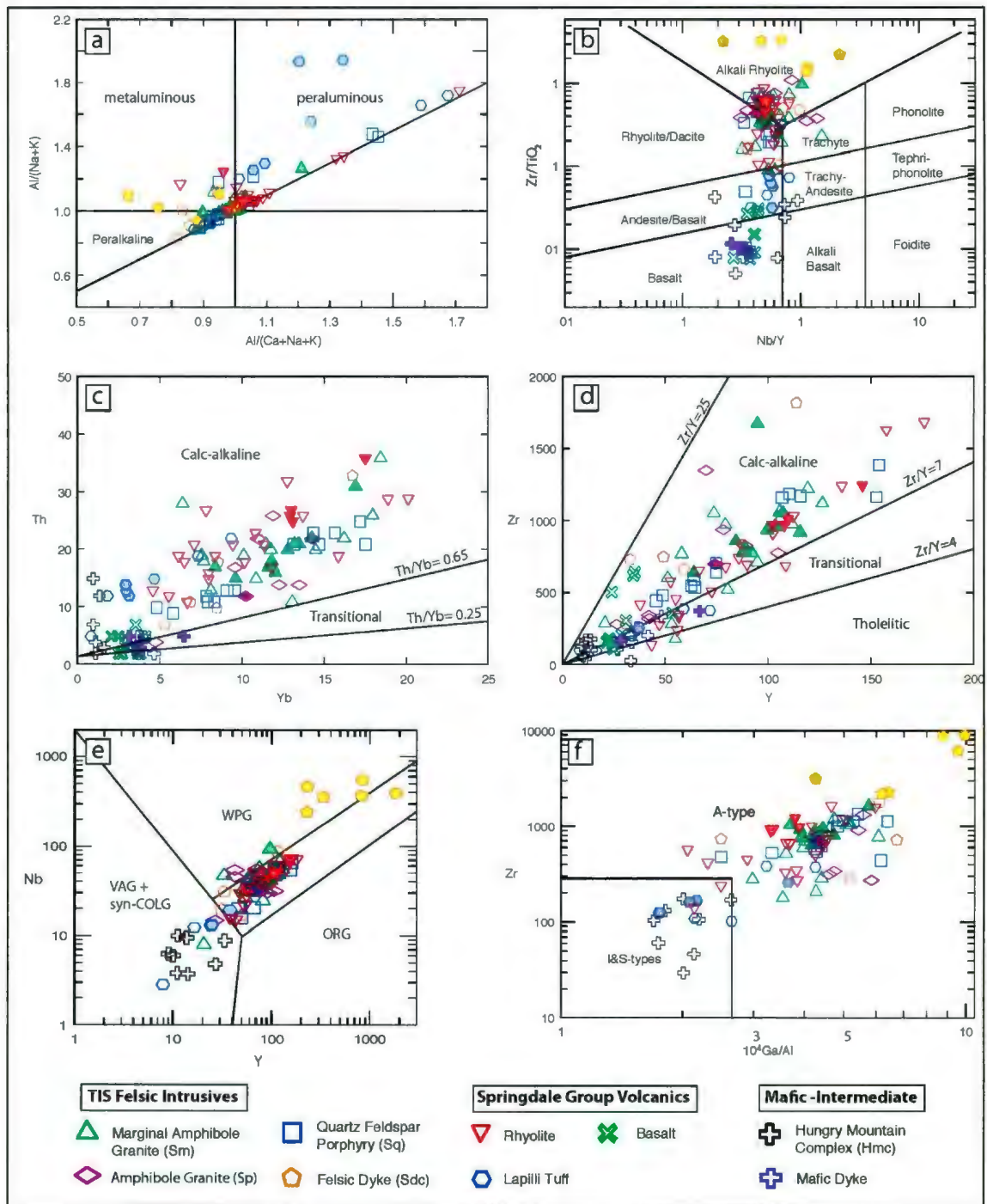


Figure 0.13: Trace element discrimination diagrams for the TIS, Springdale Group and mafic to intermediate rocks using the same symbol key as the previous diagram. **(a)** The Shand's index uses the aigpatic index [$AI = \text{molecular Al}/(\text{molecular Na} + \text{K})$] and alumina saturation index [$ASI = \text{molecular Al}/(\text{molecular Ca} + \text{Na} + \text{K})$] to classify the TIS and associated rocks as peralkaline to weakly metaluminous and peraluminous (Frost et al., 2001). **(b)** A revised Winchester and Floyd (1977; Pearce 1996) diagram uses Nb/Y vs. Zr/TiO_2 to classify the TIS and associated rocks as mostly alkali rhyolite to subalkaline rhyolite/dacite. **(c)** Immobile element pairs Th vs. Yb show the correlation of TIS and associated rocks samples in the calc-alkaline field ($Th/Yb > 0.65$). **(d)** Immobile element pairs Zr vs. Y correlate between samples of the TIS and associated rocks in the calc-alkaline field. **(e)** The Y vs. Nb plot (Pearce et al., 1984) classify the TIS and Springdale Group volcanic rocks as within plate granite (WPG), whereas the Hungry Mountain Complex plots in the volcanic arc (VAG) and syn-collisional granite (COLG) field. **(f)** Ga/Al against Zr can discriminate A-type granites from other I- and S-type granites (Whalen et al., 1987).

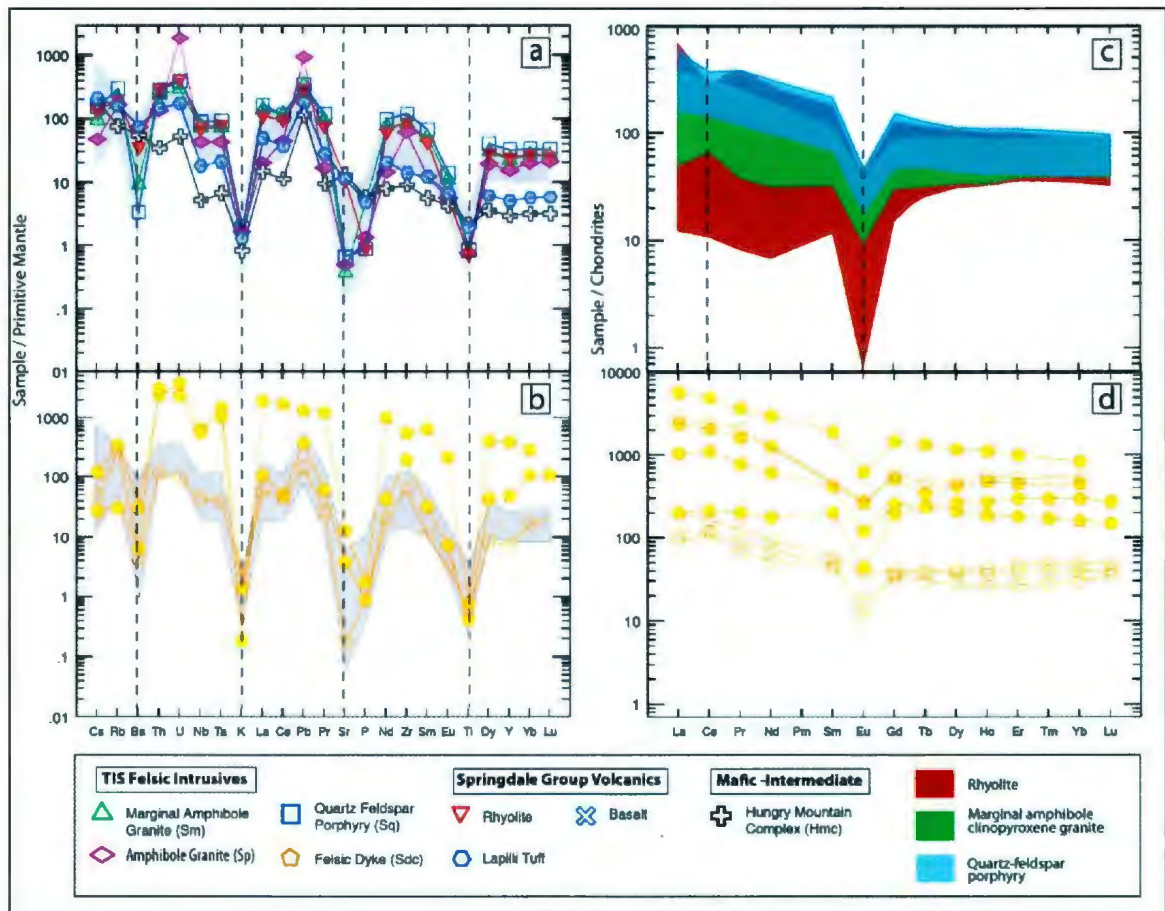


Figure 0.14: Primitive mantle normalized multi-element plots compare regional signatures of TIS granitic rocks (shaded) to (a) mineralized samples from The Koorae Prospect and a U mineralized amphibole granite from the Railway showing and (b) mineralized felsic dykes. Two types of mineralized felsic dykes show different patterns but similar enrichments in Th, U, Nb and Ta. Negative anomalies in Ba, K, Sr, P and Ti are marked by dashed lines and are common in most felsic samples. (c) Chondrite normalized REE plots (Sun and McDonough, 1989) compare the range of signatures seen in amphibole-clinopyroxene granite, quartz-feldspar porphyries and the Springdale Group rhyolite. All units are marked by strong negative Eu anomalies. Positive Ce anomalies are associated with decreased HREE in host amphibole-clinopyroxene granite at the Koorae Prospect while negative Ce anomalies in some rhyolite show enriched HREE. The rhyolite samples show a broad range of LREE to MREE signatures resulting from alteration. Quartz-feldspar porphyry samples show slightly elevated LREE compared to amphibole-clinopyroxene granite. (d) Chondrite-normalized REE patterns (Sun and McDonough, 1989) for late felsic dykes showing strong REE enrichments in mineralized samples compared to non mineralized samples. All samples show slight negative sloping patterns and negative Eu anomalies.

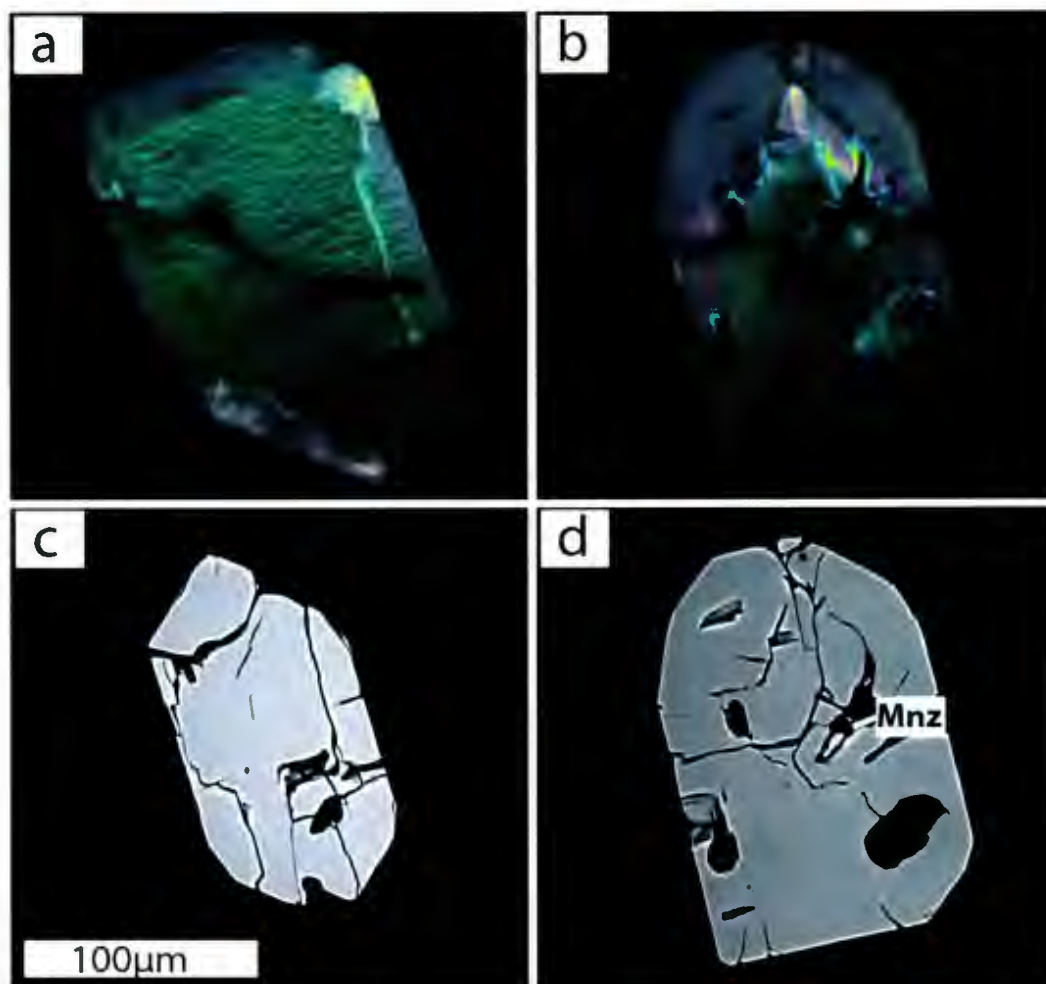


Figure 0.15: Zircons separated from mineralized rhyolite, imaged using cathode luminescence (CL; a,b) and backscatter (c,d) from SEM. The scale provided corresponds to all images.

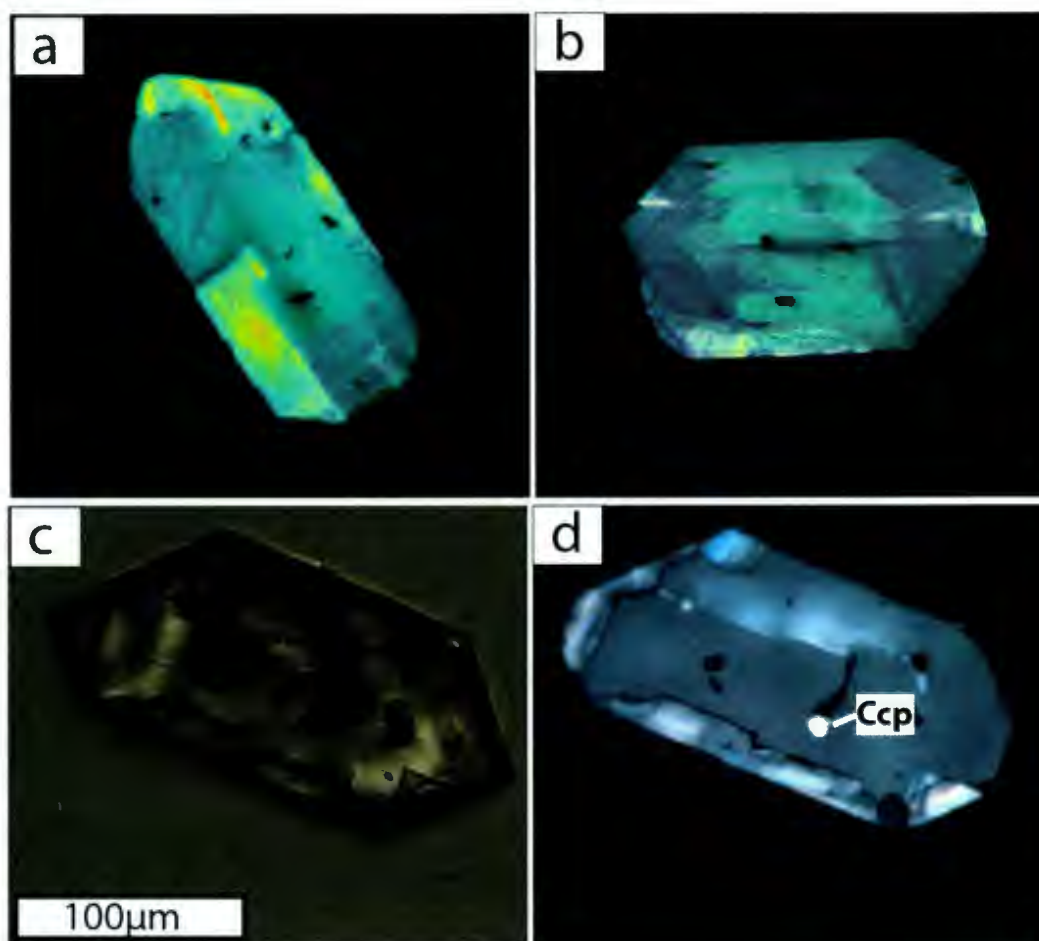


Figure 0.16: Zircons separated from mineralized granite, imaged using cathode luminescence (CL; a,b) and petrographic microscope using transmitted light (c) and reflected light (d). The scale provided corresponds to all images.

Fraction	Weight (mg) ^a	Concentration		Measured		Corrected Atomic Ratios ^c						Age (Ma)				
		U	Pb rad ^b	Pb total common	206 Pb/ 204 Pb	208Pb/ 206 Pb	206Pb/ 238U	±	207Pb/ 235U	±	207Pb/ 206Pb	±	206/ 238U	207Pb/ 235U	207Pb/ 206Pb	
GRANITE																
Z1 5 clr euh prms	0.0012	545	40.1	6.5	4347	0.1800	0.06908	54	0.5285	40	0.05549	22	431	431	432	
Z2 3 med clr euh prm	0.004	410	30.2	2.0	4039	0.1845	0.06901	38	0.5271	30	0.05540	24	430	430	428	
Z3 3 med clr euh prm	0.004	493	36.7	14.0	683	0.2000	0.06886	38	0.5252	46	0.05532	40	429	429	425	
RHYOLITE																
Z1 4 clr euh prm	0.006	1406	101.8	4.0	9177	0.1648	0.06898	64	0.5262	46	0.05532	14	430	429	425	
Z2 4 clr euh prm	0.006	771	55.9	2.4	8190	0.1752	0.06853	40	0.5246	28	0.05552	18	427	428	433	
Z3 3 clr euh prm	0.004	470	34.2	1.7	5510	0.1747	0.06864	48	0.5244	34	0.05540	18	428	428	429	
Notes; All minerals were chemically abraded (CA-TIMS, Mattinson 2005) prior to dissolution. Z=zircon; 3,4,5= number of grains in the analysis; prms= prism, clr= clear, euh=euhedral, med= medium																
a. weights of grains were estimated, with potential uncertainties of 25-50% for small samples.																
b. radiogenic lead																
c. Atomic ratios corrected for fractionation, spike, laboratory blank of 2 picograms (pg) common lead, and initial common lead at the age of the sample calculated from the model of Stacey and Kramers (1975), and 0.3 pg U blank. Two sigma uncertainties are reported after the ratios and refer to the final digits.																

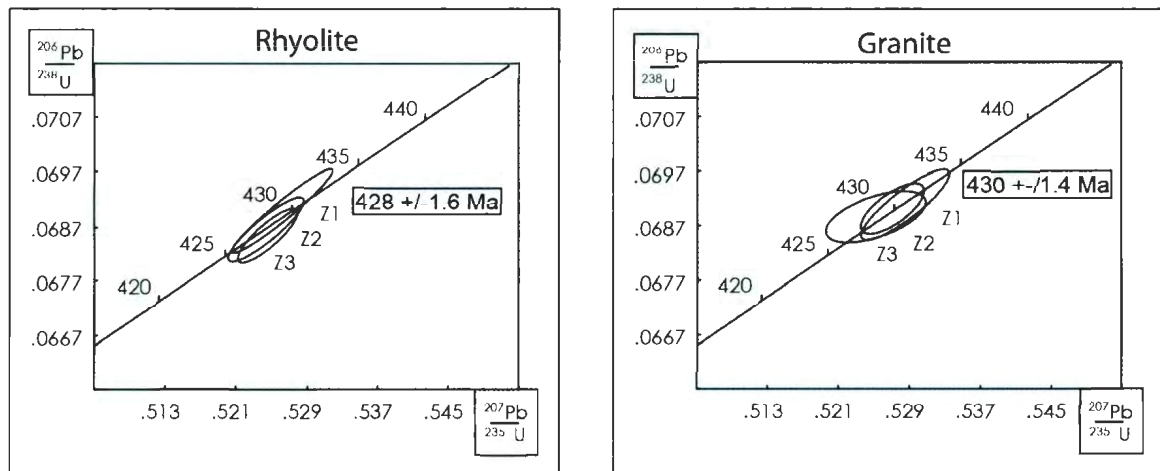


Figure 0.17: Concordia plots for zircons analyzed from the Koorae Prospect rhyolite (left) and mineralized amphibole-clinopyroxene granite (right). Three zircon fractions were analyzed by TIMS for each rock type and are shown in Figs. 2.15 and 2.16. Samples provide a concordant age of 428 ± 1.6 Ma and 430 ± 1.4 Ma for rhyolite and granite, respectively. The ages are also highlighted on each plot.

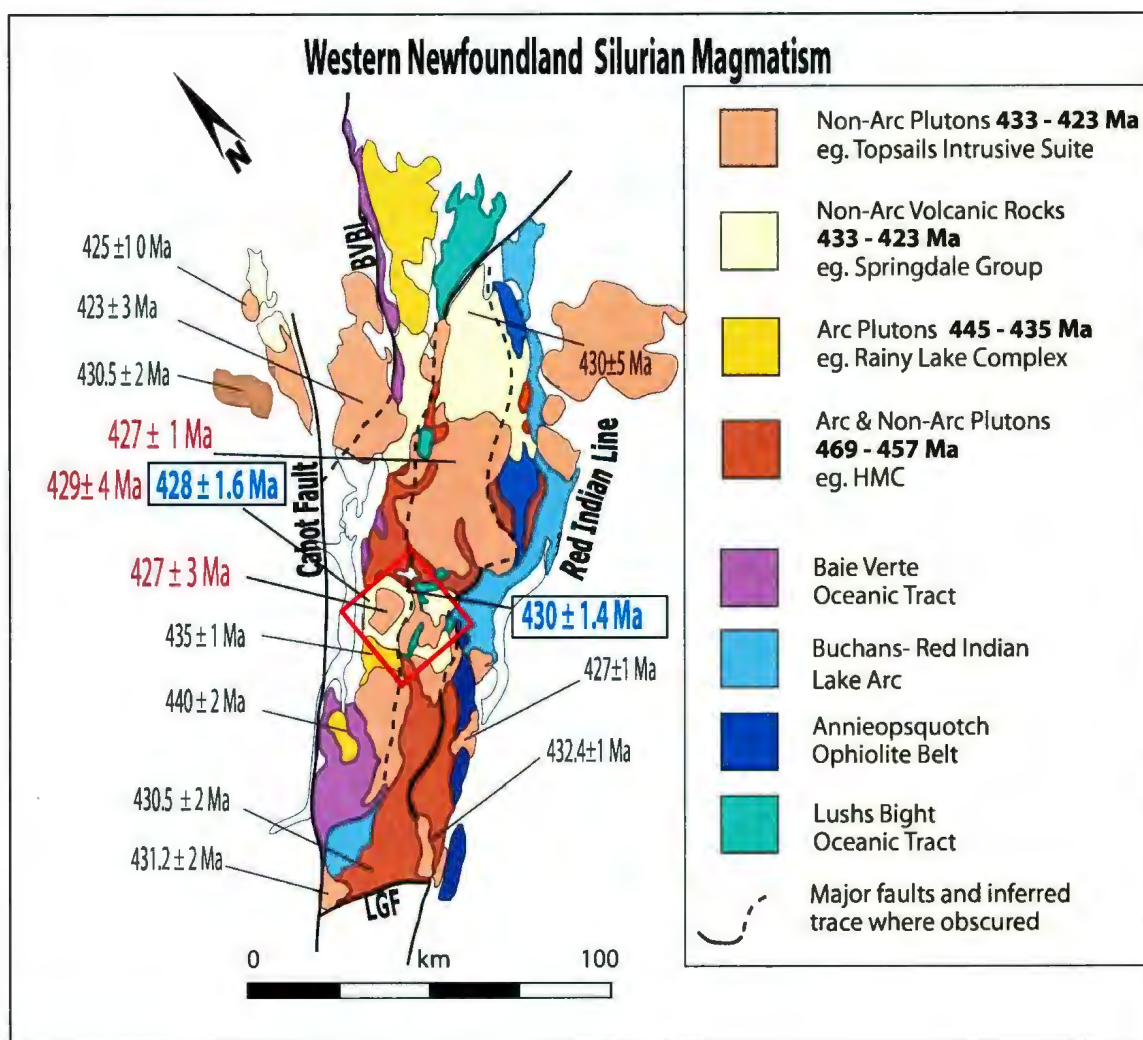


Figure 0.18: Regional map of the Notre Dame subzone highlighting the age of Silurian non-arc magmatism. Ages of the TIS are highlighted in red (Whalen et al., 1987b, 2006) and blue (this report). The map area under investigation in this manuscript is highlighted in the red box. An outline of Newfoundland is seen as a semi-transparent grey line. Modified from van Staal (2005) and Whalen et al. (2006).

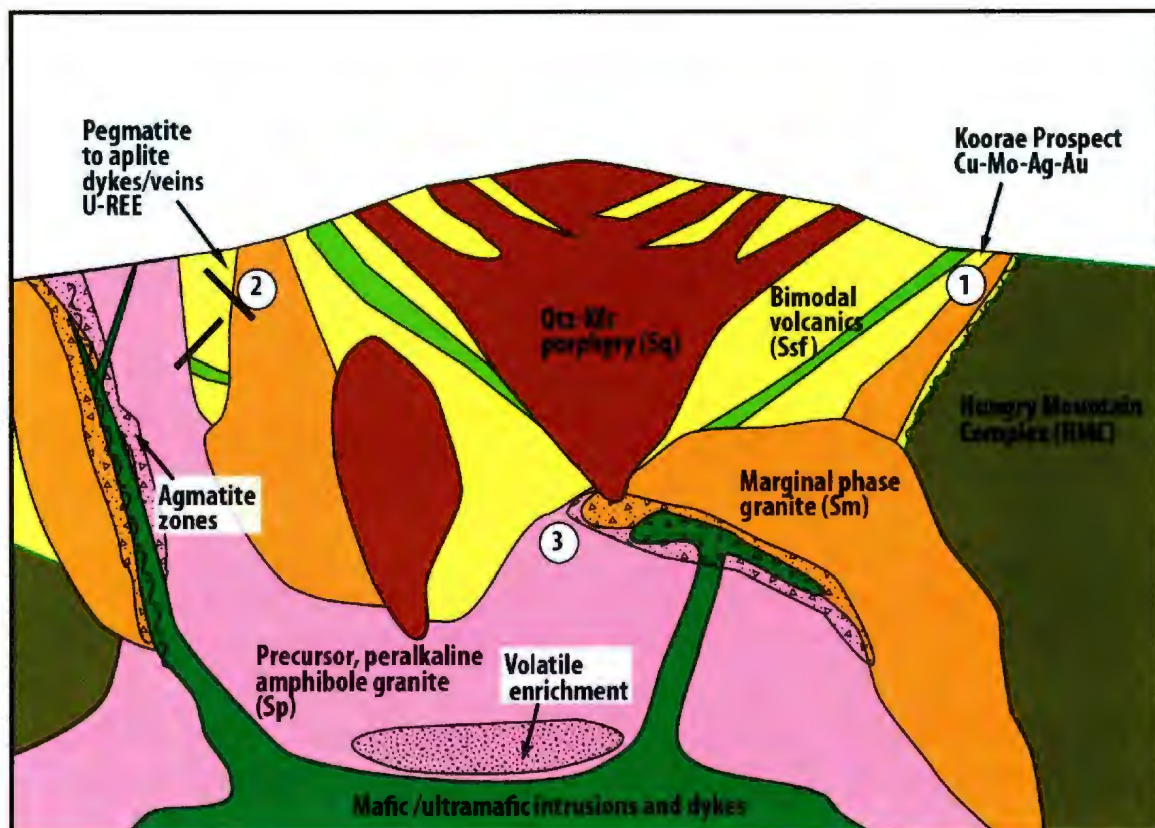


Figure 0.19: A schematic diagram illustrating the principal geological components and environments of the TIS in the Hinds Lake area. (1) The Koorae prospect Cu-Mo-Ag-Au mineralization hosted in a sill-like amphibole-clinopyroxene granite intruding the Springdale Group near a faulted unconformity with the Hungry Mountain Complex. (2) U-REE hosted pegmatite to aplite dykes (LRMa and LRMb) and veins that crosscut the youngest units of the TIS. (3) Uranium hosted in local peralkaline granite (Railway) near the margins of the intrusions.

Table 0.5: Ore deposit models analogous to Cu-Mo-Ag-Au and U-REE mineralization in the TIS and Springdale group describing the resource, tectonic setting, geology, geochemistry, alteration, and mineralization style for IOCG and peralkaline U-REE deposits. Source of information for IOCG is from Groves and Vielreicher (2001), Williams et al. (2005) and McPhie et al. (2011) while those for peralkaline U-REE are from Schonenberger et al. (2008).

	IOCG (Olympic Dam-type)	Peralkaline U-REE
Deposit	Olympic Dam of South Australia, Gawler Craton (2 Bt @ 1.6wt% Cu, 3.5 g/t Ag, 0.6 g/t Au, 0.6 kg/t U ₃ O ₈ ; Goad et al., 2000)	Ilimaussaq of South Greenland (~861 Mt @ 270 ppm U ₃ O ₈ , 1.07% TREO; www.ggg.gl)
Tectonic Setting	Post-orogenic, crustal scale fault zones, craton edges, bimodal mafic magmatism, largely undeformed	Intracratonic riftin, large scale melting of asthenospheric mantle, Extreme fractionatio.
Geological Attributes	Gawler SLIP (salicic large igneous province), A-type granites, igneous-volcanic hosted, post mineral mafic dyke swarms	Alkaline or peralkaline melts, roof zone region, late phase magmatism.
Geochemistry	low Ti Fe-oxides associated, F- and REE-rich, low S sulfides,	Silica undersaturated, LREE/HREE, U and Th increase with fractionation, while Be, Zr, Cl, F, Zn, W are independent.
Alteration	Hematite, magnetite, sericite, carbonate, low Ti Fe-oxides, iron silicates	Texturally late aegirine and sodic-amphibole including arfvedsonite.
Mineralization Style	magmatic-hydrothermal, hematite breccias, chalcopyrite-pyrite (deep), chalcocite-bornite (shallow), U-oxides	Alkali granite to Lujavrite (nephline syenite), magmatic layering 3-50 meters, veins and pegmatites.

Chapter 3: Summary and Direction for Future Research

3.1 KEY CONCLUSIONS

The TIS and Springdale Group near Hinds Lake, west-central Newfoundland consist of numerous marginal granite intrusions, hypabyssal quartz-feldspar porphyry and coeval volcanic rocks that are host to magmatic-hydrothermal Cu-Mo-Ag-Au mineralization at the Koorae Prospect. In addition, U-REE mineralization in felsic dykes is also present. The Cu-Mo-Ag-Au mineralization is hosted in older peralkaline amphibole-clinopyroxene granite, whereas the U-REE is associated with later fractionated felsic dykes.

The Koorae Cu-Mo-Ag-Au Prospect is the most significant occurrence in the TIS and provides an age of magmatic-hydrothermal mineralization between 430 ± 1.4 Ma (host granite) and 428 ± 1.8 Ma (host rhyolite). Key results from this study regarding the Koorae Prospect include:

1. Host rocks include marginal amphibole-clinopyroxene granite, rhyolitic flows, and lapilli tuff proximal to the basement unconformity with the HMC. The granite intrudes parallel to the volcanic stratigraphy. Rhyolite flow margins are preferentially mineralized and altered. The lapilli tuff is mostly barren, whereas breccias are the most strongly mineralized of all units.
2. The amphibole-clinopyroxene granite is strongly granophyric and porphyritic. Arfvedsonite and aegirine-augite are replaced by Cu sulfides in miarolitic cavities and is cogenetic with magnetite, hematite, aegirine-augite, fluorite and zircon. Sulfides include chalcopyrite, bornite, pyrite, chalcocite, molybdenite and

covellite. Silver and Au mineralization are hosted by hessite and clausthalite inclusions. Quartz, chlorite, fluorite, aegirine-augite and hematite are associated with the Cu and REE mineralization and hydrothermal alteration.

3. The geochemistry of igneous-volcanic rocks is high silica, alkalic to calc-alkaline with A-type and WPG signatures. They have high Ga/Al, Zr, Nb, Y and REE (except Eu) typical of peralkaline rocks of the TIS. Igneous rocks are weakly altered compared to volcanic rocks and all show significant mobility of HFSE, Rb, Ba and Sr. Mineralized igneous rocks correlate with a lack of amphiboles, whereas non-mineralized samples contain amphiboles.

The second and younger style of mineralization in the TIS is U-REE bearing felsic dykes that crosscut the quartz-feldspar porphyry suggesting that it is younger or equivalent to 427 ± 3 Ma (Whalen et al., 1987b). Key results from this study regarding the late U-REE-bearing dykes include:

1. Host rocks to U-REE include aplite to pegmatitic dykes, whereas U-Th is hosted in marginal phase granite and peralkaline amphibole granite. Dykes are structurally controlled near intrusive contacts and often parallel to northeast trending faults and fractures. Uranium-Th is commonly isolated near granite contacts.
2. The mineralogy of felsic dykes is variable from fresh clinopyroxene alkali feldspar granite to altered, quartz-rich pegmatite and aplite. Uranium-REE is associated with enriched accessory minerals including monazite- (La, Ce), allanite- (La), zircon, thorite and uranpyrochlore. The U and REE phases are

hosted in: primary interstitial calcic clinopyroxene, quartz, carbonate, titanite and fluorite of unaltered granitic dykes; magmatic quartz, magnetite, ilmenite and titanite of altered aplite dykes; and magmatic-hydrothermal quartz, carbonate, chlorite, ilmenite and calcic pyroxene alteration of pegmatite veins.

3. Geochemistry of felsic dykes is alkaline to calc-alkaline with A-type and WPG signatures. There is strong variability of alkalis resulting from silica and potassic alteration. The dykes are enriched U, Th, Nb, Y, Zr and REE (except Eu) and have high Ga/Al, Nb/Y, Zr/TiO₂ ratios and depletions of Ba, K, Sr, P and Ti. Ratios of U/Th and Zr/Y suggest they are from a common source.

3.2 POTENTIAL DIRECTION FOR FUTURE RESEARCH

This study has established a relationship between Cu-Mo-Ag-Au and U-REE mineralization within the geological framework and igneous petrogenesis/temporal framework of the TIS and Springdale Group. Detailed mapping, investigation of mineral paragenesis, analytical geochemistry and geochronology has demonstrated that the TIS and Springdale Group are a potential setting for IOCG-type and peralkaline U-REE mineralization. Further scientific research should address the following issues to provide a more robust regional geological and metallogenic framework of the TIS and Springdale Group to apply to further research and exploration for mineralization.

Geochronology of the TIS is limited and many ages are overlapping, thus preventing accurate interpretation of intrusive events and the longevity of A-type magmatism. Further geochronology is required of the amphibole granite in the central portion of the complex and the number of marginal phase granites, quartz-feldspar

porphyries and felsic dykes to provide a more concrete temporal framework. An accurate age of late stage granitic to pegmatitic dykes should provide an upper age limit of the TIS and a better understanding of the extent of igneous fractionation and host rocks to U-REE mineralization.

This research focused on peralkaline igneous and hypabyssal intrusions of the TIS and did not include other non-peralkaline marginal phase granites. A better understanding of the mineralogical and geochemical affects of mixing between peralkaline and non-peralkaline melts may provide insight into their affects on metal transport and deposition. Evidence from the Koorae Prospect suggest that Cu-Mo-Ag-Au mineralization is not limited to peralkaline rocks and suggests that similar potential might exist in peraluminous to metaluminous granites. Other units that were not the subject of this study and have received little documentation regarding their alteration and mineralization include the Rainy Lake Complex and the Hungry Mountain Complex. Local occurrences of hydrothermal pyrite and chalcopyrite in the HMC indicate that intermediate rocks also provide suitable hosts for sulfide mineralization especially near unconformable contacts and regional faults.

Regional faults and unconformities in the Hinds Lake Area are poorly defined and may provide a strong influence on resurgent igneous intrusions, hydrothermal alteration and mineralization. The orientation of the host amphibole-clinopyroxene granite at the Koorae Prospect, suggest a structural influence within the volcanic stratigraphy. Regional felsic and mafic dykes also appear to follow a northeast orientation similar to a regional inferred fault (Fig. 2.2). Other important structures that are poorly defined include the

Silurian-Ordovician unconformity separating the TIS and Springdale Group from the older HMC and Buchans Group. It has been documented that these unconformities are fault modified and given that alteration and mineralization is preferentially hosted in these zones, further mapping is needed to define them. Additional structures include a potential collapse caldera in the Springdale Group surrounding a composite quartz-feldspar porphyry and requires further delineation of the volcanic stratigraphy and alteration zones. Further detailed mapping in the TIS should also focus on igneous intrusive contacts as these areas may provide the best understanding of the nature of emplacement and are more likely to host mineralized felsic dykes and hydrothermal alteration.

Clinopyroxene and amphibole are associated with both Cu-Mo-Ag-Au and U-REE mineralization and thus identifying their major and trace element geochemistry may help understand their influence on mineralization with regard to metal transport and REE complexing with fluorine and chlorine. Microprobe analysis of amphibole and clinopyroxene in host rocks may identify trace element zoning or trends to be applied as geochemical vectors to fertile host rocks. Fluid inclusion data from quartz associated with various stages of mineralization may also provide important information regarding the salinity of fluids as well as pressure and temperature conditions during mineralization.

REFERENCES

- Adam, J., Green, T. H., and Sie, S. H., 1993, Proton microprobe determined partitioning of Rb, Sr, Ba, Y, Nb, and Ta between experimentally produced amphiboles and silicate melts with variable F content: *Chemical Geology*, v. 109, p. 29-49.
- Armbrust, G.A., Oyarzún, M.J., and Arias, J., 1977, Rubidium as a guide to ore in Chilean porphyry copper deposits: *Economic Geology*, v. 72, p. 1086-1100.
- Barrett, T.J., and MacLean, W.H., 1994, Chemostratigraphy and hydrothermal alteration in exploration for VHMS deposits in greenstones and younger volcanic rocks, *in* Lentz, D.R., ed., *Alteration and alteration processes associated with ore-forming systems*, Short Course Notes - Geological Association of Canada, v. 11, p. 433-467.
- Barrett, T.J., and MacLean, W.H., 1999, Volcanic sequences, lithogeochemistry, and hydrothermal alteration in some bimodal volcanic-associated massive sulfide systems: *Reviews in Economic Geology*, v. 8, p. 101-131.
- Bonin, B., Grelou-Orsini, C., and Vialette, Y., 1978, Age, origin and evolution of the anorogenic complex of Evisa (Corsica): A K-Li-Rb-Sr study: *Contributions to Mineralogy and Petrology*, v. 65, p. 425-432.
- Burnham, O.M., and Schweyer, J., 2004, Trace element analysis of geological samples by inductively coupled plasma mass spectrometry at the Geoscience Laboratories; revised capabilities due to improvements to instrumentation, *in* Baker, C.L., Debicki, E.J., Parker, J.R., Kelly, R.I., Ayer, J.A., and Easton, R.M., eds., *Summary of field work and other activities 2004: Open File Report – Ontario Geological Survey* p. 54.1-54.5.
- Case, G., and Zagorevski, A., 2009, Volcanic red bed copper mineralization in the Hinds Lake area, central Newfoundland: Current Research (2009) Newfoundland and Labrador Department of Natural Resources Geological Survey, Report 09-1, p. 131-146.
- Cawood, P.A., Dunning, G.R., Lux, D., and van Gool, J.A.M., 1994, Timing of peak metamorphism and deformation along the Appalachian margin of Laurentia in Newfoundland: Silurian, not Ordovician: *Geology*, v. 22, p. 399-402.
- Collerson, K.D., 1982, Geochemistry and rubidium-strontium geochronology of associated Proterozoic peralkaline and subalkaline anorogenic granites from Labrador: *Contributions to Mineralogy and Petrology*, v. 81, p. 126-147.
- Collins, W., Beams, S., White, A., and Chappell, B., 1982, Nature and origin of A-type granites with particular reference to southeastern Australia: *Contributions to Mineralogy and Petrology*, v. 80, p. 189-200.
- Coyle, M., and Strong, D.F., 1987, Geology of the Springdale Group - a newly recognized Silurian epicontinental-type caldera in Newfoundland: *Canadian Journal of Earth Sciences*, v. 24, p. 1135-1148.

- Dahlquist, J. A., Alasino, P. H., et al., 2010, Fault controlled Carboniferous A-type magmatism in the proto-Andean foreland (Sierras Pampeanas, Argentina): Geochemical constraints and petrogenesis. *Lithos* v. 115, p. 65-81.
- Dilles, J. A., and Gans, P. B., 1995, The chronology of Cenozoic volcanism and deformation in the Yerington area, western Basin and Range and Walker Lane: Geological Society of America (GSA), v. 107, p. 474-486
- Dunning, G.R., 1987, Geology of the Annieopsquotch Complex, southeast Newfoundland: *Canadian Journal of Earth Sciences*, v. 24, p. 1162-1174
- Dunning, G.R., O'Brien, S.J., Colman-Sadd, S.P., Blackwood, R.F., Dickson, W.L., O'Neill, P.P., and Krogh, T.E., 1990, Silurian Orogeny in the Newfoundland Appalachians: *Journal of Geology*, v. 98, p. 895-913
- Eby, G.N., 1990, The A-type granitoids: A review of their occurrence and chemical characteristics and speculations on their petrogenesis: *Lithos*, v. 26, p. 115-134.
- Frost, B.R., Barnes, C.G., Collins, W.J., Arculus, R.J., Ellis, D.J., and Frost, C.D., 2001, A geochemical classification for granitic rocks: *Journal of Petrology*, v. 42, p. 2033-2048.
- Goad, R.E., Mumin, A.H., Duke, N.A., Neale, K.L., and Camier, W.J., The NICO and Sue-Dianne Proterozoic, Iron Oxide-hosted, Polymetallic Deposits, Northwest Territories: Application of the Olympic Dam Model in Exploration, Exploration and Mining Geology, v. 9, p. 123-140.
- Groves, D.I., and Vielreicher, N.M., 2001, The Phalabowra (Palabora) carbonatite-hosted magnetite-copper sulfide deposit, South Africa: An end-member of the iron-oxide copper-gold-rare earth element deposit group?: *Mineralium Deposita*, v. 36, p. 189-194.
- Groves, D.I., Bierlein, F.P., Meinert, L.D., and Hitzman, M.W., 2010, Iron oxide copper-gold (IOCG) deposits through earth history: Implications for origin, lithospheric setting, and distinction from other epigenetic iron oxide deposits: *Economic Geology*, v. 105, p. 641-654.
- Hezarkhani, A., Williams-Jones, A.E., and Gammons, C.H., 1999, Factors controlling copper solubility and chalcopyrite deposition in the Sungun porphyry copper deposit, Iran: *Mineralium Deposita*, v. 34, p. 770-783.
- Ike, E.C., Bowden, P., and Martin, R.F., 1985, Amphibole in the porphyries of the Tibchi anorogenic ring-complex, Nigeria: Product of deuteritic adjustments: *Canadian Mineralogist*, v. 23, p. 447-456.
- Jenner, G.A., 1996, Trace element geochemistry of igneous rocks: geochemical nomenclature and analytical geochemistry: Geological Association of Canada Short Course Notes, v. 12, p. 51-77

- Krogh, T.E., 1973, A low-contamination method for hydrothermal decomposition of zircon and extraction of U and Pb for isotopic age determinations: *Geochimica et Cosmochimica Acta*, v. 37, p. 485-494.
- Large, R.R., McPhie, J., Gemmell, J.B., Herrmann, W., and Davidson, G.J., 2001, The spectrum of ore deposit types, volcanic environments, alteration halos, and related exploration vectors in submarine volcanic successions: Some examples from Australia: *Economic Geology*, v. 96, p. 913-938.
- Le Bas, M.J., Le Maitre, R.W., Streckeisen, A., and Zanettin, B.A., 1986, Chemical classification of volcanic rocks based on the total alkali-silica diagram: *Journal of Petrology*, v. 27, p. 745-750.
- Linnen, R.L., and Cuney M., 2005, Granite related rare-element deposits and experimental constraints on Ta-Nb-W-Sn-Zr-Hf mineralization, *in* Linnen, R.L., and Cuney, M., eds., *Rare-element geochemistry and mineral deposits*, Short Course Notes – Geological Association of Canada, v. 17, pp. 45-68
- Longerich, H.P., 1995, Analysis of pressed pellets of geological samples using wavelength-dispersive x-ray fluorescence spectrometry: *X-Ray Spectrometry*, v. 24, p. 123-136.
- Ludwig, K.R., 2003, User's Manual for Isoplot/Ex, Version 3.0, A geochronological toolkit for Microsoft Excel, Berkeley Geochronology Center Special Publication, v. 4, 73 p.
- Marshall, D., Anglin, C.D., and Mumin, H., 2004, Ore mineral atlas, Geological Association of Canada, Mineral Deposits Division, 112 p.
- Mattinson, J.M., 2005, Zircon U-Pb chemical abrasion ("CA-TIMS") method: Combined annealing and multi-step partial dissolution analysis for improved precision and accuracy of zircon ages: *Chemical Geology*, v. 220, p. 47-66.
- McPhie, J., Kamenetsky, V., Allen, S., Ehrig, K., Agangi, A., and Bath, A., 2011, The fluorine link between a supergiant ore deposit and a silicic large igneous province: *Geology*, v. 39, p. 1003-1006.
- Middlemost, E.A.K., 1975, The basalt clan: *Earth-Science Reviews*, v. 11, p. 337-364.
- Mitchell, R.H., 1990, A review of the compositional variation of amphiboles in alkaline plutonic complexes: *Lithos*, v. 26, p. 135-156.
- Miyashiro, A., 1978, Nature of alkalic volcanic rock series: *Contributions to Mineralogy and Petrology*, v. 66, p. 91-104.
- Newfoundland and Labrador Geological Survey, Assessment file NFLD/ 1320, Thurlow, J.G., Barbour, D., Ford, G., and Head, T., 1982, Assessment report on geological, geochemical, geophysical and diamond drilling exploration for 1981
- Pearce, J., 1996, Sources and settings of granitic rocks: *Episodes*, v. 19, p. 120-125.

- Pearce, J.A., Harris, N.B.W., and Tindle, A.G., 1984, Trace-element discrimination diagrams for the tectonic interpretation of granitic rocks: *Journal of Petrology*, v. 25, p. 956-983.
- Pupin, J.P., 1980, Zircon and granite petrology: *Contributions to Mineralogy and Petrology*, v. 73, p. 207-220.
- Schonenberger, J., Koehler, J., and Markl, G., 2008, REE systematics of fluorides, calcite and siderite in peralkaline plutonic rocks near Gardar Province, South Greenland, v. 247, p. 16-35
- Stacey, J.S., and Kramers, J.D., 1975, Approximation of terrestrial lead isotope evolution by a two-stage model: *Earth and Planetary Science Letters*, v. 26, p. 207-221.
- Strong, D.F., and Taylor, R.P., 1984, Magmatic-subsolidus and oxidation trends in composition of amphiboles from silica-saturated peralkaline igneous rocks: *Tschermaks Mineralogische und Petrographische Mitteilungen*, v. 32, p. 211-222.
- Sun, S.S., and McDonough, W.F., 1989, Chemical and isotopic systematics of oceanic basalts; implications for mantle composition and processes, *in* Saunders, A.D., and Norry, M.J., eds., *Magmatism in the ocean basins*, Geological Society Special Publications, v. 42, p. 313-345.
- Taylor, R.P., Strong, D.F., and Kean, B.F., 1980, The Topsails Igneous Complex - Silurian-Devonian peralkaline magmatism in western Newfoundland: *Canadian Journal of Earth Sciences*, v. 17, p. 425-439.
- Taylor, R.P., Strong, D.F., and Fryer, B.J., 1981, Volatile control of contrasting trace element distributions in peralkaline granitic and volcanic rocks: *Contributions to Mineralogy and Petrology*, v. 77, p. 267-271.
- Taylor, R.P., and Fryer, B.J., 1982, Rare earth element geochemistry as an aid to interpreting hydrothermal ore deposits, *in* Evans, A.M., ed., *Metallization associated with acid magmatism*, Volume 6, John Wiley & Sons, p. 357-365.
- Thurlow, J.G., 1981, The Buchans Group – its stratigraphic and structural setting, *in* Swanson, E.A., Strong, D.F., and Thurlow, J.G., eds., *The Buchans orebodies – fifty years of geology and mining*, Geological Association of Canada Special Paper, Issue 22, p. 79-89.
- van Staal, C.R., 2005, North America: Northern Appalachians, *in* Selley, R.C., Cocks, L.R.M., and Pilmer, I.R., eds., *Encyclopedia of geology*, Volume 4: Oxford, United Kingdom, Elsevier Academic Press, p. 81-92.
- van Staal, C.R., 2007, Pre-Carboniferous tectonic evolution and metalogeny of the Canadian Appalachians, *in* Goodfellow W.D., eds., *Mineral Deposits of Canada: A Synthesis of Major Deposit Types, District Metallogeny, the Evolution of Geological Provinces & Exploration Methods*: Geological Association of Canada Mineral Deposits Division Special Publication No.5, p. 793-828

- van Staal, C.R., Whalen, J.B., McNicoll, V.J., Pehrsson, S., Lissenberg, C.J., Zagorevski, A., van Breeman, O., and Jenner, G.A., 2007, The Notre Dame Arc and the Taconic Orogeny in Newfoundland, *in* Hatcher, R.D., Jr., Carlson, M.P., McBride, J.H., and Martinez Catalan, J.R., eds. 4-D framework of continental crust, Geological Society of America Memoir, Volume 200, p. 511-552.
- Whalen, J.B., 1989, The Topsails Igneous Suite, Western Newfoundland - an early Silurian subduction-related magmatic suite: *Canadian Journal of Earth Sciences*, v. 26, p. 2421-2434.
- Whalen, J. B. and B. W. Chappell (1988a). "Opaque mineralogy and mafic mineral chemistry of I- and S-type granites of the Lachlan fold belt, southeast Australia." *Am. Mineral.* **73**(Copyright (C) 2011 American Chemical Society (ACS). All{van Staal, 2007 #312} Rights Reserved.): 281-296.
- Whalen, J.B., and Currie, K.L., 1988b, Topsails igneous terrane, Newfoundland, Geological Survey of Canada, "A" Series Map
- Whalen, J.B., and Currie, K.L., 1982, Volcanic and plutonic rocks in the Rainy Lake area, Newfoundland: *Current Research, Part A, Issue 82-1A*, p. 17-22.
- Whalen, J.B., and Currie, K.L., 1983, The Topsails igneous terrane of western Newfoundland: *Geological Survey of Canada, Issue 83-1A*, p. 15-23.
- Whalen, J.B., and Currie, K.L., 1984, The Topsails igneous terrane, western Newfoundland – evidence for magma mixing: *Contributions to Mineralogy and Petrology*, v. 87, p. 319-327.
- Whalen, J.B., and Currie, K.L., 1990, The Topsails igneous suite, western Newfoundland: Fractionation and magma mixing in an "orogenic" A-type granite suite, *in* Stein, H.J., and Hannah, J.L., eds., *Ore-bearing granite systems, petrogenesis and mineralizing processes*, Geological Society of America Special Paper 246, p. 287-299.
- Whalen, J.B., Currie, K.L., and Chappell, B.W., 1987a, A-type granites: geochemical characteristics, discrimination and petrogenesis: *Contributions to Mineralogy and Petrology*, v. 95, p. 407-419.
- Whalen, J.B., Currie, K.L., and van Breeman, O., 1987b, Episodic Ordovician-Silurian plutonism in the Topsails igneous terrane, western Newfoundland: *Transactions of the Royal Society of Edinburgh: Earth Sciences*, v. 78, p. 17-28.
- Whalen, J.B., Jenner, G.A., Longstaffe, F.J., Robert, F., and Gariépy, C., 1996, Geochemical and isotopic (O, Nd, Pb and Sr) constraints on a type granite petrogenesis based on the Topsails Igneous Suite, Newfoundland Appalachians: *Journal of Petrology*, v. 37, p. 1463-1489.
- Whalen, J.B., McNicoll, V.J., van Staal, C.R., Lissenberg, C.J., Longstaffe, F.J., Jenner, G.A., and van Breeman, O., 2006, Spatial, temporal and geochemical characteristics of Silurian collision-zone magmatism, Newfoundland

- Appalachians: An example of a rapidly evolving magmatic system related to slab break-off: *Lithos*, v. 89, p. 377-404.
- White, A.J.R., and Chappell, B.W., 1983, Granitoid types and their distribution in the Lachlan Fold Belt, southeastern Australia, *in* Roddick, J.A., ed., Circum-Pacific plutonic terranes, Geological Society of America Memoir, Volume 159, p. 21-34.
- Williams, J.P., Barton, M.D., Johnson, D.A., Fontbote, L., de Haller, A., Mark., G., Oliver., N.H.S., and Marschik., R., 2005, Iron oxide copper-gold deposits: geology, space-time distribution, and possible modes of origin: *Economic Geology 100th Anniversary Volume*, p. 371-405
- Williams, H., 1979, Appalachian Orogen in Canada: *Canadian Journal of Earth Sciences*, v. 16, p. 792-807.
- Williams, H., and St. Julien, P., 1982, The Baie Verte-Brompton Line – early Paleozoic continent-ocean interface in the Canadian Appalachians, *in* St. Julien, P., and Beland, J. eds., Major structural zones and faults of the Northern Appalachians, Geological Association of Canada Special Paper, Issue 24, p. 177-207.
- Williams, H., Colman-Sadd, S.P., and Swinden, H.S., 1988, Tectonic-stratigraphic subdivisions of central Newfoundland: *Current Research*, Part B, Issue 88-1B, p. 91-98.
- Winchester, J.A., and Floyd, P.A., 1977, Geochemical discrimination of different magma series and their differentiation products using immobile elements: *Chemical Geology*, v. 20, p. 325-343.

APPENDIX A: LITHOGEOCHEMICAL ANALYTICAL METHODS, QUALITY CONTROL AND QUALITY ASSURANCE

A.1 INTRODUCTION

Samples from the TIS were collected southwest of Hinds Lake over an area approximately 20 x 30 km during field work in 2009 and 2010. Chip samples weighed approximately 5kg and were taken from surface outcrop both regionally and at the Koorae Prospect. Weathered surfaces were removed in the field or later with a diamond rotary saw. Samples were crushed using a steel jaw crusher and subsequently pulverized at Saskatchewan Research Council (SRC) in Saskatoon. Powders were subsequently analysed using a combination of inductively coupled plasma mass spectroscopy (ICP-MS), inductively coupled plasma optical emission spectroscopy (ICP-OES), and X-ray fluorescence (XRF).

Major elements (SiO_2 , Fe_2O_3 , K_2O , Al_2O_3 , Na_2O , MgO , MnO , P_2O_5 , CaO and TiO_2) were determined via a lithium metaborate fusion and an ICP-OES finish at SRC. Loss on ignition (LOI) was determined via conventional heating and weight difference methods at SRC. Trace elements were determined by ICP-MS (Ba, Be, Bi, Cd, Ce, Co, Cr, Cs, Cu, Dy, Er, Eu, Ga, Gd, Hf, Ho, In, La, Li, Lu, Mo, Nb, Nd, Ni, Pb, Pr, Rb, Sb, Sc, Sm, Sn, Sr, Ta, Tb, Th, Ti, Tl, Tm, U, V, W, Y, Yb, Zn and Zr) and were obtained via a closed vessel multi-acid (total) digestion prior to analysis and a finish by ICP-MS (Burnham and Schweyer, 2004) at the Ontario Geosciences Laboratories (OGL) in Sudbury, Ontario. There were overlimits in some of the elements above, therefore, additional data were collected. Values above the upper detection limits for Ba, Be, Ce, Cu, Hf, Nd, Sn, Th and V were substituted for by values obtained by lithium metaborate

fusion and an ICP-OES finish at SRC. For values of Zr, Nb, and Y above upper detection limits additional values were substituted for by values obtained from pressed pellet X-ray fluorescence at Memorial University using the methods of Longerich (1995).

A.2 PRECISION

Precision and accuracy was calculated using replicate analysis of a variety of known and unknown reference materials from each laboratory and analytical method. The precision and accuracy of ICP-MS at OGL was calculated using known standards AGV-2 (n=2), BHVO-2 (n=2), GSP-2 (n=2) and MRB-29 (n=6). Precisions and accuracy of ICP-OES analysis for total digestion, whole rock analysis and partial digestion at SRC used known standards AGV-2 (n=2), GSP-2 (n=1), SY-3 and internal standard G-2 and CAR 110 (n=4). Precision and accuracy for XRF analysis at MUN used AGV-1 (n=9), BCR-2 (n=8), BHVO-1 (n=34), DNC-1 (n=8), DTS-1 (n=34), JG-2 (n=3), PACS-1 (n=18) and SYS-3 (n=52).

The measure of precision is given by the percent relative standard deviation:

$$\%RSD_i = 100 \times s_i / \mu_i$$

where:

$\%RSD_i$ = percent relative standard deviation for element i

s_i = standard deviation of the mean from the series of analytical runs for element i

μ_i = mean value of element i over a series of analytical runs.

In general, %RSD values between 0 and 3% are excellent, 3 to 7% are very good, 7 to 10% are good, and above 10% are poor (e.g., Jenner 1996). In general, %RSD

increases (precision decreases) as one approaches the limit of detection (LOD) for an instrument (e.g., Jenner 1996) and should be considered for each standard. Furthermore, values that lie between the LOD and the limit of quantification ($LOQ = 3.3 \times LOD$; Jenner 1996), are also subject to poor precision; thus, %RSD values in Tables should only be considered valid for elemental concentrations above the LOQ.

Analytical error for each element calculated from replicate analysis of standards is given in Tables, and is presented as the 2σ error:

$$2 \sigma_i = 2 \times s_i / \sqrt{n}$$

where:

σ_i = standard error of the mean of analytical runs for element i

s_i = standard deviation of the mean of analytical runs for element i

n = number of measurements of element i.

The $2 \sigma_i$ value implies that if a sample was repeatedly analyzed, the value of element I in that sample will have a value between $\mu \pm 2\sigma_i$ 95% of the time (ie., 95% confidence level).

Percent relative standard deviation (%RSD) and $2\sigma_i$ errors for each analytical method are presented for reference materials analyzed at OGL (Tables A.1), SRC (Tables A.2) and MUN (Tables A.3) during this project.

A.3 ACCURACY

Accuracy was determined using reference materials with known or accepted values. Both international and internal reference materials were utilized, and internal reference materials from the GeoLabs are compared to the long term averages for said reference materials. The measure of accuracy is given the percent relative difference of the mean value of the analytical runs for an element as compared to the accepted value for the standard, and is given by:

$$\%RD = 100 \times (\mu - STD_i) / STD_i$$

where:

μ_i = mean value of element i in the standard over a number of analytical runs

STD_i = "known" or "certified" value of i in the standard or reference material

Values for %RD can be negative or positive reflecting values less than or greater than known values. In general, values of %RD values that are $\pm 0 - 3\%$ are considered to have excellent accuracy, values from ± 3 to 7% are considered to represent very good accuracy, and ± 7 to 10% good accuracy. Values above 10% should be considered indicators of poor accuracy. Accuracy is expected to decrease as the LOD is approached (e.g., Jenner 1996) and should be considered for poorly accurate results. Furthermore, values that lie between the LOD and the LOQ are also subject to poor accuracy; thus, %RD values in the following data should only be considered valid for elemental concentrations above the LOQ.

Table A.1: Precision and accuracy results for standard reference materials analyzed by ICP-MS at OGL.

	LOD	BHVO-2 Mean (n=2)	STD	%RSD	accepted	%RD	2 σ
Ba	0.8	133.08	1.15	0.86	131.00	1.59	1.62
Be	0.04	0.94	0.00	0.41	1.00	-5.85	0.01
Bi	0.15	0.01	0.00	7.86	-	-	0.00
Cd	0.013	0.12	0.00	3.20	0.06	102.50	0.01
Ce	0.12	38.52	0.04	0.11	37.50	2.72	0.06
Co	0.13	46.95	0.13	0.27	45.00	4.33	0.18
Cr	3	301.10	1.30	0.43	280.00	7.54	1.83
Cs	0.013	0.10	0.00	1.78	0.10	-0.50	0.00
Cu	1.4	133.73	3.57	2.67	127.00	5.30	5.05
Dy	0.09	5.51	0.06	1.05	5.31	3.80	0.08
Er	0.007	2.61	0.03	1.19	2.54	2.68	0.04
Eu	0.0031	2.15	0.01	0.53	2.07	3.86	0.02
Ga	0.04	19.89	0.88	4.45	22.00	-9.58	1.25
Gd	0.09	6.35	0.02	0.33	6.24	1.72	0.03
Hf	0.14	4.39	0.05	1.21	4.36	0.57	0.08
Ho	0.0025	1.01	0.00	0.03	0.98	3.32	0.00
In	0.0018	0.09	0.00	1.63	-	-	0.00
La	0.04	15.90	0.22	1.38	15.20	4.60	0.31
Li	0.4	3.94	0.28	7.14	4.80	-17.83	0.40
Lu	0.002	0.28	0.00	1.02	0.27	1.46	0.00
Mo	0.08	4.08	0.20	4.93	4.00	1.94	0.28
Nb	0.028	17.91	0.02	0.09	18.10	-1.06	0.02
Nd	0.06	25.55	0.26	1.03	24.50	4.29	0.37
Ni	1.6	125.39	0.34	0.27	119.00	5.37	0.48
Pb	0.6	1.66	0.12	7.20	1.60	3.97	0.17
Pr	0.014	5.56	0.07	1.17	5.35	3.91	0.09
Rb	0.23	9.53	0.10	1.03	9.11	4.56	0.14
Sb	0.04	0.11	0.01	5.97	-	-	0.01
Sc	1.1	32.96	0.65	1.97	32.00	2.99	0.92
Sm	0.012	6.31	0.06	0.89	6.07	4.01	0.08
Sn	0.16	1.21	0.62	51.06	1.70	-28.88	0.87
Sr	0.6	389.32	2.75	0.71	396.00	-1.69	3.90
Ta	0.023	1.14	0.00	0.40	1.14	0.13	0.01
Tb	0.0023	0.95	0.01	1.41	0.92	3.37	0.02
Th	0.018	1.24	0.03	2.05	1.22	1.72	0.04
Ti	7	15483.23	491.54	3.17	16300.00	-5.01	695.25
Tl	0.005	0.02	0.00	1.81	-	-	0.00
Tm	0.0019	0.34	0.00	1.24	-	-	0.01
U	0.011	0.43	0.01	1.64	0.40	6.95	0.01
V	0.8	323.08	9.27	2.87	-	-	13.11
W	0.05	0.25	0.00	1.15	-	-	0.00
Y	0.05	25.62	0.07	0.28	-	-	0.10
Yb	0.009	2.04	0.03	1.25	-	-	0.04
Zn	7	105.66	2.81	2.66	-	-	3.97
Zr	6	172.55	1.69	0.98	-	-	2.39

	LOD	AGV-2 Mean (n=2)	STD	%RSD	Accepted	%RD	2σ
Ba	0.8	1115.14	73.66	6.61	1130.00	-1.31	104.17
Be	0.04	1.93	0.16	8.53	2.30	-16.07	0.23
Bi	0.15	0.06	0.02	31.43	-	-	0.03
Cd	0.013	0.11	0.00	4.44	-	-	0.01
Ce	0.12	68.52	5.85	8.54	68.60	-0.12	8.27
Co	0.13	16.56	0.50	2.99	16.00	3.48	0.70
Cr	3	18.82	0.86	4.59	17.00	10.73	1.22
Cs	0.013	1.20	0.01	1.06	1.20	0.25	0.02
Cu	1.4	53.26	2.48	4.65	53.00	0.48	3.50
Dy	0.09	3.57	0.21	5.83	3.47	2.77	0.29
Er	0.007	1.84	0.07	4.00	1.81	1.55	0.10
Eu	0.0031	1.57	0.06	3.91	1.53	2.84	0.09
Ga	0.04	19.32	1.39	7.22	20.00	-3.42	1.97
Gd	0.09	4.50	0.24	5.35	4.52	-0.51	0.34
Hf	0.14	5.23	0.08	1.59	5.00	4.68	0.12
Ho	0.0025	0.66	0.03	4.90	0.65	2.15	0.05
In	0.0018	0.04	0.00	1.59	-	-	0.00
La	0.04	38.22	2.73	7.14	37.90	0.85	3.86
Li	0.4	9.42	1.69	17.97	11.00	-14.33	2.40
Lu	0.002	0.25	0.01	4.29	0.25	0.20	0.02
Mo	0.08	1.99	0.02	0.93	-	-	0.03
Nb	0.028	13.67	0.21	1.53	14.50	-5.70	0.30
Nd	0.06	31.11	2.44	7.83	30.50	2.00	3.44
Ni	1.6	19.84	0.62	3.12	20.00	-0.82	0.87
Pb	0.6	13.17	0.71	5.42	13.20	-0.19	1.01
Pr	0.014	8.20	0.48	5.89	7.84	4.65	0.68
Rb	0.23	71.12	2.14	3.01	66.30	7.27	3.03
Sb	0.04	0.47	0.03	7.19	-	-	0.05
Sc	1.1	13.17	1.75	13.27	13.00	1.32	2.47
Sm	0.012	5.69	0.35	6.17	5.49	3.55	0.50
Sn	0.16	1.91	0.50	26.14	2.30	-16.96	0.71
Sr	0.6	651.05	23.76	3.65	661.00	-1.50	33.61
Ta	0.023	0.84	0.01	0.75	0.87	-2.93	0.01
Tb	0.0023	0.63	0.03	4.51	0.64	-2.03	0.04
Th	0.018	6.19	0.03	0.51	6.10	1.43	0.05
Ti	7	5899.02	537.50	9.11	-	-	760.14
Tl	0.005	0.26	0.01	5.36	0.27	-2.22	0.02
Tm	0.0019	0.26	0.02	6.01	0.26	-0.38	0.02
U	0.011	1.97	0.06	2.95	1.86	5.70	0.08
V	0.8	117.63	3.95	3.36	122.00	-3.58	5.59
W	0.05	0.53	0.01	1.86	-	-	0.01
Y	0.05	18.94	1.42	7.51	19.00	-0.34	2.01
Yb	0.009	1.64	0.09	5.72	1.62	1.45	0.13
Zn	7	89.03	5.50	6.18	86.00	3.53	7.78
Zr	6	237.32	7.92	3.34	230.00	3.18	11.19

	LOD	GSP-2 Mean (n=2)	STD	%RSD	Accepted	%RD	2 σ
Ba	0.8	1344.51	60.94	4.53	1340.00	0.34	86.18
Be	0.04	1.33	0.03	1.91	1.50	-11.33	0.04
Bi	0.15	0.04	0.00	1.94	-	-	0.00
Cd	0.013	0.17	0.01	3.80	-	-	0.01
Ce	0.12	460.73	4.45	0.97	410.00	12.37	6.30
Co	0.13	7.54	0.01	0.17	7.30	3.27	0.02
Cr	3	22.61	0.72	3.17	20.00	13.04	1.01
Cs	0.013	1.21	0.02	1.76	-	-	0.03
Cu	1.4	45.51	2.44	5.36	43.00	5.83	3.45
Dy	0.09	6.09	0.09	1.50	6.10	-0.24	0.13
Er	0.007	2.43	0.01	0.47	2.20	10.55	0.02
Eu	0.0031	2.39	0.04	1.84	2.30	3.78	0.06
Ga	0.04	21.40	1.96	9.15	22.00	-2.74	2.77
Gd	0.09	12.12	0.14	1.16	12.00	1.04	0.20
Hf	0.14	14.11	1.14	8.06	14.00	0.79	1.61
Ho	0.0025	1.00	0.03	3.04	1.00	-0.05	0.04
In	0.0018	0.05	0.00	4.12	-	-	0.00
La	0.04	196.23	2.65	1.35	180.00	9.01	3.75
Li	0.4	31.58	6.21	19.65	36.00	-12.27	8.78
Lu	0.002	0.24	0.00	0.59	-	-	0.00
Mo	0.08	2.33	0.01	0.27	2.10	10.88	0.01
Nb	0.028	26.10	0.41	1.58	27.00	-3.34	0.58
Nd	0.06	214.85	1.93	0.90	200.00	7.33	2.74
Ni	1.6	17.13	0.79	4.62	17.00	0.75	1.12
Pb	0.6	42.06	1.11	2.63	42.00	0.13	1.57
Pr	0.014	58.63	1.16	1.98	51.00	14.95	1.65
Rb	0.23	252.86	12.26	4.85	-	-	17.33
Sb	0.04	0.39	0.02	4.48	-	-	0.03
Sc	1.1	6.93	0.32	4.68	6.30	9.95	0.46
Sm	0.012	27.63	0.33	1.19	27.00	2.34	0.46
Sn	0.16	6.23	1.90	30.43	-	-	2.68
Sr	0.6	233.44	8.84	3.79	240.00	-2.73	12.51
Ta	0.023	0.87	0.01	1.22	-	-	0.02
Tb	0.0023	1.28	0.00	0.17	-	-	0.00
Th	0.018	112.06	0.33	0.30	105.00	6.72	0.47
Ti	7	3711.77	308.95	8.32	-	-	436.92
Tl	0.005	1.26	0.04	2.98	-	-	0.05
Tm	0.0019	0.30	0.00	1.17	-	-	0.01
U	0.011	2.59	0.03	1.09	2.40	7.83	0.04
V	0.8	52.66	2.96	5.62	52.00	1.27	4.19
W	0.05	0.41	0.01	2.96	-	-	0.02
Y	0.05	26.64	0.82	3.09	28.00	-4.87	1.16
Yb	0.009	1.71	0.02	1.45	1.60	6.97	0.04
Zn	7	112.93	10.59	9.37	120.00	-5.89	14.97
Zr	6	552.72	28.85	5.22	550.00	0.50	40.81

	LOD	MRB-29 Mean (n=6)	STD	%RSD	Accepted	%RD	2 σ
Ba	0.8	294.52	3.08	1.04	291.00	1.21	4.35
Be	0.04	1.01	0.06	5.47	-	-	0.08
Bi	0.15	0.04	0.01	32.31	-	-	0.02
Cd	0.013	0.65	1.28	196.17	-	-	1.81
Ce	0.12	50.78	0.28	0.55	51.21	-0.84	0.40
Co	0.13	52.57	0.81	1.54	51.50	2.07	1.15
Cr	3	288.70	9.40	3.25	291.00	-0.79	13.29
Cs	0.013	0.25	0.01	4.54	0.25	-1.13	0.02
Cu	1.4	160.10	28.36	17.72	149.00	7.45	40.11
Dy	0.09	5.52	0.08	1.38	5.37	2.74	0.11
Er	0.007	2.94	0.06	2.01	2.90	1.32	0.08
Eu	0.0031	1.99	0.03	1.62	1.95	2.09	0.05
Ga	0.04	18.44	1.27	6.86	-	-	1.79
Gd	0.09	6.20	0.11	1.83	6.22	-0.34	0.16
Hf	0.14	4.50	0.06	1.40	4.59	-1.93	0.09
Ho	0.0025	1.06	0.01	0.97	1.05	1.37	0.01
In	0.0018	0.08	0.00	2.05	-	-	0.00
La	0.04	22.87	0.44	1.93	22.70	0.75	0.62
Li	0.4	10.04	1.20	11.99	12.20	-17.67	1.70
Lu	0.002	0.37	0.00	1.24	0.37	-1.13	0.01
Mo	0.08	0.79	0.01	1.83	-	-	0.02
Nb	0.028	13.07	0.24	1.84	13.30	-1.71	0.34
Nd	0.06	29.17	0.33	1.14	29.10	0.23	0.47
Ni	1.6	114.88	2.14	1.86	115.10	-0.19	3.02
Pb	0.6	4.98	0.24	4.74	-	-	0.33
Pr	0.014	6.83	0.11	1.61	6.74	1.36	0.16
Rb	0.23	15.11	0.26	1.71	15.20	-0.60	0.36
Sb	0.04	0.06	0.01	9.03	-	-	0.01
Sc	1.1	34.54	1.22	3.53	33.20	4.02	1.73
Sm	0.012	6.59	0.10	1.50	6.39	3.13	0.14
Sn	0.16	2.09	0.71	33.82	-	-	1.00
Sr	0.6	309.36	4.11	1.33	316.00	-2.10	5.81
Ta	0.023	0.83	0.03	3.22	0.81	2.30	0.04
Tb	0.0023	0.92	0.01	1.60	0.93	-0.61	0.02
Th	0.018	2.66	0.08	3.15	2.69	-1.14	0.12
Ti	7	11092.23	649.20	5.85	-	-	918.12
Tl	0.005	0.07	0.00	4.31	-	-	0.00
Tm	0.0019	0.40	0.01	1.91	0.40	0.79	0.01
U	0.011	0.66	0.02	2.62	0.66	0.71	0.02
V	0.8	316.25	13.90	4.39	317.00	-0.24	19.65
W	0.05	0.24	0.00	1.88	0.20	20.42	0.01
Y	0.05	27.36	0.32	1.16	26.80	2.09	0.45
Yb	0.009	2.52	0.03	1.32	2.54	-0.81	0.05
Zn	7	109.76	4.80	4.37	106.00	3.55	6.78
Zr	6	174.80	2.91	1.67	179.00	-2.34	4.12

Table A.2: Precision and accuracy results using standard reference materials analysed by ICP-OES for total digestion at the SRC.

SRC-Total Digestion	LOD	CAR110 Mean (n=4)	STD	%RSD	Accepted	%RD	2σ
Ag	0.20	4.10	0.14	3.45	3.80	-	0.14
Al ₂ O ₃	0.01	13.53	0.10	0.71	13.20	2.46	0.10
Ba	1.00	1705.00	10.00	0.59	1683.00	1.31	10.00
Be	0.20	3.75	0.13	3.44	3.60	4.17	0.13
Cd	0.20	-	-	-	1.00	-	-
Ce	1.00	812.25	5.91	0.73	783.00	3.74	5.91
Co	1.00	76.25	2.99	3.92	75.00	1.67	2.99
Cr	1.00	194.25	3.20	1.65	193.00	0.65	3.20
Cu	1.00	214.00	8.76	4.09	221.00	-3.17	8.76
Dy	0.20	12.55	0.10	0.80	12.30	2.03	0.10
Er	0.20	8.50	0.22	2.54	8.60	-1.16	0.22
Eu	0.20	9.95	0.17	1.74	9.70	2.58	0.17
Fe ₂ O ₃	0.01	4.44	0.06	1.42	4.45	-0.22	0.06
Ga	1.00	20.75	0.50	2.41	20.00	3.75	0.50
Gd	0.50	24.50	1.00	4.08	25.00	-2.00	1.00
Hf	0.50	6.75	0.50	7.41	7.00	-3.57	0.50
Ho	0.40	3.00	0.00	0.00	3.00	0.00	0.00
K ₂ O	0.00	3.17	0.03	0.83	3.11	1.85	0.03
La	1.00	413.25	7.50	1.81	424.00	-2.54	7.50
Li	1.00	84.75	1.26	1.48	83.00	2.11	1.26
MgO	0.00	3.34	0.02	0.65	3.29	1.52	0.02
MnO	0.00	0.08	0.01	6.45	0.08	-3.13	0.01
Mo	1.00	68.50	3.70	5.40	65.00	5.38	3.70
Na ₂ O	0.01	1.31	0.01	0.38	1.32	-0.57	0.01
Nb	1.00	14.50	0.58	3.98	16.00	-9.38	0.58
Nd	1.00	358.25	4.57	1.28	355.00	0.92	4.57
Ni	1.00	411.25	4.86	1.18	402.00	2.30	4.86
P ₂ O ₅	0.00	0.90	0.02	1.94	0.87	2.87	0.02
Pb	1.00	441.00	13.49	3.06	424.00	4.01	13.49
Pr	1.00	90.25	0.50	0.55	93.00	-2.96	0.50
Sc	1.00	10.00	0.00	0.00	11.00	-9.09	0.00
Sm	0.50	45.00	0.82	1.81	46.00	-2.17	0.82
Sn	1.00	2.75	1.26	45.76	2.00	37.50	1.26
Sr	1.00	712.00	7.07	0.99	704.00	1.14	7.07
Ta	1.00	1.25	0.50	40.00	1.00	25.00	0.50
Tb	0.30	3.00	0.00	0.00	2.00	50.00	0.00
Th	1.00	120.25	2.36	1.96	117.00	2.78	2.36
TiO ₂	0.00	0.50	0.01	1.63	0.50	0.00	0.01
U ^{ICP}	2.00	3272.50	33.04	1.01	3350.00	-2.31	33.04
V	1.00	243.00	5.89	2.42	240.00	1.25	5.89
W	1.00	2.50	0.71	28.28	3.00	-16.67	0.71
Y	1.00	59.75	0.96	1.60	60.00	-0.42	0.96
Yb	0.10	4.50	0.08	1.81	4.20	7.14	0.08
Zn	1.00	122.25	6.40	5.23	117.00	4.49	6.40
Zr	1.00	282.25	6.18	2.19	276.00	2.26	6.18

SRC-Total Digestion	LOD	AGV-2 Mean (n=2)	STD	%RSD	Accepted	%RD	2σ
Ag	0.20	-	-	-	-	-	-
Al ₂ O ₃	0.01	17.00	0.14	0.83	16.91	0.53	0.20
Ba	1.00	1110.00	14.14	1.27	1140.00	-2.63	20.00
Be	0.20	2.00	0.00	0.00	2.30	-13.04	0.00
Cd	0.20	1.00	0.00	0.00	-	-	0.00
Ce	1.00	62.50	0.71	1.13	68.00	-8.09	1.00
Co	1.00	14.00	0.00	0.00	16.00	-12.50	0.00
Cr	1.00	18.50	0.71	3.82	17.00	8.82	1.00
Cu	1.00	56.50	0.71	1.25	53.00	6.60	1.00
Dy	0.20	3.10	0.00	0.00	3.60	-13.89	0.00
Er	0.20	1.85	0.07	3.82	1.79	3.35	0.10
Eu	0.20	1.65	0.07	4.29	1.54	7.14	0.10
Fe ₂ O ₃	0.01	6.66	0.06	0.85	6.69	-0.45	0.08
Ga	1.00	20.50	0.71	3.45	20.00	2.50	1.00
Gd	0.50	3.00	0.00	0.00	4.69	-36.03	0.00
Hf	0.50	4.00	0.00	0.00	5.08	-21.26	0.00
Ho	0.40	-	-	-	0.71	-	-
K ₂ O	0.00	2.92	0.02	0.73	2.88	1.22	0.03
La	1.00	36.00	0.00	0.00	38.00	-5.26	0.00
Li	1.00	10.00	0.00	0.00	11.00	-9.09	0.00
MgO	0.00	1.80	0.01	0.79	1.79	0.56	0.02
MnO	0.00	0.09	0.00	0.00	-	-	0.00
Mo	1.00	-	-	-	-	-	0.00
Na ₂ O	0.01	4.04	0.04	0.88	4.19	-3.70	0.05
Nb	1.00	11.50	0.71	6.15	15.00	-23.33	1.00
Nd	1.00	27.50	0.71	2.57	30.00	-8.33	1.00
Ni	1.00	19.50	0.71	3.63	19.00	2.63	1.00
P ₂ O ₅	0.00	0.48	0.00	0.00	0.48	0.00	0.00
Pb	1.00	15.00	0.00	0.00	13.00	15.38	0.00
Pr	1.00	6.00	0.00	0.00	8.30	-27.71	0.00
Sc	1.00	12.00	0.00	0.00	13.00	-7.69	0.00
Sm	0.50	4.00	0.00	0.00	5.70	-29.82	0.00
Sn	1.00	1.00	-	0.00	2.30	-56.52	0.00
Sr	1.00	661.50	17.68	2.67	658.00	0.53	25.00
Ta	1.00	-	-	-	0.89	-	0.00
Tb	0.30	-	-	-	0.64	-	0.00
Th	1.00	5.00	0.00	0.00	6.10	-18.03	0.00
TrO ₂	0.00	1.03	0.01	0.69	1.05	-2.38	0.01
U ^{ICP}	2.00	2.00	0.00	0.00	1.88	6.38	0.00
V	1.00	123.50	2.12	1.72	120.00	2.92	3.00
W	1.00	-	-	-	-	-	0.00
Y	1.00	19.50	0.71	3.63	20.00	-2.50	1.00
Yb	0.10	1.90	0.00	0.00	1.60	18.75	0.00
Zn	1.00	87.50	0.71	0.81	86.00	1.74	1.00
Zr	1.00	227.50	2.12	0.93	230.00	-1.09	3.00

SRC-Total Digestion	LOD	GSP-2 Mean (n=1)	Accepted	%RD
Ag	0.20	<0.2	-	-
Al ₂ O ₃	0.01	14.80	14.90	-0.67
Ba	1.00	1330.00	1340.00	-0.75
Be	0.20	1.30	1.50	-13.33
Cd	0.20	1.00	-	-
Ca	1.00	412.00	410.00	0.49
Co	1.00	7.00	7.30	-4.11
Cr	1.00	21.00	20.00	5.00
Cu	1.00	44.00	43.00	2.33
Dy	0.20	5.70	6.10	-6.56
Er	0.20	2.60	2.20	18.18
Eu	0.20	2.60	2.30	13.04
Fe ₂ O ₃	0.01	4.90	4.90	0.00
Ga	1.00	23.00	22.00	4.55
Gd	0.50	11.00	12.00	-8.33
Hf	0.50	2.00	14.00	-85.71
Ho	0.40	1.00	1.00	0.00
K ₂ O	0.00	5.48	5.38	1.86
La	1.00	192.00	180.00	6.67
Li	1.00	34.00	36.00	-5.56
MgO	0.00	0.95	0.96	-1.04
MnO	0.00	0.04	-	-
Mo	1.00	3.00	2.10	42.86
Na ₂ O	0.01	2.65	2.78	-4.68
Nb	1.00	22.00	27.00	-18.52
Nd	1.00	187.00	200.00	-6.50
Ni	1.00	16.00	17.00	-5.88
P ₂ O ₅	0.00	0.30	0.29	3.45
Pb	1.00	43.00	42.00	2.38
Pr	1.00	46.00	51.00	-9.80
Sc	1.00	6.00	6.30	-4.76
Sm	0.50	24.00	27.00	-11.11
Sn	1.00	4.00	-	-
Sr	1.00	242.00	240.00	0.83
Ta	1.00	<1	-	-
Tb	0.30	<1	-	-
Th	1.00	99.00	105.00	-5.71
TiO ₂	0.00	0.65	0.66	-1.52
U, ICP	2.00	<2	2.40	-
V	1.00	55.00	52.00	5.77
W	1.00	<1	-	-
Y	1.00	24.00	28.00	-14.29
Yb	0.10	1.50	1.60	-6.25
Zn	1.00	116.00	120.00	-3.33
Zr	1.00	71.00	550.00	-87.09

SRC-Total Digestion	LOD	SY3 Mean (n=1)	Accepted	%RD
Ag	0.20	<0.2	1.50	-
Al ₂ O ₃	0.01	12.00	11.76	2.04
Ba	1.00	441.00	450.00	-2.00
Be	0.20	21.00	20.00	5.00
Cd	0.20	1.00	-	-
Ce	1.00	2110.00	2230.00	-5.38
Co	1.00	9.00	8.80	2.27
Cr	1.00	10.00	11.00	-9.09
Cu	1.00	14.00	17.00	-17.65
Dy	0.20	114.00	118.00	-3.39
Er	0.20	65.20	68.00	-4.12
Eu	0.20	17.30	17.00	1.76
Fe ₂ O ₃	0.01	6.38	6.49	-1.69
Ga	1.00	30.00	27.00	11.11
Gd	0.50	102.00	105.00	-2.86
Hf	0.50	10.00	9.70	3.09
Ho	0.40	27.00	29.50	-8.47
K ₂ O	0.00	4.30	4.23	1.65
La	1.00	1320.00	1340.00	-1.49
Li	1.00	94.00	92.00	2.17
MgO	0.00	2.78	2.67	4.12
MnO	0.00	0.30	0.32	-6.25
Mo	1.00	1.00	1.00	0.00
Na ₂ O	0.01	4.05	4.12	-1.70
Nb	1.00	139.00	148.00	-6.08
Nd	1.00	637.00	670.00	-4.93
Ni	1.00	10.00	11.00	-9.09
P ₂ O ₅	0.00	0.53	0.54	-1.85
Pb	1.00	139.00	133.00	4.51
Pr	1.00	207.00	223.00	-7.17
Sc	1.00	6.00	6.80	-11.76
Sm	0.50	102.00	109.00	-6.42
Sn	1.00	5.00	6.50	-23.08
Sr	1.00	307.00	302.00	1.66
Ta	1.00	27.00	30.00	-10.00
Tb	0.30	18.00	18.00	0.00
Th	1.00	981.00	1003.00	-2.19
TiO ₂	0.00	0.14	0.15	-6.67
U ^{ICP}	2.00	642.00	650.00	-1.23
V	1.00	53.00	50.00	6.00
W	1.00	<1	1.10	-
Y	1.00	696.00	718.00	-3.06
Yb	0.10	65.60	62.00	5.81
Zn	1.00	234.00	244.00	-4.10
Zr	1.00	334.00	320.00	4.38

Table A.3: Precision and accuracy results using standard reference materials analyzed by ICP-OES for whole rock and partial digestion at the SRC.

SRC- Whole Rock	LOD	G2 Mean (n=4)	STD	%RSD	Accepted	%RD	2 σ
Al ₂ O ₃	0.01	15.18	0.13	0.83	15.39	-1.40	0.13
Ba	2.00	1910.00	11.55	0.60	1880.00	1.60	11.55
CaO	0.01	1.94	0.02	1.26	1.96	-1.02	0.02
Cr	2.00	8.50	1.29	15.19	-	-	1.29
Fe ₂ O ₃	0.01	2.68	0.03	1.12	2.66	0.56	0.03
K ₂ O	0.01	4.47	0.05	1.10	4.48	-0.22	0.05
MgO	0.01	0.78	0.01	1.22	0.75	4.33	0.01
MnO	0.01	0.03	0.00	0.00	0.03	0.00	0.00
Na ₂ O	0.01	4.06	0.05	1.16	4.08	-0.49	0.05
P ₂ O ₅	0.01	0.12	0.01	4.08	0.14	-12.50	0.01
Sc	2.00	3.00	0.00	0.00	3.50	-14.29	0.00
SiO ₂	0.10	68.73	0.56	0.81	69.14	-0.60	0.56
Sr	2.00	461.75	3.86	0.84	478.00	-3.40	3.86
TiO ₂	0.01	0.48	0.01	1.70	0.48	0.00	0.01
Y	2.00	13.50	1.73	12.83	11.00	22.73	1.73
Zr	2.00	290.50	3.11	1.07	309.00	-5.99	3.11
SUM	-	98.46	0.71	0.72	-	-	0.71
LOI	0.10	-	-	-	-	-	-

Partial Digestion	LOD	CAR110 Mean (n=4)	STD	%RSD	Accepted	%RD	2 σ
Ag	0.10	2.93	0.10	3.27	3.20	-8.59	0.10
As	0.20	413.00	2.16	0.52	402.00	2.74	2.16
Au [*]	2.00	-	-	-	-	-	-
Bi	0.20	20.75	0.96	4.61	21.00	-1.19	0.96
Co	0.10	64.75	0.50	0.77	67.00	-3.36	0.50
Cu	0.10	206.50	6.03	2.92	209.00	-1.20	6.03
Ge	0.20	-	-	-	-	-	-
Hg	0.20	-	-	-	-	-	-
Mo	0.10	59.50	1.29	2.17	57.00	4.39	1.29
Ni	0.10	358.50	9.15	2.55	354.00	1.27	9.15
Pb	0.02	396.25	10.24	2.58	402.00	-1.43	10.24
Sb	0.20	-	-	-	-	-	-
Sb	0.20	2.75	0.50	18.18	4.00	-31.25	0.50
Te	0.20	1.00	0.00	0.00	1.00	0.00	0.00
U, ^{FI}	0.02	3155.00	20.82	0.66	3198.00	-1.34	20.82
V	0.10	128.00	3.92	3.06	136.00	-5.88	3.92
Zn	0.10	92.50	2.08	2.25	95.00	-2.63	2.08

SRC- Whole Rock	LOD	AGV-2 Mean (n=2)	STD	%RSD	Accepted	%RD	2σ
Al ₂ O ₃	0.01	17.25	0.07	0.41	16.91	2.01	0.10
Ba	2.00	1130.00	28.28	2.50	1140.00	-0.88	40.00
CaO	0.01	5.23	0.10	1.89	5.20	0.58	0.14
Cr ICP	2.00	16.00	1.41	8.84	17.00	-5.88	2.00
Fe ₂ O ₃	0.01	6.61	0.01	0.11	6.69	-1.27	0.01
K ₂ O	0.01	2.91	0.01	0.49	2.88	1.04	0.02
MgO	0.01	1.76	0.05	2.82	1.79	-1.96	0.07
MnO	0.01	0.10	0.00	0.00	-	-	0.00
Na ₂ O	0.01	4.22	0.06	1.51	4.19	0.60	0.09
P ₂ O ₅	0.01	0.47	0.00	0.00	0.48	-2.08	0.00
Sc	2.00	12.00	0.00	0.00	13.00	-7.69	0.00
SiO ₂	0.10	59.80	0.28	0.47	59.30	0.84	0.40
Sr	2.00	657.00	8.49	1.29	658.00	-0.15	12.00
TiO ₂	0.01	1.03	0.00	0.00	1.05	-1.90	0.00
Y	2.00	20.50	0.71	3.45	20.00	2.50	1.00
Zr	2.00	220.00	5.66	2.57	230.00	-4.35	8.00
SUM	-	99.37	0.59	0.59	-	-	0.83
LOI	0.10	-	-	-	-	-	-

Partial Digestion	LOD	AGV-2 Mean (n=2)	STD	%RSD	Accepted	%RD	2σ
Ag	0.10	-	-	-	-	-	-
As	0.20	1.00	0.00	0.00	-	-	0.00
Au ^r	2.00	-	-	-	-	-	-
Bi	0.20	-	-	-	-	-	-
Co	0.10	6.00	0.00	0.00	16.00	-62.50	0.00
Cu	0.10	45.50	0.71	1.55	53.00	-14.15	1.00
Ge	0.20	-	-	-	-	-	-
Hg	0.20	-	-	-	-	-	-
Mo	0.10	1.00	0.00	0.00	-	-	0.00
Ni	0.10	8.00	0.00	0.00	19.00	-57.89	0.00
Pb	0.02	3.00	0.00	0.00	13.00	-76.92	0.00
Sb	0.20	-	-	-	0.60	-	-
Sb	0.20	-	-	-	-	-	-
Te	0.20	-	-	-	-	-	-
U ^{FI}	0.02	0.64	0.05	7.79	1.88	-66.22	0.07
V	0.10	49.50	2.12	4.29	120.00	-58.75	3.00
Zn	0.10	45.00	1.41	3.14	86.00	-47.67	2.00

SRC-Whole Rock	LOD	SY3 (n=1)	Accepted	%RD
Al ₂ O ₃	0.01	11.90	11.76	1.19
Ba	2.00	437.00	450.00	-2.89
CaO	0.01	8.32	8.25	0.85
Cr ICP	2.00	9.00	11.00	-18.18
Fe ₂ O ₃	0.01	6.47	6.49	-0.31
K ₂ O	0.01	4.26	4.23	0.71
MgO	0.01	-	-	-
MnO	0.01	2.65	2.67	-0.75
Na ₂ O	0.01	0.33	0.32	3.13
P ₂ O ₅	0.01	4.04	4.12	-1.94
Sc	2.00	0.52	0.54	-3.70
SiO ₂	0.10	7.00	6.80	2.94
Sr	2.00	59.90	59.68	0.37
TiO ₂	0.01	307.00	302.00	1.66
Y	2.00	98.53	-	-
Zr	2.00	0.14	0.15	-6.67
SUM	-	731.00	718.00	1.81
LOI	0.10	308.00	320.00	-3.75

Partial Digestion	LOD	SY3	Accepted	%RD
Ag	0.10	<0.2	1.50	-
As	0.20	6.00	18.80	-68.09
Au [*]	2.00	-	-	-
Bi	0.20	<1	0.80	-
Co	0.10	2.00	8.80	-77.27
Cu	0.10	13.00	17.00	-23.53
Ge	0.20	<1	1.40	-
Hg	0.20	<1	0.02	-
Mo	0.10	1.00	1.00	0.00
Ni	0.10	2.00	11.00	-81.82
Pb	0.02	128.00	133.00	-3.76
Sb	0.20	<1	0.31	-
Sb	0.20	<1	0.03	-
Te	0.20	1.00	-	-
U,Fl	0.02	498.00	650.00	-23.38
V	0.10	23.00	50.00	-54.00

SRC-Whole Rock	LOD	GSP-2 Mean (n=1)
Al ₂ O ₃	0.01	15.30
Ba	2.00	1390.00
CaO	0.01	2.16
Cr ICP	2.00	22.00
Fe ₂ O ₃	0.01	4.80
K ₂ O	0.01	5.47
MgO	0.01	-
MnO	0.01	0.98
Na ₂ O	0.01	0.04
P ₂ O ₅	0.01	2.85
Sc	2.00	0.29
SiO ₂	0.10	6.00
Sr	2.00	66.30
TiO ₂	0.01	248.00
Y	2.00	104.86
Zr	2.00	0.67
SUM	-	27.00
LOI	0.10	541.00

Partial Digestion	LOD	GSP-2 Mean (n=1)
Ag	0.10	<0.2
As	0.20	2.00
Au [*]	2.00	-
Bi	0.20	<1
Co	0.10	6.00
Cu	0.10	43.00
Ge	0.20	<1
Hg	0.20	<1
Mo	0.10	2.00
Ni	0.10	13.00
Pb	0.02	16.00
Sb	0.20	<1
Sb	0.20	<1
Te	0.20	<1
U, ^{Fl}	0.02	1.42
V	0.10	34.00
Zn	0.10	106.00

Table A.4: Precision and accuracy results using standard reference materials for analysis by pressed pellet XRF at MUN.

	LOD	AGV-1 Mean (n=9)	STD	%RSD	Accepted	%RD	2 σ
Al ₂ O ₃	0.08	16.96	0.13	0.77	17.15	-1.11	0.09
As	17.09	5.15	4.53	87.88	0.88	82.92	3.02
Ba	22.12	1233.49	24.35	1.97	1200.00	2.72	16.23
CaO	0.003	4.84	0.04	0.89	4.94	-2.03	0.03
Ca	40.80	99.00	10.26	10.36	67.60	31.72	6.84
Cl	35.18	640.83	30.47	4.75	119.00	81.43	20.31
Cr	7.40	4.24	3.37	79.47	9.40	-121.63	2.25
Cu	4.53	57.29	2.33	4.07	58.00	-1.24	1.56
Fe ₂ O ₃ T	0.01	6.62	0.03	0.43	6.77	-2.31	0.02
Ga	4.42	21.26	1.91	8.96	20.20	4.98	1.27
K ₂ O	0.003	2.77	0.02	0.66	0.04	98.48	0.01
MgO	0.01	1.40	0.03	1.95	1.53	-9.08	0.02
MnO	0.002	0.10	0.00	1.51	0.10	-1.98	0.00
Na ₂ O	0.02	3.81	0.02	0.63	4.26	-11.88	0.02
Nb	0.95	17.51	0.36	2.03	14.60	16.61	0.24
Ni	4.92	17.95	2.86	15.94	15.50	13.63	1.91
P ₂ O ₅	0.003	0.46	0.00	0.78	0.50	-9.77	0.00
Pb	5.09	36.78	1.81	4.93	37.40	-1.68	1.21
Rb	0.94	70.03	0.64	0.91	66.60	4.90	0.43
S	18.49	951.57	12.16	1.28	-	-	8.11
Sc	8.29	11.87	1.92	16.15	12.30	-3.58	1.28
SiO ₂	0.01	60.49	0.47	0.78	58.84	2.73	0.31
Sr	1.58	690.41	2.41	0.35	660.00	4.40	1.61
Th	4.24	5.81	1.65	28.41	6.40	-10.12	1.10
TiO ₂	0.00	1.02	0.02	1.90	1.05	-3.15	0.01
U	4.92	0.62	2.56	410.63	1.93	-209.64	1.71
V	6.61	113.57	6.54	5.76	119.00	-4.78	4.36
Y	0.84	18.32	0.17	0.91	19.00	-3.70	0.11
Zn	2.38	74.90	2.86	3.82	87.00	-16.16	1.91
Zr	1.54	260.14	1.87	0.72	231.00	11.20	1.25
total	-	99.09	0.70	0.71	-	-	0.47

	LOD	BCR-2 Mean (n=8)	STD	%RSD	Accepted	%RD	2σ
Al ₂ O ₃	0.08	14.71	0.06	0.42	13.50	8.94	0.04
As	17.09	3.90	3.96	101.60	-	-	2.80
Ba	22.12	720.63	24.01	3.33	683.00	5.51	16.98
CaO	0.003	6.96	0.02	0.26	7.12	-2.24	0.01
Ca	40.80	75.59	13.58	17.97	53.00	42.62	9.61
Cl	35.18	559.75	34.77	6.21	-	-	24.59
Cr	7.40	17.36	2.33	13.43	18.00	-3.53	1.65
Cu	4.53	20.52	1.13	5.52	19.00	8.01	0.80
Fe ₂ O ₃ T	0.01	12.98	0.04	0.28	13.80	-5.97	0.03
Ga	4.42	22.15	0.91	4.10	23.00	-3.69	0.64
K ₂ O	0.003	1.82	0.01	0.64	1.79	1.49	0.01
MgO	0.01	2.97	0.04	1.23	3.59	-17.19	0.03
MnO	0.002	0.19	0.00	1.11	-	-	0.00
Na ₂ O	0.02	3.21	0.03	0.89	3.16	1.50	0.02
Nb	0.95	14.70	0.25	1.72	-	-	0.18
Ni	4.92	26.33	9.09	34.51	-	-	6.43
P ₂ O ₅	0.003	0.29	0.00	0.81	0.35	-16.66	0.00
Pb	5.09	10.12	1.41	13.88	11.00	-7.99	0.99
Rb	0.94	47.23	0.53	1.11	48.00	-1.60	0.37
S	18.49	786.58	27.46	3.49	-	-	19.42
Sc	8.29	30.55	3.20	10.49	33.00	-7.43	2.27
SiO ₂	0.01	56.52	0.20	0.35	54.10	4.48	0.14
Sr	1.58	339.04	1.75	0.52	346.00	-2.01	1.24
Th	4.24	4.91	1.73	35.34	6.20	-20.82	1.23
TiO ₂	0.00	2.33	0.02	0.74	2.26	2.95	0.01
U	4.92	1.11	1.52	137.43	1.69	-34.36	1.08
V	6.61	421.95	5.97	1.42	416.00	1.43	4.22
Y	0.84	32.81	0.32	0.96	37.00	-11.33	0.22
Zn	2.38	87.91	1.80	2.05	127.00	-30.78	1.28
Zr	1.54	200.24	1.54	0.77	188.00	6.51	1.09
total	-	102.49	0.28	0.27	189.00	-45.77	0.20

	LOD	BHVO-1 Mean (n=34)	STD	%RSD	Accepted	%RD	2 σ
Al ₂ O ₃	0.08	14.37	0.14	1.01	13.70	4.86	0.34
As	17.09	3.24	7.21	222.73	0.50	547.25	76.40
Ba	22.12	136.89	12.25	8.95	133.00	2.93	3.07
CaO	0.003	11.02	0.13	1.21	11.40	-3.31	0.42
Ce	40.80	49.67	14.79	29.78	38.10	30.37	10.21
Cl	35.18	1107.51	29.13	2.63	92.00	1103.82	0.90
Cr	7.40	310.91	4.76	1.53	287.00	8.33	0.53
Cu	4.53	136.97	1.95	1.42	137.00	-0.02	0.49
Fe ₂ O ₃ T	0.01	12.09	0.07	0.59	12.40	-2.49	0.20
Ga	4.42	20.59	1.59	7.71	21.00	-1.96	2.65
K ₂ O	0.003	0.50	0.01	1.52	0.53	-4.91	0.52
MgO	0.01	7.03	0.11	1.60	7.22	-2.64	0.55
MnO	0.002	0.17	0.00	1.31	0.17	-2.86	0.45
Na ₂ O	0.02	2.33	0.02	1.05	2.30	1.45	0.36
Nb	0.95	23.65	0.38	1.59	18.60	27.17	0.54
Ni	4.92	124.37	2.66	2.14	118.00	5.40	0.73
P ₂ O ₅	0.003	0.30	0.01	2.28	0.27	9.98	0.78
Pb	5.09	2.73	1.99	72.87	0.00	94204.86	24.99
Rb	0.94	9.35	0.39	4.19	9.19	1.69	1.44
S	18.49	1144.50	24.54	2.14	93.00	1130.65	0.74
Sc	8.29	32.62	3.26	9.98	31.00	5.24	3.42
SiO ₂	0.01	49.16	0.38	0.77	49.80	-1.29	0.26
Sr	1.58	410.22	2.09	0.51	396.00	3.59	0.17
Th	4.24	0.34	1.66	-483.16	1.23	-127.88	-165.72
TiO ₂	0.00	2.79	0.03	1.17	2.75	1.49	0.40
U	4.92	1.05	2.13	-202.22	0.41	-357.65	-69.36
V	6.61	317.13	7.53	2.37	318.00	-0.27	0.81
Y	0.84	24.94	0.34	1.35	26.00	-4.10	0.46
Zn	2.38	100.91	2.55	2.53	106.00	-4.81	0.87
Zr	1.54	191.77	1.34	0.70	174.00	10.21	0.24
total	-	100.41	0.85	0.85	-	-	0.29

	LOD	DNC-1 Mean (N=8)	STD	%RD	Accepted	%RSD	2 σ
Al ₂ O ₃	0.08	19.54	0.11	0.55	18.34	6.53	0.08
As	17.09	0.05	5.44	-10212.72	0.12	-144.40	3.85
Ba	22.12	118.11	13.60	11.51	118.00	0.09	9.61
CaO	0.003	11.12	0.05	0.46	11.49	-3.25	0.04
Ce	40.80	21.63	18.49	85.47	-	-	13.07
Cl	35.18	678.08	28.65	4.23	60.00	1030.14	20.26
Cr	7.40	306.73	3.21	1.05	270.00	13.60	2.27
Cu	4.53	82.72	3.22	3.89	100.00	-17.28	2.27
Fe ₂ O ₃ T	0.01	9.96	0.03	0.27	9.97	-0.09	0.02
Ga	4.42	12.77	1.10	8.58	15.00	-14.85	0.78
K ₂ O	0.003	0.26	0.00	1.33	0.23	12.32	0.00
MgO	0.01	10.34	0.14	1.31	10.13	2.08	0.10
MnO	0.002	0.15	0.00	0.97	0.15	-3.16	0.00
Na ₂ O	0.02	1.90	0.03	1.34	1.89	0.78	0.02
Nb	0.95	2.45	0.26	10.74	3.00	-18.25	0.19
Ni	4.92	244.65	2.93	1.20	247.00	-0.95	2.07
P ₂ O ₅	0.003	0.10	0.00	2.10	0.07	50.00	0.00
Pb	5.09	7.23	1.41	19.50	6.30	14.71	1.00
Rb	0.94	3.58	0.19	5.18	4.50	-20.53	0.13
S	18.49	1297.16	32.23	2.48	-	-	22.79
Sc	8.29	33.14	2.44	7.35	31.00	6.91	1.72
SiO ₂	0.01	44.32	0.30	0.68	47.15	-6.00	0.21
Sr	1.58	142.03	0.81	0.57	144.00	-1.37	0.57
Th	4.24	0.97	1.56	-161.83	-	-	1.10
TiO ₂	0.00	0.46	0.01	1.51	0.48	-4.82	0.00
U	4.92	1.07	1.93	-180.76	-	-	1.36
V	6.61	145.29	2.49	1.71	148.00	-1.83	1.76
Y	0.84	15.57	0.34	2.15	18.00	-13.49	0.24
Zn	2.38	56.81	1.15	2.02	70.00	-18.84	0.81
Zr	1.54	37.38	0.47	1.25	38.00	-1.64	0.33
total	-	98.71	0.55	0.56	-	-	0.39

	LOD	DTS-1 Mean (n=34)	STD	%RD	Accepted	%RSD	2 σ
Al ₂ O ₃	0.08	0.00	0.02	-1652.91	0.19	-100.56	0.01
As	17.09	0.53	4.57	-867.47	0.03	-1649.85	1.57
Ba	22.12	9.29	6.37	68.57	1.70	446.73	2.19
CaO	0.003	0.16	0.00	1.85	0.17	-8.02	0.00
Ce	40.80	4.25	11.29	265.42	0.07	5975.50	3.87
Cl	35.18	773.25	35.06	4.53	11.00	6929.58	12.03
Cr	7.40	3989.38	24.18	0.61	3990.00	-0.02	8.29
Cu	4.53	6.16	2.03	33.02	7.10	-13.20	0.70
Fe ₂ O ₃ T	0.01	9.32	0.03	0.35	8.68	7.42	0.01
Ga	4.42	1.88	1.39	-74.16	-	-	0.48
K ₂ O	0.003	0.04	0.00	8.73	0.00	3855.13	0.00
MgO	0.01	49.57	0.24	0.48	49.59	-0.04	0.08
MnO	0.002	0.13	0.00	1.37	0.12	6.18	0.00
Na ₂ O	0.02	0.21	0.04	17.67	0.01	2033.89	0.01
Nb	0.95	0.53	0.33	61.50	-	-	0.11
Ni	4.92	2360.08	7.61	0.32	2360.00	0.00	2.61
P ₂ O ₅	0.003	0.11	0.00	1.45	0.00	5536.18	0.00
Pb	5.09	7.32	1.46	19.97	12.00	-39.01	0.50
Rb	0.94	0.11	0.32	286.37	-	-	0.11
S	18.49	1122.25	34.38	3.06	12.00	9252.11	11.79
Sc	8.29	2.03	2.33	115.13	3.50	-42.11	0.80
SiO ₂	0.01	39.20	0.30	0.77	40.41	-2.99	0.10
Sr	1.58	0.18	0.44	241.12	0.32	-43.32	0.15
Th	4.24	0.49	1.26	-256.72	0.01	-5019.51	0.43
TiO ₂	0.00	0.01	0.00	23.57	0.01	47.04	0.00
U	4.92	0.27	1.40	-515.06	0.00	-7660.00	0.48
V	6.61	9.25	1.77	19.15	11.00	-15.91	0.61
Y	0.84	0.02	0.25	-1358.92	-	-	0.08
Zn	2.38	96.85	5.65	5.83	46.00	110.53	1.94
Zr	1.54	0.48	0.51	-106.84	-	-	0.18
total	-	100.01	0.42	0.42	-	-	0.14

	LOD	DNC-1 Mean (N=8)	STD	%RD	Accepted	%RSD	2σ
Al ₂ O ₃	0.08	19.54	0.11	0.55	18.34	6.53	0.08
As	17.09	0.05	5.44	-10212.72	0.12	-144.40	3.85
Ba	22.12	118.11	13.60	11.51	118.00	0.09	9.61
CaO	0.003	11.12	0.05	0.46	11.49	-3.25	0.04
Ce	40.80	21.63	18.49	85.47	-	-	13.07
Cl	35.18	678.08	28.65	4.23	60.00	1030.14	20.26
Cr	7.40	306.73	3.21	1.05	270.00	13.60	2.27
Cu	4.53	82.72	3.22	3.89	100.00	-17.28	2.27
Fe ₂ O ₃ T	0.01	9.96	0.03	0.27	9.97	-0.09	0.02
Ga	4.42	12.77	1.10	8.58	15.00	-14.85	0.78
K ₂ O	0.003	0.26	0.00	1.33	0.23	12.32	0.00
MgO	0.01	10.34	0.14	1.31	10.13	2.08	0.10
MnO	0.002	0.15	0.00	0.97	0.15	-3.16	0.00
Na ₂ O	0.02	1.90	0.03	1.34	1.89	0.78	0.02
Nb	0.95	2.45	0.26	10.74	3.00	-18.25	0.19
Ni	4.92	244.65	2.93	1.20	247.00	-0.95	2.07
P ₂ O ₅	0.003	0.10	0.00	2.10	0.07	50.00	0.00
Pb	5.09	7.23	1.41	19.50	6.30	14.71	1.00
Rb	0.94	3.58	0.19	5.18	4.50	-20.53	0.13
S	18.49	1297.16	32.23	2.48	-	-	22.79
Sc	8.29	33.14	2.44	7.35	31.00	6.91	1.72
SiO ₂	0.01	44.32	0.30	0.68	47.15	-6.00	0.21
Sr	1.58	142.03	0.81	0.57	144.00	-1.37	0.57
Th	4.24	0.97	1.56	-161.83	-	-	1.10
TiO ₂	0.00	0.46	0.01	1.51	0.48	-4.82	0.00
U	4.92	1.07	1.93	-180.76	-	-	1.36
V	6.61	145.29	2.49	1.71	148.00	-1.83	1.76
Y	0.84	15.57	0.34	2.15	18.00	-13.49	0.24
Zn	2.38	56.81	1.15	2.02	70.00	-18.84	0.81
Zr	1.54	37.38	0.47	1.25	38.00	-1.64	0.33
total	-	98.71	0.55	0.56	-	-	0.39

	LOD	PACS-1 Mean (n=18)	STD	%RSD	Accepted	%RD	2σ
Al ₂ O ₃	0.08	13.02	0.07	0.53	12.23	6.43	0.03
As	17.09	210.63	6.92	3.28	211.00	-0.17	3.26
Ba	22.12	672.72	19.12	2.84	-	-	9.01
CaO	0.003	3.16	0.02	0.65	2.92	8.06	0.01
Ce	40.80	100.65	15.02	14.92	-	-	7.08
Cl	35.18	23897.50	215.98	0.90	23900.00	-0.01	101.81
Cr	7.40	132.80	3.81	2.87	113.00	17.52	1.80
Cu	4.53	417.90	6.14	1.47	452.00	-7.55	2.89
Fe ₂ O ₃ T	0.01	7.48	0.02	0.26	6.96	7.42	0.01
Ga	4.42	15.44	1.26	8.18	-	-	0.60
K ₂ O	0.003	1.61	0.01	0.76	1.50	7.55	0.01
MgO	0.01	3.78	0.05	1.22	2.41	57.05	0.02
MnO	0.002	0.06	0.00	2.13	0.06	7.76	0.00
Na ₂ O	0.02	4.01	0.05	1.16	4.40	-8.84	0.02
Nb	0.95	10.83	0.30	2.80	-	-	0.14
Ni	4.92	54.46	3.13	5.75	44.10	23.50	1.48
P ₂ O ₅	0.003	0.44	0.00	0.88	0.23	87.32	0.00
Pb	5.09	381.16	4.11	1.08	404.00	-5.65	1.94
Rb	0.94	43.13	0.33	0.77	-	-	0.16
S	18.49	13194.09	87.48	0.66	13200.00	-0.04	41.24
Sc	8.29	13.98	3.49	24.99	-	-	1.65
SiO ₂	0.01	63.83	0.30	0.46	55.70	14.60	0.14
Sr	1.58	285.93	1.20	0.42	277.00	3.22	0.57
Th	4.24	-6.22	2.19	-35.20	-	-	1.03
TiO ₂	0.00	0.81	0.01	1.38	0.70	14.91	0.01
U	4.92	-2.20	1.61	-73.30	-	-	0.76
V	6.61	154.04	3.85	2.50	127.00	21.29	1.82
Y	0.84	17.22	0.22	1.30	-	-	0.11
Zn	2.38	479.70	9.17	1.91	824.00	-41.78	4.32
Zr	1.54	143.01	2.28	1.60	-	-	1.08
total	-	104.27	0.38	0.36	-	-	0.18

	LOD	SY-3	STD	%RSD	Accepted	%RD	2 σ
Mean (n=52)							
Al ₂ O ₃	0.08	12.61	0.13	1.03	11.76	7.25	0.04
As	17.09	25.24	5.33	21.10	18.80	34.24	1.48
Ba	22.12	448.45	11.32	2.52	450.00	-0.34	3.14
CaO	0.003	8.04	0.04	0.55	8.25	-2.57	0.01
Ca	40.80	1523.42	979.85	64.32	-	-	271.76
Cl	35.18	1162.10	213.02	18.33	150.00	674.73	59.08
Cr	7.40	3.71	3.04	81.81	11.00	-86.25	0.84
Cu	4.53	13.33	4.89	36.72	17.00	-21.59	1.36
Fe ₂ O ₃ T	0.01	6.19	0.09	1.44	6.49	-4.60	0.02
Ga	4.42	28.37	1.65	5.80	27.00	5.08	0.46
K ₂ O	0.003	4.23	0.08	1.99	4.23	-0.07	0.02
MgO	0.01	2.91	0.06	2.23	2.67	8.90	0.02
MnO	0.002	0.30	0.01	2.06	0.32	-5.51	0.00
Na ₂ O	0.02	4.21	0.02	0.53	4.12	2.09	0.01
Nb	0.95	177.20	105.18	59.36	148.00	19.73	29.17
Ni	4.92	66.78	35.66	53.41	11.00	507.06	9.89
P ₂ O ₅	0.003	0.49	0.05	10.08	0.54	-9.30	0.01
Pb	5.09	119.48	24.64	20.62	133.00	-10.16	6.83
Rb	0.94	207.70	9.03	4.35	206.00	0.83	2.51
S	18.49	1044.74	178.58	17.09	510.00	104.85	49.53
Sc	8.29	3.41	4.12	120.86	6.80	-49.89	1.14
SiO ₂	0.01	63.14	0.36	0.57	59.68	5.79	0.10
Sr	1.58	287.17	11.99	4.18	302.00	-4.91	3.33
Th	4.24	713.15	269.24	37.75	1003.00	-28.90	74.67
TiO ₂	0.00	0.13	0.00	2.56	0.15	-16.36	0.00
U	4.92	578.57	212.02	36.65	650.00	-10.99	58.80
V	6.61	22.96	18.52	80.66	50.00	-54.09	5.14
Y	0.84	424.54	225.21	53.05	718.00	-40.87	62.46
Zn	2.38	284.06	54.54	19.20	244.00	16.42	15.13
Zr	1.54	328.55	24.16	7.35	320.00	2.67	6.70
total	-	103.24	0.41	0.39	-	-	0.11

APPENDIX B: LITHOGEOCHEMISTRY OF THE TOPSAILS INTRUSIVE SUITE

Geochemical investigation of the TIS required the use of numerous major and trace elements selected from a variety of analytical methods and laboratories. A list of the geochemical results for the entire sample suite is provided in Table B1 that include sample type information as well as the Aigpatic Index ($AI = \text{molar Al} / \text{molar (Na + K)}$), Alumina Saturation Index ($ASI = \text{molar Al} / \text{molar (Na + K + Ca)}$) and Ga^*/Al ratio ($Ga^*=69.723$). Major element oxides (SiO_2 , Al_2O_3 , Fe_2O_3 , K_2O , Na_2O , MgO , MnO , P_2O_5 , CaO and TiO_2 where selected from whole rock analysis by ICP-OES at SRC. Trace elements were mostly selected from ICP-MS analysis from the OGL however because some samples returned over limit values in certain elements the results were substituted for ICP-OES results from SRC (Be, Ce, Cu, Hy, Nd, Sn, Th, V and F) and XRF results from MUN (Zr, Nb, Y, S and Cl).

Table B.1: Geochemical results for the TIS samples providing the sample type details and location. Easting and northing are Nad 27 specific.

Sample #		3001	3002	3003	3004	3005	3006	3007	3008
Year		2009	2009	2009	2009	2009	2009	2009	2009
Rock Type		rhyolite	rhyolite	Am-Pyx granite	Am-Bt granite	Qtz-Kfs porphyry	rhyolite breccia	rhyolite	rhyolite breccia
Rock Unit		Ssf	Ssf	Sp	Sm	Sq	Ssf	Ssf	Ssf
Sample type		float	outcrop	outcrop	outcrop	outcrop	outcrop	outcrop	outcrop
Easting (m)		489288	489287	491660	491563	488530	480295	481510	480608
Northing (m)		5427605	5427609	5414336	5414297	5421339	5427781	5427710	5427557
SiO ₂	(wt%; ICP-OES; WR)	76.80	76.40	75.20	76.20	76.20	79.00	81.40	79.10
Al ₂ O ₃	(wt%; ICP-OES; WR)	11.20	10.40	11.40	12.10	10.80	10.90	9.74	10.80
Fe ₂ O ₃	(wt%; ICP-OES; WR)	2.26	2.37	3.38	2.33	2.79	1.70	1.40	2.85
K ₂ O	(wt%; ICP-OES; WR)	4.97	4.90	4.75	4.77	4.41	5.19	3.96	3.49
Na ₂ O	(wt%; ICP-OES; WR)	3.16	2.90	4.49	4.01	4.10	1.49	0.76	2.61
MgO	(wt%; ICP-OES; WR)	0.04	0.05	0.06	0.05	0.04	0.14	0.17	0.27
MnO	(wt%; ICP-OES; WR)	0.02	0.03	0.06	0.01	0.05	0.01	0.02	0.04
P ₂ O ₅	(wt%; ICP-OES; WR)	0.03	0.07	0.04	0.02	0.03	0.02	0.02	0.03
CaO	(wt%; ICP-OES; WR)	0.12	0.48	0.25	0.13	0.21	0.03	0.09	0.07
TiO ₂	(wt%; ICP-OES; WR)	0.17	0.25	0.32	0.17	0.18	0.12	0.10	0.19
Ba	(ppm; ICP-OES; WR)	58.00	93.00	82.00	590.00	31.00	43.00	33.00	72.00
LOI	(wt%; ICP-OES; WR)	0.40	0.60	0.10	0.70	0.40	1.10	1.60	1.20
ASI		1.04	0.95	0.88	1.01	0.91	1.34	1.71	1.32
Ga ⁺ /Al		2.52	2.51	4.50	3.39	4.93	2.77	2.96	3.88
Al		1.06	1.03	0.91	1.03	0.94	1.35	1.76	1.34
Cl	(ppm; XRF)	128.94	213.76	150.77	158.68	120.77	83.66	99.78	104.56
Nb	(ppm; XRF)	40.16	38.71	15.01	8.20	56.00	33.74	30.62	56.60
S	(ppm; XRF)	127.96	123.85	115.76	153.74	118.09	124.11	125.08	118.63
Y	(ppm; XRF)	76.69	74.59	26.19	20.17	106.43	56.32	46.92	135.50
Zr	(ppm; XRF)	618.26	662.96	282.93	294.38	1165.77	338.33	282.36	1245.76
Bi	(ppm; ICP-MS)	0.18	-	-	-	0.38	-	0.24	0.40
Cd	(ppm; ICP-MS)	0.12	0.12	0.15	0.23	0.30	0.04	0.05	0.20
Co	(ppm; ICP-MS)	0.28	1.73	0.42	0.54	0.20	0.30	0.65	0.32
Cr	(ppm; ICP-MS)	35.00	16.00	8.00	13.00	21.00	9.00	7.00	10.00
Cs	(ppm; ICP-MS)	0.47	0.58	0.58	0.25	1.67	2.20	3.32	3.28
Dy	(ppm; ICP-MS)	14.13	14.61	7.09	5.36	26.79	10.28	8.07	27.63
Er	(ppm; ICP-MS)	9.22	9.13	4.64	2.37	17.79	7.43	6.05	16.75
Eu	(ppm; ICP-MS)	0.29	0.65	0.76	1.50	1.73	0.06	0.06	2.31

Sample #		3001	3002	3003	3004	3005	3006	3007	3008
Ga	(ppm; ICP-MS)	19.29	17.82	35.10	28.02	36.38	20.61	19.70	28.67
Gd	(ppm; ICP-MS)	12.28	13.72	5.38	7.38	20.91	4.20	3.69	26.87
Ho	(ppm; ICP-MS)	3.00	3.06	1.51	0.93	5.79	2.36	1.87	5.68
In	(ppm; ICP-MS)	0.12	0.10	0.13	0.15	0.24	0.08	0.09	0.20
La	(ppm; ICP-MS)	72.98	82.53	11.78	51.55	60.45	7.32	10.76	114.80
Li	(ppm; ICP-MS)	1.40	3.60	23.00	1.90	55.90	3.20	6.60	9.30
Lu	(ppm; ICP-MS)	1.33	1.34	0.74	0.49	2.60	1.13	0.88	2.33
Mo	(ppm; ICP-MS)	0.40	0.58	0.64	0.90	4.98	1.30	0.08	0.55
Nd	(ppm; ICP-MS)	67.43	76.22	19.77	51.08	76.27	6.56	10.66	126.59
Ni	(ppm; ICP-MS)	-	4.80	-	-	-	-	-	-
Pb	(ppm; ICP-MS)	12.70	9.40	5.90	5.90	38.80	11.20	11.70	10.00
Pr	(ppm; ICP-MS)	18.11	20.13	4.62	13.08	18.67	1.73	2.82	31.17
Rb	(ppm; ICP-MS)	182.85	179.84	118.55	93.22	229.44	190.45	189.31	156.65
Sb	(ppm; ICP-MS)	0.49	0.49	0.08	0.05	0.24	1.85	0.43	0.47
Sc	(ppm; ICP-MS)	1.70	2.50	-	1.10	1.10	1.20	1.20	-
Sm	(ppm; ICP-MS)	13.62	15.49	5.34	9.33	19.70	2.34	2.82	27.95
Sr	(ppm; ICP-MS)	10.36	21.12	5.44	16.50	4.32	9.98	7.73	18.34
Ta	(ppm; ICP-MS)	2.48	2.32	0.93	0.40	4.22	2.33	2.26	3.64
Tb	(ppm; ICP-MS)	2.12	2.27	1.04	0.99	3.91	1.24	0.97	4.33
Ti	(ppm; ICP-MS)	923.00	1525.00	1874.00	1013.00	1355.00	650.00	601.00	1134.00
Tl	(ppm; ICP-MS)	0.88	0.88	0.55	0.46	1.09	1.06	1.22	0.81
Tm	(ppm; ICP-MS)	1.39	1.38	0.71	0.35	2.66	1.17	0.94	2.45
U	(ppm; ICP-MS)	7.34	7.05	2.48	0.60	8.86	3.81	5.48	7.18
W	(ppm; ICP-MS)	1.02	1.37	0.23	0.42	1.52	1.95	0.28	1.67
Yb	(ppm; ICP-MS)	9.04	9.08	4.71	2.59	17.44	7.75	6.11	15.81
Zn	(ppm; ICP-MS)	42.00	41.00	69.00	61.00	185.00	88.00	104.00	147.00
Be	(ppm; ICP-OES)	3.00	2.80	3.40	2.40	5.70	2.50	4.50	9.50
Ca	(ppm; ICP-OES)	109.00	152.00	34.00	98.00	102.00	29.00	29.00	152.00
Cu	(ppm; ICP-OES)	1.00	-	-	7.00	-	2.00	-	3.00
Hf	(ppm; ICP-OES)	13.00	14.00	4.00	1.00	23.00	9.00	7.00	24.00
Nd	(ppm; ICP-OES)	52.00	61.00	15.00	42.00	41.00	4.00	8.00	95.00
Sn	(ppm; ICP-OES)	8.00	6.00	7.00	4.00	10.00	7.00	7.00	10.00
Th	(ppm; ICP-OES)	23.00	22.00	4.00	2.00	21.00	27.00	19.00	19.00
V	(ppm; ICP-OES)	9.00	18.00	9.00	10.00	7.00	10.00	7.00	9.00
F	(ppm; fusion)	200.00	2600.00	200.00	-	400.00	400.00	600.00	400.00

	3009	3010	3011	3012	3013	3014	3015	3016	3017	3018
	2009	2009	2009	2009	2009	2009	2009	2009	2009	2009
	Qtz-Ksp	Qtz-Ksp	rhyolite	Qtz-Ksp	rhyolite	rhyolite	Qtz-Ksp	rhyolite	Qtz-Ksp	Am-Pyx
	porphyry	porphyry		porphyry			porphyry		porphyry	granite
	Sq	Sq	Ssf	Sq	Ssf	Ssf	Sq	Ssf	Sq	Sp
	outcrop	outcrop	float	outcrop	outcrop	outcrop	outcrop	outcrop	outcrop	outcrop
	480587	482905	484032	485947	485965	479915	478003	478003	486292	531004
	5427537	5422717	5422774	5423197	5423291	5424425	5423970	5423970	5420339	5433773
SiO2	76.90	75.80	78.20	75.00	77.00	72.50	77.40	77.40	76.80	75.40
Al2O3	12.40	11.80	11.70	12.00	12.00	13.70	10.30	9.62	10.90	11.40
Fe2O3	2.62	2.80	1.26	2.63	1.39	2.09	3.62	2.67	2.71	2.77
K2O	3.56	4.87	1.41	4.85	5.17	4.80	2.47	6.07	4.66	4.15
Na2O	2.80	3.97	5.65	4.19	3.58	4.46	3.95	1.48	3.87	3.89
MgO	0.31	0.15	0.05	0.08	0.03	0.34	0.10	0.04	0.03	0.14
MnO	0.05	0.07	-	0.05	-	0.05	0.02	0.04	0.04	0.10
P2O5	0.05	0.04	0.02	0.03	0.03	0.06	0.04	0.02	0.02	0.03
CaO	0.05	0.19	0.06	0.32	0.04	0.49	0.08	0.18	0.11	0.04
TiO2	0.30	0.26	0.10	0.28	0.26	0.39	0.21	0.18	0.19	0.16
Ba	50.00	162.00	34.00	167.00	123.00	588.00	52.00	118.00	32.00	520.00
LOI	1.70	0.70	1.00	0.60	0.80	1.10	1.00	0.80	0.60	1.00
ASI	1.45	0.97	1.07	0.94	1.04	1.02	1.11	1.03	0.94	1.04
Ga/Al	3.26	3.39	2.63	3.30	3.32	2.23	3.58	2.55	4.05	3.35
Al	1.47	1.00	1.08	0.99	1.04	1.09	1.12	1.07	0.96	1.05
Cl	135.25	235.27	168.38	137.34	167.69	168.01	97.95	224.83	124.42	168.09
Nb	35.18	37.39	35.03	32.81	39.78	29.11	73.37	41.97	56.98	31.42
S	156.36	130.70	199.55	125.08	158.13	144.00	134.32	131.24	120.41	121.79
Y	63.59	74.30	60.38	62.17	74.17	54.94	175.50	102.14	115.29	74.09
Zr	595.64	643.54	284.84	555.29	709.90	463.44	1690.87	917.15	1176.17	703.53
Bi	-	0.16	0.20	0.15	0.16	0.23	0.17	-	0.30	0.15
Cd	0.14	0.23	0.06	0.17	0.28	0.17	0.24	0.16	0.18	0.14
Co	0.90	0.57	0.14	0.47	0.20	2.35	0.93	0.57	-	0.51
Cr	6.00	12.00	6.00	10.00	11.00	14.00	17.00	14.00	18.00	10.00
Cs	7.42	1.07	0.26	0.90	0.33	1.05	0.79	0.74	1.42	0.38
Dy	13.46	15.46	11.23	12.91	14.51	10.79	34.23	20.89	22.77	14.60
Er	8.30	9.24	7.49	8.02	9.44	6.65	21.20	12.55	14.99	10.15
Eu	1.22	1.65	0.12	1.56	1.09	1.29	2.09	1.90	1.39	1.00

	3009	3010	3011	3012	3013	3014	3015	3016	3017	3018
Ga	27.68	27.33	21.08	27.11	27.27	20.85	25.24	16.77	30.22	26.13
Gd	10.90	14.91	5.16	12.37	10.52	10.47	27.18	19.92	16.66	7.71
Ho	2.81	3.15	2.45	2.67	3.10	2.19	7.18	4.24	4.87	3.25
In	0.18	0.18	0.07	0.17	0.13	0.07	0.13	0.13	0.20	0.15
La	59.44	85.22	2.93	73.08	44.15	71.59	70.78	98.08	42.97	14.46
Li	6.60	24.70	3.90	26.90	1.70	9.70	1.80	1.80	43.00	4.00
Lu	1.22	1.35	1.05	1.21	1.45	0.96	2.89	1.75	2.15	1.57
Mo	0.37	1.63	4.50	3.37	3.01	4.79	1.54	1.12	4.89	2.03
Nd	59.56	86.96	3.21	75.03	46.85	62.97	94.15	103.36	51.97	20.30
Ni	-	-	-	-	-	1.60	2.50	-	-	-
Pb	6.30	18.40	4.20	17.00	11.40	55.10	10.80	8.60	27.90	68.90
Pr	15.59	22.20	0.79	19.19	11.61	17.05	22.47	26.04	12.75	4.87
Rb	215.89	125.37	48.69	122.58	134.15	152.17	87.96	195.27	178.27	110.57
Sb	0.39	0.15	0.46	0.09	0.39	0.43	1.01	0.79	0.18	0.42
Sc	1.60	1.60	1.80	1.50	1.40	5.00	1.30	-	-	1.50
Sm	11.80	16.83	2.15	14.60	9.92	11.90	24.24	21.35	14.56	5.79
Sr	13.88	14.04	12.73	27.11	13.85	9.74	9.69	52.72	12.34	10.90
Ta	1.81	1.97	2.17	1.98	2.07	1.79	4.48	2.72	3.36	1.82
Tb	2.00	2.42	1.47	2.03	2.06	1.70	5.20	3.27	3.27	1.89
Ti	1505.00	1531.00	641.00	1551.00	1584.00	2348.00	1178.00	1146.00	1174.00	1016.00
Tl	1.02	0.62	0.25	0.66	0.77	0.90	0.47	1.11	0.99	0.62
Tm	1.22	1.37	1.14	1.18	1.43	0.99	3.12	1.84	2.25	1.54
U	3.36	3.75	6.72	2.99	5.05	6.19	8.22	3.93	7.20	40.89
W	0.48	0.26	0.30	0.40	0.67	1.06	1.59	4.36	1.30	0.48
Yb	7.88	9.05	7.28	7.78	9.50	6.47	20.07	11.75	14.62	10.18
Zn	167.00	103.00	42.00	90.00	76.00	76.00	102.00	81.00	147.00	140.00
Be	5.80	3.10	2.60	2.80	1.50	3.10	3.70	2.00	5.90	4.20
Ce	192.00	166.00	8.00	127.00	81.00	79.00	156.00	145.00	88.00	72.00
Cu	1.00	1.00	-	1.00	5.00	7.00	-	1.00	-	21.00
Hf	10.00	11.00	8.00	10.00	12.00	7.00	32.00	18.00	23.00	14.00
Nd	49.00	69.00	2.00	54.00	38.00	37.00	70.00	79.00	36.00	13.00
Sn	6.00	6.00	7.00	6.00	7.00	5.00	15.00	8.00	11.00	11.00
Th	11.00	13.00	21.00	12.00	13.00	18.00	29.00	17.00	21.00	12.00
V	11.00	10.00	10.00	10.00	11.00	23.00	13.00	9.00	8.00	11.00
F	900.00	400.00	200.00	300.00	100.00	900.00	700.00	100.00	200.00	-

	3019	3020	3021	3022	3023	3024	3025	3026	3027	3028
	2009	2009	2009	2009	2009	2009	2009	2009	2009	2009
	Am-Pyx granite Sp	Am-Pyx granite Sp	rhyolite Ssf	lapilli tuff Ssf	basalt Ssm	basalt Ssm	grano- diorite HMC	rhyolite Ssf	rhyolitic tuff Ssf	aplite dyke Sdc
	outcrop	outcrop	outcrop	outcrop	outcrop	outcrop	outcrop	outcrop	outcrop	outcrop
	531020	532283	493571	494842	494579	493152	494860	494827	494827	486897
	5433802	5432834	5424740	5420183	5416909	5426101	5420185	5420197	5420197	5413235
SiO ₂	77.20	74.70	75.30	74.50	51.50	58.60	65.50	75.60	70.20	77.00
Al ₂ O ₃	11.70	11.80	12.30	13.90	17.70	17.00	13.90	11.90	14.30	11.60
Fe ₂ O ₃	2.17	2.45	2.30	1.32	10.40	6.47	3.66	2.50	2.86	2.44
K ₂ O	3.56	4.35	3.75	2.27	0.30	0.64	5.12	4.36	4.59	3.46
Na ₂ O	4.53	4.53	4.26	4.98	3.49	6.14	2.68	3.86	2.54	4.55
MgO	0.10	0.17	0.26	0.80	4.50	3.48	1.60	0.10	1.09	0.05
MnO	0.03	0.05	0.05	0.06	0.17	0.08	0.08	0.04	0.11	0.02
P ₂ O ₅	0.03	0.04	0.03	0.05	0.41	0.18	0.16	0.02	0.11	0.02
CaO	0.06	0.24	0.42	1.15	6.49	2.94	3.49	0.48	1.33	0.20
TiO ₂	0.20	0.17	0.23	0.22	2.25	1.13	0.38	0.16	0.33	0.10
Ba	341.00	410.00	1080.00	878.00	121.00	144.00	2060.00	285.00	575.00	243.00
LOI	0.80	0.60	1.10	1.20	2.60	3.70	2.80	0.80	1.70	0.60
ASI	1.02	0.94	1.04	1.09	0.99	1.05	0.85	1.00	1.24	1.00
Ga/Al	3.24	3.37	1.59	1.35	1.82	1.56	1.40	3.21	2.80	4.87
Al	1.03	0.97	1.11	1.31	2.92	1.57	1.40	1.08	1.56	1.03
Cl	142.29	125.11	104.48	78.56	89.46	190.93	187.93	48.26	58.38	157.66
Nb	32.23	30.86	22.21	13.64	11.54	10.48	6.42	52.55	19.59	476.92
S	110.27	132.40	126.65	132.62	148.94	134.68	410.05	946.61	132.82	111.30
Y	104.55	88.53	52.20	23.87	28.58	30.43	8.89	111.99	37.02	227.04
Zr	782.66	831.59	583.68	128.30	213.01	311.49	134.38	1041.08	262.71	2291.01
Bi	0.22	0.20	-	-	-	-	-	0.15	0.18	1.43
Cd	0.11	0.47	0.09	0.07	0.07	0.09	0.05	0.29	0.09	0.29
Co	0.36	0.51	0.40	2.44	32.64	30.21	10.24	1.43	4.90	0.48
Cr	9.00	8.00	17.00	19.00	18.00	40.00	30.00	15.00	29.00	15.00
Cs	0.30	0.56	0.82	0.91	1.09	0.98	1.00	1.11	2.94	0.99
Dy	21.65	18.64	10.62	4.55	6.38	6.21	1.94	22.38	7.71	32.65
Er	14.13	12.16	6.78	2.83	3.57	3.65	1.02	13.94	4.78	33.65
Eu	2.02	2.48	1.70	0.88	2.19	1.63	0.91	1.00	1.14	1.22

	3019	3020	3021	3022	3023	3024	3025	3026	3027	3028
Ga	25.95	27.22	13.34	12.80	21.98	18.10	13.31	26.15	27.42	39.39
Gd	14.90	15.88	8.98	4.22	6.68	5.92	2.60	19.56	7.03	15.43
Ho	4.65	3.90	2.24	0.93	1.27	1.25	0.37	4.63	1.60	8.41
In	0.12	0.16	0.09	0.03	0.09	0.05	0.02	0.14	0.05	0.17
La	33.61	60.08	37.26	33.38	23.60	20.70	35.40	79.98	42.26	76.56
Li	3.00	16.60	2.90	6.10	29.80	64.50	10.70	1.90	14.10	0.70
Lu	1.99	1.82	0.99	0.44	0.47	0.53	0.14	1.98	0.69	8.20
Mo	0.69	0.65	0.47	3.55	0.41	0.42	1.88	1.59	0.38	1.90
Nd	41.63	72.81	40.69	26.77	30.38	24.70	23.44	87.68	37.81	58.76
Ni	-	-	-	4.10	27.60	57.90	13.80	-	15.10	-
Pb	9.60	24.70	17.90	9.20	12.60	6.40	21.00	21.70	15.80	27.10
Pr	10.06	17.87	10.00	7.56	6.91	6.01	6.65	22.14	10.15	16.90
Rb	93.71	112.75	110.54	74.51	16.04	26.61	123.03	129.10	188.63	225.18
Sb	0.14	0.19	1.19	0.30	0.72	1.01	0.46	0.21	0.21	0.47
Sc	1.80	1.50	8.60	4.40	26.30	22.30	9.60	-	6.90	-
Sm	11.84	16.97	9.01	5.04	6.88	5.81	3.67	20.05	7.59	14.47
Sr	7.19	5.92	12.08	11.93	46.92	181.64	473.06	233.68	389.87	80.80
Ta	2.02	1.78	1.27	1.00	0.60	0.63	0.34	3.49	1.34	62.68
Tb	3.07	2.78	1.58	0.70	1.04	0.99	0.35	3.42	1.18	3.85
Ti	1142.00	928.00	1427.00	1318.00	13442.00	6970.00	2344.00	988.00	2314.00	559.00
Tl	0.47	0.56	0.74	0.45	0.11	0.13	0.72	0.69	0.89	0.44
Tm	2.09	1.86	1.01	0.43	0.50	0.54	0.15	2.13	0.71	6.76
U	6.11	4.76	3.78	4.60	0.70	2.38	2.77	9.30	4.89	78.62
W	0.36	0.30	3.44	0.88	1.05	0.93	0.53	0.79	2.19	3.25
Yb	13.43	12.22	6.64	2.86	3.14	3.51	0.93	13.67	4.63	53.81
Zn	40.00	152.00	36.00	66.00	134.00	75.00	68.00	41.00	59.00	51.00
Be	3.40	5.00	2.50	1.90	1.20	2.20	1.10	6.50	4.60	45.80
Ce	146.00	129.00	86.00	52.00	46.00	39.00	52.00	157.00	78.00	82.00
Cu	-	-	-	150.00	21.00	14.00	479.00	1410.00	25.00	3.00
Hf	15.00	17.00	10.00	3.00	4.00	6.00	1.00	21.00	6.00	91.00
Nd	29.00	51.00	38.00	19.00	24.00	19.00	18.00	64.00	29.00	37.00
Sn	8.00	7.00	4.00	1.00	-	-	-	6.00	3.00	63.00
Th	14.00	14.00	11.00	14.00	3.00	7.00	15.00	26.00	15.00	208.00
V	11.00	10.00	10.00	24.00	226.00	125.00	95.00	10.00	38.00	8.00
F	-	500.00	500.00	300.00	600.00	800.00	400.00	100.00	700.00	300.00

	3029	3030	3031	3032	3033	3034	3035	3036	3037	3038
	2009	2009	2009	2009	2009	2009	2009	2009	2009	2009
	Am-Pyx granite Smg	rhyolite Ssf	rhyolite Ssf	rhyolite Ssf	rhyolite Ssf	Am-Pyx granite Smg	diabase dyke Sda	lapilli tuff Ssf	tuff Ssf	diorite Sa
	outcrop	outcrop	outcrop	outcrop	outcrop	outcrop	outcrop	outcrop	outcrop	outcrop
	494701	491455	491726	491729	494825	494797	494803	494807	515165	488639
	5420085	5426493	5423754	5423754	5420196	5420194	5420189	5420185	5458980	5396212
SiO2	76.20	78.10	77.20	69.70	76.80	75.50	49.60	69.00	76.10	56.30
Al2O3	11.00	11.70	11.00	12.90	11.20	11.10	15.70	15.50	10.90	14.10
Fe2O3	2.76	1.03	0.98	4.51	2.47	3.03	11.60	3.33	3.34	8.98
K2O	4.36	3.70	7.54	5.25	4.20	4.53	1.66	2.66	4.20	2.20
Na2O	3.80	4.08	1.27	3.03	3.94	3.64	2.72	3.09	4.44	3.69
MgO	0.04	0.07	0.04	1.03	0.03	0.08	6.11	2.60	0.11	3.62
MnO	-	-	-	0.11	0.03	0.07	0.20	0.07	0.06	0.13
P2O5	0.03	0.01	0.02	0.19	0.02	0.03	0.50	0.16	0.03	0.34
CaO	0.04	0.03	0.04	1.15	0.25	0.24	8.48	1.99	0.14	8.08
TiO2	0.19	0.11	0.10	0.83	0.16	0.23	2.34	0.53	0.18	2.26
Ba	56.00	56.00	110.00	249.00	330.00	566.00	293.00	647.00	54.00	269.00
LOI	0.60	1.00	1.10	1.70	0.60	0.80	1.70	2.10	0.70	1.00
ASI	1.00	1.09	1.07	1.01	0.98	0.98	0.72	1.34	0.90	0.61
Ga/Al	4.00	3.43	1.92	3.27	2.98	3.63	1.84	1.67	4.27	2.30
Al	1.00	1.09	1.07	1.21	1.02	1.02	2.50	1.95	0.92	1.67
Cl	94.89	120.52	126.14	88.65	53.65	110.01	98.66	74.68	141.27	233.07
Nb	51.54	51.96	33.37	36.61	52.72	43.90	10.59	13.66	72.51	17.42
S	117.07	117.75	2952.97	4342.03	142.91	2247.96	1387.24	215.22	131.87	133.77
Y	105.24	66.12	55.64	71.46	109.40	88.53	35.78	24.23	175.62	40.81
Zr	1067.95	657.39	244.36	384.26	1019.03	814.94	253.81	170.79	1726.54	279.07
Bi	0.29	0.39	0.42	-	-	0.35	-	0.24	0.64	-
Cd	0.16	0.09	0.03	0.11	0.19	0.49	0.20	0.12	0.25	0.08
Co	0.19	0.14	0.36	7.35	1.00	1.86	47.31	10.51	0.25	24.78
Cr	24.00	5.00	13.00	20.00	38.00	14.00	152.00	24.00	16.00	68.00
Cs	0.97	0.43	1.23	1.43	1.08	0.78	17.34	3.41	0.79	0.22
Dy	20.58	14.17	9.42	14.10	21.41	19.02	7.50	4.97	33.68	8.38
Er	14.35	9.10	7.12	9.79	13.48	11.79	4.25	3.05	22.03	4.94
Eu	1.46	0.19	0.07	1.09	0.92	1.77	2.51	1.19	1.89	2.11

	3029	3030	3031	3032	3033	3034	3035	3036	3037	3038
Ga	30.10	27.42	14.42	28.82	22.84	27.57	19.72	17.70	31.79	22.20
Gd	15.93	10.36	3.24	12.66	18.48	17.99	7.97	4.99	26.65	8.13
Ho	4.56	3.03	2.20	3.07	4.48	3.94	1.49	1.03	7.31	1.70
In	0.20	0.18	0.28	0.13	0.08	0.25	0.08	0.04	0.20	0.09
La	69.89	4.73	3.77	67.45	75.16	96.87	23.40	34.96	66.06	29.27
Li	0.80	4.00	1.20	16.10	1.00	1.60	13.70	24.00	5.00	3.30
Lu	2.13	1.37	0.99	1.35	1.88	1.75	0.55	0.47	3.05	0.69
Mo	1.18	0.69	2.04	1.09	11.12	7.57	1.07	0.19	0.54	0.88
Nd	79.72	11.98	4.80	63.96	82.62	99.16	33.12	29.70	90.26	34.92
Ni	-	-	-	5.30	-	-	82.00	11.60	-	27.00
Pb	20.80	7.30	18.10	23.70	19.70	40.50	6.00	13.80	68.20	3.90
Pr	20.05	2.36	1.24	17.05	20.94	25.15	7.48	7.97	21.49	8.39
Rb	149.97	125.48	315.75	220.24	107.68	120.21	115.25	103.19	189.82	54.22
Sb	0.27	0.28	0.59	1.23	0.22	0.09	0.14	0.51	0.43	0.13
Sc	-	-	1.80	10.10	-	1.30	34.00	11.00	-	27.40
Sm	17.15	7.23	1.82	13.46	18.82	19.89	7.84	5.69	24.36	8.14
Sr	181.51	53.65	314.24	667.86	0.14	6.18	14.82	24.87	70.14	54.08
Ta	3.18	2.93	2.11	2.27	3.36	2.76	0.77	0.93	4.53	1.10
Tb	2.93	2.11	1.06	2.15	3.28	2.96	1.24	0.79	4.95	1.33
Ti	1139.00	678.00	601.00	4911.00	929.00	1672.00	14298.00	3506.00	1084.00	12226.00
Tl	0.81	0.66	2.33	1.32	0.62	0.53	0.86	0.49	0.94	0.27
Tm	2.19	1.42	1.09	1.50	2.01	1.78	0.59	0.47	3.27	0.72
U	6.75	6.79	6.72	8.66	8.82	5.50	1.31	4.28	6.95	2.45
W	1.14	1.34	0.42	1.84	1.01	1.01	0.27	1.54	0.72	0.60
Yb	14.42	9.40	7.04	9.29	13.03	11.57	3.77	3.11	20.92	4.61
Zn	139.00	67.00	12.00	94.00	22.00	108.00	101.00	67.00	205.00	84.00
Be	5.70	3.30	2.70	4.60	6.30	4.60	0.90	2.10	8.20	2.00
Ce	125.00	26.00	8.00	122.00	153.00	171.00	46.00	69.00	189.00	60.00
Cu	4.00	2.00	9.00	4.00	11.00	2340.00	59.00	16.00	11.00	7.00
Hf	20.00	16.00	7.00	9.00	20.00	14.00	5.00	4.00	34.00	5.00
Nd	58.00	7.00	2.00	51.00	62.00	73.00	28.00	26.00	68.00	29.00
Sn	11.00	8.00	13.00	4.00	5.00	9.00	-	-	13.00	-
Th	20.00	21.00	21.00	22.00	25.00	17.00	3.00	12.00	67.00	9.00
V	10.00	12.00	8.00	72.00	9.00	10.00	268.00	70.00	9.00	245.00
F	-	-	200.00	1100.00	-	-	400.00	700.00	100.00	600.00

	3039	3040	3041	3088	3089	3094	3095	3096	3097	3098
	2009	2009	2009	2010	2010	2010	2010	2010	2010	2010
	gabbro	granite	rhyolite	Qtz-Ksp	mafic	mafic	tuff	Qtz-Ksp	diorite	Afs- granite
	dyke	porphyry	porphyry	porphyry	volcanic	volcanic		porphyry		
	Sda	Ssya	Ssf	Smg	Sda	Ssm	Ssf	Sq	HMC	HMC
	outcrop	outcrop	outcrop	outcrop	outcrop	outcrop	outcrop	float	outcrop	outcrop
	488640	524424	523527	484762	484748	539433	491635	491636	491631	491667
	5396212	5418481	5418301	5420173	5420181	5451820	5427086	5427088	5427077	5427125
SiO2	48.90	74.50	72.50	78.10	55.80	49.00	71.70	75.30	58.30	70.60
Al2O3	15.20	12.10	14.30	10.80	16.90	19.40	14.30	11.30	16.20	9.25
Fe2O3	12.30	3.35	2.20	2.99	8.21	10.00	2.90	2.61	7.87	9.44
K2O	1.48	4.52	4.26	4.70	1.15	1.41	2.39	4.49	1.42	1.49
Na2O	3.28	4.39	4.70	3.39	5.71	4.48	3.31	4.02	2.52	0.04
MgO	5.62	0.08	0.40	0.04	4.04	6.19	1.15	0.08	3.74	3.76
MnO	0.21	0.08	0.05	0.04	0.24	0.16	0.05	0.07	0.14	0.16
P2O5	0.41	0.05	0.07	0.02	0.30	0.21	0.14	-	0.08	0.09
CaO	7.89	0.27	1.06	0.23	5.68	7.73	1.74	0.30	5.99	0.61
TiO2	2.57	0.28	0.39	0.19	1.20	1.38	0.39	0.23	0.58	0.45
Ba	303.00	1140.00	809.00	390.00	464.00	262.00	2140.00	128.00	459.00	100.00
LOI	1.90	0.60	0.50	0.30	1.40	1.00	3.00	1.30	3.30	4.40
ASI	0.71	0.96	1.00	0.97	0.81	0.85	1.28	0.94	0.98	3.32
Ga/Al	2.10	3.19	1.78	3.22	1.37	1.36	1.56	3.08	1.55	1.65
Al	2.17	1.00	1.16	1.01	1.59	2.18	1.78	0.98	2.85	5.51
Cl	180.88	122.99	144.05	105.74	152.48	1416.86	114.94	203.28	121.76	100.01
Nb	10.75	23.82	16.08	46.83	9.01	6.51	4.08	41.93	9.07	3.93
S	495.80	129.69	120.49	744.05	161.56	369.84	889.99	1274.89	469.48	5190.23
Y	33.28	60.77	37.39	88.82	22.47	24.52	8.65	80.16	32.89	10.77
Zr	215.06	568.30	424.27	810.31	189.34	113.16	105.97	735.69	30.21	47.47
Bi	-	0.17	-	0.63	-	-	-	0.16	0.25	2.29
Cd	0.44	0.23	0.14	0.25	0.21	0.46	0.12	0.37	0.07	0.08
Co	40.91	0.33	1.69	1.14	27.82	47.79	7.23	0.61	21.04	38.12
Cr	150.00	6.00	15.00	10.00	50.00	81.00	33.00	6.00	50.00	49.00
Cs	0.92	0.95	2.17	0.64	1.75	16.60	4.40	0.51	3.92	3.02
Dy	7.00	11.76	6.81	19.62	4.61	4.95	1.84	17.45	7.12	2.12
Er	3.89	7.93	4.43	12.03	2.62	2.87	0.98	10.49	4.00	1.20
Eu	2.29	2.28	1.27	1.68	1.56	1.61	0.91	1.82	1.54	0.63

	3099	3100	3152	3153	3176	3177	3178	3179	3180	3181
	2010	2010	2010	2010	2010	2010	2010	2010	2010	2010
	gabbro	tuff	granitic dyke	Am-Bt granite	ultramafic	Qtz-Ksp porphyry	Qtz-Ksp porphyry	aplite dyke	aplite dyke	Am-Pyx granite
	HMC	Ssf	Sdc	Sm	Ssm	Sq	Sq	Sdc	Sdc	Sm
	outcrop	outcrop	outcrop	outcrop	outcrop	outcrop	outcrop	outcrop	outcrop	outcrop
	491747	491756	494490	489171	486484	486582	493278	494373	494463	489157
	5427111	5427017	5410307	5410303	5408625	5408555	5413777	5410309	5410294	5410311
SiO2	52.70	74.00	76.30	75.70	38.20	79.80	77.00	77.00	77.00	75.40
Al2O3	16.80	14.60	11.20	12.20	19.60	10.00	10.70	10.30	11.10	11.60
Fe2O3	11.00	2.60	3.68	2.66	19.30	1.76	2.73	3.04	2.12	2.71
K2O	1.39	2.89	4.66	4.67	4.33	5.03	4.84	6.75	3.72	4.70
Na2O	1.03	3.43	4.38	4.25	0.34	1.66	3.70	2.18	4.28	4.50
MgO	5.76	0.69	0.17	0.12	6.04	0.21	0.07	0.14	0.05	0.09
MnO	0.14	0.01	0.07	0.09	0.50	0.03	0.06	0.12	0.01	0.07
P2O5	0.09	0.11	0.02	-	0.85	-	-	-	-	-
CaO	8.77	0.24	0.46	0.30	1.73	0.72	0.19	0.45	0.18	0.30
TiO2	0.77	0.34	0.27	0.21	4.66	0.16	0.19	0.23	0.13	0.20
Ba	271.00	421.00	133.00	808.00	110.00	629.00	58.00	158.00	62.00	710.00
LOI	1.80	1.90	0.40	0.50	4.60	0.60	0.30	0.40	0.20	0.30
ASI	0.88	1.59	0.86	0.97	2.34	1.05	0.92	0.88	0.97	0.89
Ga/Al	1.34	1.65	3.98	3.08	2.35	2.56	3.71	3.28	3.36	3.30
Al	5.25	1.66	0.91	1.01	3.74	1.22	0.94	0.95	1.00	0.93
Cl	194.05	116.30	146.54	178.17	1955.27	98.37	140.46	113.06	129.16	231.72
Nb	6.14	2.87	20.07	42.04	19.49	20.90	49.17	247.58	40.90	45.12
S	1049.37	348.40	151.52	123.14	23340.70	193.79	145.40	150.69	115.34	142.89
Y	9.68	7.85	30.70	94.32	53.17	63.97	106.11	224.19	58.77	57.72
Zr	61.88	110.93	290.65	718.18	365.34	542.33	1037.50	3241.80	668.76	775.56
Bi	-	-	-	0.21	-	-	0.17	0.82	0.22	0.25
Cd	0.06	0.07	0.13	0.45	0.21	0.10	0.19	0.52	0.09	0.29
Co	44.57	3.86	1.22	0.66	49.98	0.38	0.56	1.09	0.48	0.56
Cr	36.00	25.00	5.00	8.00	38.00	13.00	9.00	9.00	6.00	6.00
Cs	1.88	3.32	0.34	0.39	7.69	0.58	0.69	0.88	0.38	1.70
Dy	1.99	1.56	7.19	20.47	7.69	13.61	21.49	55.72	10.81	12.02
Er	1.11	0.87	4.51	12.29	4.38	8.31	13.54	30.70	7.91	8.59
Eu	0.69	0.67	0.99	3.17	2.24	1.94	1.57	6.99	0.64	1.77

	3183	3184	3185	3186	3187	3188	3230	3231	3232	3233
	2010	2010	2010	2010	2010	2010	2010	2010	2010	2010
	Am-Pyx Granite	Granite dike	Gabbro	Gabbro	Diabase dike	Am-Pyx Granite	Rhyolite	Qtz-Ksp Porphyry	Qtz-Ksp Porphyry	Qtz-Ksp Porphyry
	Sp	Sdc	Ssy	Sa	Sda	Smg	Ssf	Sq	Sq	Sq
	outcrop	outcrop	outcrop	outcrop	outcrop	outcrop	outcrop	outcrop	outcrop	outcrop
	483294	486648	484557	482201	482370	494886	491614	486756	486571	487727
	5404148	5403392	5403367	5405397	5405425	5420310	5426872	5420166	5420343	5420458
SiO2	76.50	72.00	46.20	52.00	44.00	76.10	79.40	78.60	87.60	77.40
Al2O3	12.10	14.70	13.80	15.20	14.20	11.00	10.50	9.84	5.09	10.70
Fe2O3	1.69	2.76	16.50	10.60	15.50	3.25	1.76	2.69	2.42	2.77
K2O	5.20	2.46	0.59	1.03	0.84	4.57	5.04	3.55	1.13	4.66
Na2O	3.76	6.32	2.70	3.37	3.64	3.63	2.68	3.36	1.34	4.05
MgO	0.13	0.45	6.03	6.40	6.06	0.13	0.20	0.69	0.76	0.04
MnO	0.01	0.02	0.19	0.16	0.23	0.03	0.02	0.06	0.04	0.05
P2O5	-	0.07	0.23	0.18	1.05	0.10	-	-	-	-
CaO	0.09	1.40	9.82	7.71	8.33	0.21	0.24	0.19	0.07	0.20
TiO2	0.16	0.46	3.04	2.09	3.97	0.24	0.11	0.17	0.08	0.20
Ba	592.00	510.00	243.00	182.00	342.00	660.00	48.00	34.00	40.00	31.00
LOI	0.40	0.50	0.80	1.30	2.70	0.60	0.80	0.90	1.00	0.40
ASI	1.01	0.94	0.60	0.74	0.64	0.97	1.02	1.01	1.43	0.89
Ga/Al	2.68	1.92	1.93	1.62	2.01	3.27	3.28	3.82	4.75	3.74
Al	1.02	1.13	2.72	2.28	2.06	1.01	1.06	1.05	1.49	0.91
Cl	201.35	128.16	174.84	235.20	179.17	117.19	133.40	161.51	122.91	99.34
Nb	33.78	17.09	6.81	12.99	17.72	42.99	40.53	54.89	20.66	57.76
S	115.40	307.35	714.05	269.22	1161.04	345.64	230.10	125.67	161.96	133.57
Y	55.28	48.92	26.29	26.30	47.67	91.91	72.35	152.21	45.23	109.69
Zr	315.42	750.32	123.28	140.72	340.32	778.49	515.15	1168.90	451.67	1192.97
Bi	0.25	-	-	-	-	-	0.15	0.30	1.00	0.32
Cd	0.12	0.13	0.16	0.17	0.20	0.19	0.11	0.41	0.07	0.26
Co	0.93	6.07	56.38	44.03	40.86	1.57	0.31	0.52	1.87	0.40
Cr	9.00	7.00	44.00	136.00	95.00	6.00	6.00	7.00	10.00	9.00
Cs	0.30	0.13	0.49	1.87	2.20	0.75	1.28	0.54	0.12	1.39
Dy	10.16	9.64	5.44	5.31	10.08	22.24	12.28	32.92	8.16	22.48
Er	7.16	6.51	3.07	3.16	5.46	12.58	8.37	17.46	5.77	14.31
Eu	1.01	2.26	1.72	1.49	3.89	2.33	0.15	3.21	0.53	1.65

	3234	3235	3242	3243	3244	3245	3246	3247	3248	3249
	2010	2010	2010	2010	2010	2010	2010	2010	2010	2010
	Pyx granite	Am-Pyx granite	Am-Pyx granite	diabase dyke	tuff breccia	lapilli tuff	Am-Pyx granite	Am-Pyx granite	diabase dyke	mafic volcanic
	Sdc	Sp	Smg	Sda	Ssf	Ssf	Smg	Smg	Sda	Ssm
	outcrop	outcrop	outcrop	outcrop	outcrop	outcrop	outcrop	outcrop	outcrop	outcrop
	486797	486797	494716	494720	494744	494763	494759	494745	494753	494746
	5413180	5413180	5420146	5420146	5420160	5420169	5420183	5420151	5420171	5420164
SiO ₂	77.00	77.90	78.00	49.60	77.80	69.50	74.30	78.80	51.80	54.00
Al ₂ O ₃	10.80	11.40	11.40	13.10	10.40	14.20	9.89	11.00	15.60	15.30
Fe ₂ O ₃	2.55	1.70	2.32	13.50	2.85	3.21	3.21	2.51	10.30	6.67
K ₂ O	0.86	4.53	2.65	2.08	3.54	3.03	4.20	4.50	1.55	0.60
Na ₂ O	5.84	4.30	4.79	2.87	3.46	2.46	3.95	3.82	2.85	5.99
MgO	0.36	0.06	0.07	3.83	0.24	1.83	0.04	0.05	6.03	2.68
MnO	0.05	0.03	0.04	0.26	0.05	0.07	0.06	0.02	0.16	0.42
P ₂ O ₅	-	-	0.10	1.28	0.16	0.11	-	-	0.35	0.30
CaO	2.07	0.07	0.09	7.33	0.32	2.48	0.12	0.12	8.09	5.93
TiO ₂	0.14	0.09	0.23	3.15	0.20	0.50	0.17	0.21	1.88	1.06
Ba	62.00	38.00	253.00	389.00	394.00	591.00	22.00	77.00	339.00	80.00
LOI	1.00	0.30	0.90	2.40	1.00	1.90	0.10	0.30	1.70	6.40
ASI	0.76	0.94	1.04	0.65	1.03	1.20	0.88	0.97	0.74	0.72
Ga/Al	4.77	3.54	2.83	2.35	3.00	1.60	4.43	3.42	1.62	1.71
Al	1.02	0.95	1.06	1.88	1.09	1.94	0.90	0.99	2.45	1.46
Cl	296.25	287.35	136.07	62.77	119.62	67.07	55.13	118.06	139.70	105.64
Nb	369.73	46.63	54.00	17.04	49.86	13.27	94.61	53.18	9.79	8.47
S	119.78	119.66	794.33	928.04	8397.34	127.72	121.87	129.11	449.02	162.37
Y	329.18	41.98	106.66	66.45	99.13	23.81	94.41	103.12	28.32	21.33
Zr	2210.11	323.97	1057.69	378.06	938.85	164.00	1680.66	962.58	173.92	163.78
Bi	0.19	0.26	0.68	-	1.37	0.26	0.51	0.29	-	-
Cd	0.38	0.16	1.24	0.24	0.19	0.11	0.34	0.36	0.24	0.07
Co	1.38	0.51	2.32	25.07	5.20	10.43	0.30	0.55	41.07	21.54
Cr	8.00	6.00	8.00	8.00	9.00	46.00	11.00	10.00	103.00	46.00
Cs	0.35	1.10	0.30	6.01	0.56	1.72	1.60	0.76	2.40	0.97
Dy	68.20	10.55	21.28	13.89	21.17	4.74	22.02	22.88	5.91	3.94
Er	49.41	8.07	14.27	7.53	13.03	2.84	14.85	13.95	3.45	2.24
Eu	2.54	0.47	1.29	4.94	1.69	1.18	1.67	1.95	1.93	1.25

	3250	3251	3252	3253	3254	3255	3256	3257	3258	3509
	2010	2010	2010	2010	2010	2010	2010	2010	2010	2009
	Am-Pyx granite	tuff	rhyolite	mafic dyke	grano- diorite	rhyolite	diorite	rhyolite	Bl-granite	Qtz-Kfs porphyry
	Smg	Ssf	Ssf	Sda	HMC	Ssf	HMC	Ssf	HMC	Sq
	outcrop	outcrop	outcrop	outcrop	outcrop	outcrop	outcrop	outcrop	outcrop	outcrop
	494805	494856	494862	494858	494859	494858	494872	494862	494723	489929
	5420195	5420217	5420208	5420204	5420188	5420212	5420216	5420228	5420084	5423383
SiO ₂	75.60	76.40	77.60	49.30	64.80	65.60	61.00	77.90	75.00	76.40
Al ₂ O ₃	11.20	13.10	11.10	15.50	14.70	16.80	16.50	11.20	12.70	10.80
Fe ₂ O ₃	2.70	1.22	2.21	11.90	6.06	3.28	6.93	2.29	3.32	2.98
K ₂ O	4.26	2.57	4.17	1.27	1.88	5.98	1.75	3.45	0.85	4.59
Na ₂ O	4.01	4.61	3.52	2.55	3.17	4.22	2.82	4.10	5.51	3.82
MgO	0.07	0.68	0.08	5.92	2.03	0.23	3.26	0.06	0.54	0.06
MnO	0.06	0.05	0.04	0.20	0.12	0.07	0.11	0.02	0.03	0.05
P ₂ O ₅	-	0.04	-	0.54	0.13	0.14	0.23	-	0.04	0.02
CaO	0.71	1.13	0.23	8.56	3.01	2.24	5.66	0.26	0.29	0.10
TiO ₂	0.21	0.20	0.15	2.38	0.53	0.27	0.73	0.16	0.25	0.18
Ba	82.00	795.00	655.00	302.00	443.00	2020.00	892.00	695.00	112.00	31.00
LOI	0.60	0.80	0.50	1.80	2.90	1.00	2.10	0.40	1.20	0.70
ASI	0.90	1.05	1.04	0.73	1.16	0.96	0.98	1.02	1.21	0.94
Ga/Al	3.26	1.36	2.58	1.71	1.31	2.92	1.55	2.54	1.69	4.16
Al	1.00	1.26	1.08	2.78	2.03	1.25	2.53	1.07	1.27	0.96
Cl	89.18	74.72	157.82	69.11	93.60	118.80	187.08	105.60	100.28	175.97
Nb	48.69	13.37	53.38	11.87	3.85	71.92	9.66	52.30	4.88	66.77
S	197.16	145.82	162.26	615.04	219.36	3924.63	235.70	138.86	124.65	136.31
Y	115.21	24.40	107.48	36.25	13.92	145.39	13.38	101.88	26.49	153.52
Zr	922.46	128.95	978.33	258.89	105.34	1252.97	178.26	974.90	108.47	1390.42
Bi	0.33	-	0.26	-	-	>47	-	0.26	-	0.35
Cd	0.49	0.04	0.30	0.16	0.05	0.66	0.06	0.19	0.13	0.37
Co	0.44	1.92	1.06	40.23	12.92	2.77	20.10	0.90	2.08	0.17
Cr	18.00	16.00	15.00	141.00	9.00	10.00	46.00	11.00	5.00	17.00
Cs	0.83	1.00	0.83	3.51	1.48	1.30	2.69	0.85	0.55	1.26
Dy	23.32	4.43	21.44	7.62	2.70	28.22	2.75	20.03	4.49	30.32
Er	14.14	2.76	13.46	4.30	1.65	18.07	1.45	12.97	2.93	18.16
Eu	1.96	0.91	0.96	2.62	0.74	1.67	1.15	0.83	0.71	2.41

[illegible]

	3510	3511	3512	3513	3514	3515	3516	3517	3518	3519
	2009	2009	2009	2009	2009	2009	2009	2009	2009	2009
	rhyolite	Am-Pyx	Am-Pyx	Am-Pyx	Am-Pyx	Am-Pyx	Am-Pyx	mafic dyke	Am-Pyx	granite
	breccia	granite	granite	granite	granite	granite	granite		granite	
	Ssf	Sp	Sp	Smg	Smg	Smg	Smg	Sda	Smg	Smg
	outcrop	outcrop	outcrop	outcrop	outcrop	outcrop	outcrop	outcrop	outcrop	outcrop
	493615	535491	534980	542907	542799	542877	543854	544870	544821	541975
	5424780	5435534	5441518	5442681	5438277	5438514	5440908	5442707	5442597	5448240
SiO ₂	80.30	76.60	76.80	74.10	75.30	76.40	77.20	53.40	76.50	76.70
Al ₂ O ₃	11.40	10.90	11.00	12.50	11.00	10.70	11.10	16.00	11.00	11.50
Fe ₂ O ₃	1.61	2.82	3.11	2.77	2.52	3.42	2.69	10.50	2.57	2.37
K ₂ O	0.23	4.04	4.48	4.05	4.38	4.20	4.46	0.93	4.37	4.42
Na ₂ O	6.29	4.14	4.25	4.10	4.36	4.52	4.35	4.35	4.30	4.47
MgO	0.04	0.06	0.05	0.38	0.07	0.05	0.13	4.20	0.10	0.10
MnO	0.01	0.04	0.04	0.05	0.04	0.05	0.04	0.18	0.05	0.05
P ₂ O ₅	0.02	0.03	0.02	0.11	0.02	0.03	0.01	0.34	0.02	0.03
CaO	0.08	0.14	0.06	1.27	0.08	0.05	0.17	7.06	0.25	0.32
TiO ₂	0.09	0.12	0.12	0.32	0.14	0.12	0.16	1.94	0.17	0.16
Ba	23.00	44.00	16.00	531.00	114.00	39.00	96.00	254.00	285.00	283.00
LOI	0.50	0.40	0.30	0.50	0.50	0.40	0.40	0.80	0.40	0.60
ASI	1.06	0.95	0.92	0.93	0.91	0.89	0.90	0.76	0.90	0.90
Ga/Al	2.94	4.18	4.29	2.77	3.91	4.69	3.92	1.91	3.64	3.68
Al	1.08	0.97	0.93	1.12	0.92	0.89	0.93	1.96	0.93	0.95
Cl	135.43	87.15	-	188.90	441.00	133.33	145.60	570.59	156.10	216.46
Nb	35.79	45.94	57.34	25.20	57.40	33.89	56.08	6.23	67.80	143.94
S	128.71	116.07	122.54	123.15	133.72	111.98	129.83	108.58	115.29	135.14
Y	55.95	77.90	69.42	79.95	73.28	87.69	125.84	33.35	118.89	289.57
Zr	357.05	942.91	1355.29	527.88	1057.32	794.65	1127.54	162.58	1227.87	1622.10
Bi	-	0.38	0.46	0.87	0.38	0.52	0.37	-	0.16	0.50
Cd	0.06	0.14	0.36	0.33	0.27	0.28	0.26	0.17	0.29	0.41
Co	0.27	0.24	0.30	3.24	0.43	0.28	0.47	32.17	0.42	0.65
Cr	31.00	10.00	8.00	12.00	10.00	5.00	10.00	21.00	11.00	6.00
Cs	0.13	0.52	1.55	2.33	2.14	1.18	2.68	2.23	2.19	5.43
Dy	10.03	16.16	13.93	16.56	16.83	15.27	26.75	6.89	24.92	55.22
Er	7.51	12.39	10.30	10.71	13.15	11.61	17.75	4.08	17.16	43.95
Eu	0.04	1.24	0.96	1.95	1.29	0.89	2.52	1.92	2.69	3.31

	3510	3511	3512	3513	3514	3515	3516	3517	3518	3519
Ga	22.95	31.17	32.28	23.67	29.38	34.31	29.75	20.88	27.35	28.92
Gd	5.57	10.54	8.72	13.89	9.72	8.61	20.78	6.65	20.48	30.39
Ho	2.28	3.68	3.17	3.52	3.85	3.56	5.75	1.41	5.43	13.15
In	0.06	0.17	0.19	0.11	0.16	0.18	0.16	0.09	0.17	0.13
La	26.40	20.74	17.42	46.22	36.28	15.94	45.90	16.85	59.55	70.14
Li	0.90	4.60	92.30	13.50	68.90	111.30	77.90	24.70	50.50	77.60
Lu	1.14	2.21	1.84	1.58	2.40	2.08	2.63	0.55	2.78	5.74
Mo	0.59	0.24	0.40	2.27	3.83	0.63	1.21	1.08	1.64	0.65
Nd	25.45	31.08	19.28	55.19	39.50	18.29	67.09	24.19	77.86	86.10
Ni	-	-	-	1.60	-	-	-	12.80	-	-
Pb	5.00	22.60	43.10	30.40	45.50	12.60	29.20	16.90	45.90	102.90
Pr	7.16	7.23	4.73	13.55	10.58	4.74	15.88	5.46	18.73	21.43
Rb	8.69	191.79	259.65	155.51	214.38	282.48	203.46	31.01	156.75	230.90
Sb	0.58	0.14	0.78	0.24	0.53	0.46	0.77	0.24	0.48	0.83
Sc	1.30	1.10	1.20	5.60	1.10	-	1.20	35.10	1.50	1.60
Sm	5.81	9.40	6.63	13.52	9.55	5.94	19.30	6.11	20.26	24.16
Sr	478.80	477.85	378.74	9.92	106.96	6.10	22.99	3.38	1.70	1.54
Ta	2.28	2.90	3.61	1.67	3.40	2.20	3.78	0.31	4.28	11.72
Tb	1.28	2.17	1.91	2.45	2.16	2.01	3.90	1.06	3.66	6.98
Ti	547.00	725.00	728.00	1983.00	949.00	777.00	902.00	12473.00	1049.00	1022.00
Tl	0.04	0.97	0.94	0.96	1.05	1.00	1.02	0.32	1.25	1.28
Tm	1.18	2.03	1.66	1.62	2.25	1.85	2.72	0.58	2.68	6.86
U	4.17	5.84	6.79	4.26	8.06	4.36	8.69	0.81	9.48	18.83
W	1.13	0.28	0.16	1.61	2.32	0.49	0.67	1.14	0.81	3.73
Yb	7.94	14.21	11.83	10.79	16.14	13.01	17.88	3.68	18.37	43.68
Zn	13.00	167.00	266.00	101.00	208.00	247.00	217.00	142.00	233.00	208.00
Be	6.30	8.60	7.20	4.20	8.00	8.20	8.70	0.60	8.80	15.10
Ce	81.00	78.00	39.00	97.00	106.00	34.00	112.00	32.00	138.00	152.00
Cu	-	-	-	14.00	1.00	2.00	-	27.00	2.00	-
Hf	10.00	20.00	30.00	9.00	25.00	21.00	32.00	3.00	29.00	38.00
Nd	20.00	21.00	9.00	43.00	29.00	9.00	48.00	21.00	57.00	59.00
Sn	6.00	13.00	15.00	6.00	15.00	18.00	15.00	-	14.00	16.00
Th	16.00	22.00	26.00	15.00	22.00	11.00	26.00	2.00	36.00	49.00
V	9.00	8.00	8.00	27.00	10.00	9.00	9.00	320.00	10.00	11.00
F	-	500.00	900.00	500.00	900.00	1100.00	1400.00	800.00	1200.00	1800.00

	3520	3521	3546	3547	3548	3549	3812	3813	3814	3815
	2009	2009	2009	2009	2009	2009	2010	2010	2010	2010
	rhyolite	granitic dyke	rhyolite	rhyolite	granitic dyke	tuff	Am-Pyx granite	Am-Pyx granite	Am-Pyx granite	rhyolite
	Ssf	Sdc	Ssf	Ssf	Sdc	Ssf	Smg	Smg	Smg	Ssf
	outcrop	outcrop	outcrop	outcrop	outcrop	outcrop	outcrop	outcrop	outcrop	outcrop
	480208	483902	494153	494153	494440	489091	494721	494661	494662	494494
	5414776	5408943	5410452	5410452	5410350	5427212	5420287	5420430	5420432	5410310
SiO ₂	74.50	72.60	77.70	75.20	75.50	76.20	76.20	78.10	77.80	76.00
Al ₂ O ₃	13.90	7.17	7.85	11.10	10.70	10.80	11.50	11.40	11.40	13.30
Fe ₂ O ₃	2.22	9.09	8.08	2.78	4.03	3.24	2.95	2.07	2.58	2.38
K ₂ O	1.31	3.24	0.18	5.54	4.59	4.50	4.76	4.97	4.80	5.03
Na ₂ O	6.95	1.83	4.17	2.66	3.40	4.40	4.10	3.54	3.61	0.22
MgO	0.15	0.17	0.12	0.14	0.11	0.04	0.09	0.03	0.04	0.91
MnO	0.04	0.32	0.02	0.01	0.13	0.06	0.06	-	0.02	0.03
P ₂ O ₅	0.03	0.06	0.06	0.02	0.04	0.04	0.01	-	-	0.06
CaO	0.17	2.38	0.67	0.20	1.27	0.18	0.28	0.03	0.13	0.29
TiO ₂	0.20	0.27	0.26	0.13	0.26	0.18	0.26	0.20	0.20	0.37
Ba	48.00	331.00	16.00	100.00	137.00	18.00	154.00	99.00	100.00	537.00
LOI	0.60	2.30	0.40	0.80	0.20	0.70	0.40	0.50	0.40	2.40
ASI	1.06	0.66	0.95	1.03	0.83	0.87	0.93	1.01	1.00	2.10
Ga/Al	2.83	7.64	6.77	3.57	4.71	4.60	3.21	3.34	3.02	2.77
Al	1.08	1.10	1.11	1.07	1.01	0.89	0.97	1.02	1.02	2.29
Cl	56.35	80.44	132.09	130.23	101.55	87.98	86.90	119.19	129.56	120.67
Nb	38.62	372.30	563.38	51.85	88.81	75.82	39.98	44.03	40.76	63.25
S	125.28	139.87	119.75	237.04	120.76	121.52	119.64	116.29	130.50	1466.43
Y	78.96	815.32	827.38	85.95	113.43	157.09	63.63	83.99	87.45	108.33
Zr	684.86	9012.33	8878.97	853.84	1821.72	1637.27	643.22	862.98	780.66	693.36
Bi	-	0.57	0.33	1.64	0.36	0.40	-	0.63	0.42	0.27
Cd	0.08	2.48	1.08	0.15	0.38	0.36	0.11	0.19	0.17	0.20
Co	0.32	1.08	1.18	1.02	2.01	0.18	0.80	0.36	5.16	0.51
Cr	14.00	8.00	15.00	11.00	7.00	21.00	4.00	5.00	47.00	7.00
Cs	0.30	0.66	0.11	0.80	0.62	1.89	0.45	0.67	4.24	0.50
Dy	15.26	110.00	126.00	15.58	23.74	31.31	14.66	17.24	13.21	20.12
Er	8.39	75.40	87.60	11.35	15.17	19.83	9.39	11.86	8.47	13.24
Eu	0.25	16.17	15.29	0.86	2.61	2.02	1.30	0.66	0.76	0.90

	3520	3521	3546	3547	3548	3549	3812	3813	3814	3815
Ga	26.93	37.47	36.32	27.13	34.45	33.98	25.21	26.05	23.52	25.21
Gd	18.51	106.00	123.00	11.67	20.42	26.83	11.63	9.35	11.28	11.82
Ho	2.95	27.00	31.00	3.55	4.94	6.62	3.04	3.79	2.75	4.33
In	0.09	0.21	0.27	0.29	0.29	0.22	0.18	0.16	0.09	0.17
La	164.66	569.71	685.63	32.98	111.81	74.33	32.58	13.67	44.42	28.23
Li	1.80	1.70	1.50	2.10	3.60	6.50	11.30	1.20	11.30	0.80
Lu	1.19	9.00	9.00	1.69	2.52	2.76	1.46	1.78	1.15	1.90
Mo	0.83	1.73	1.87	20.07	0.97	0.56	0.81	1.28	10.11	5.29
Nd	134.95	605.17	760.00	38.70	109.37	98.47	45.81	17.68	49.35	32.10
Ni	-	-	-	-	-	-	-	-	21.50	-
Pb	6.40	57.90	15.20	18.20	19.60	49.70	10.00	27.90	31.10	24.70
Pr	37.04	156.93	198.94	9.64	29.58	23.83	11.37	4.28	12.85	8.03
Rb	36.83	258.21	5.50	171.16	172.39	206.70	122.66	140.89	165.77	131.44
Sb	0.40	0.52	0.17	0.07	0.26	0.82	0.11	0.42	0.26	0.49
Sc	5.30	-	-	-	1.40	-	1.70	1.20	3.90	1.30
Sm	22.80	128.00	128.00	10.50	22.84	25.52	11.42	5.82	11.96	8.50
Sr	64.93	3.47	2.03	6.42	392.00	311.33	9.80	4.00	69.10	4.00
Ta	2.01	22.35	33.62	2.99	5.70	4.44	2.22	2.88	4.20	2.73
Tb	2.63	21.00	21.00	2.23	3.58	4.73	2.15	2.26	2.00	2.71
Ti	1191.00	1497.00	1507.00	790.00	1542.00	1059.00	1348.00	1209.00	2058.00	1082.00
Tl	0.18	0.63	0.04	0.79	0.80	0.77	0.42	0.76	1.54	0.72
Tm	1.22	48.00	62.00	1.72	2.40	2.89	1.44	1.80	1.27	1.98
U	3.86	39.20	54.05	8.40	10.28	9.45	4.30	5.89	9.56	5.20
W	1.43	1.68	4.83	1.15	0.80	1.96	0.50	0.88	0.75	0.85
Yb	7.93	76.70	93.80	11.28	16.67	18.84	9.57	11.98	8.33	12.69
Zn	37.00	491.00	65.00	45.00	143.00	214.00	80.00	82.00	62.00	86.00
Be	2.80	48.50	33.70	4.50	10.60	8.10	2.90	4.10	3.40	6.40
Ce	138.00	1170.00	1360.00	102.00	239.00	175.00	110.00	58.00	79.00	111.00
Cu	-	-	-	34.00	-	3.00	4.00	4.00	4.00	15.00
Hf	12.00	149.00	146.00	20.00	25.00	32.00	11.00	14.00	14.00	19.00
Nd	103.00	464.00	561.00	35.00	80.00	74.00	45.00	17.00	31.00	56.00
Sn	8.00	58.00	39.00	11.00	7.00	13.00	4.00	2.00	3.00	9.00
Th	15.00	122.00	164.00	21.00	33.00	29.00	15.00	16.00	17.00	32.00
V	10.00	11.00	8.00	11.00	10.00	8.00	6.00	3.00	4.00	34.00
F	300.00	300.00	100.00	100.00	800.00	100.00	N.D.	N.D.	N.D.	N.D.

	3889	3894	3895	3896	3897	3898	3899	3900	4327	4331
	2009	2009	2009	2009	2009	2009	2009	2009	2010	2010
	rhyolite	Am-Bt granite	Am-Bt granite	mafic dyke	basalt	basalt	basalt	rhyolite	Am-Bt granite	granite
	Ssf	Sm	Sm	Sda	Ssm	Ssm	Ssm	Ssf	HMC	Smg
	outcrop	outcrop	outcrop	outcrop	outcrop	outcrop	outcrop	outcrop	outcrop	outcrop
	494155	494962	491262	488618	486803	486803	486761	491452	490693	496170
	5410450	5399593	5396951	5395757	5430909	5430909	5430906	5426491	5428754	5419328
SiO2	78.00	78.20	76.90	52.80	51.40	53.30	51.60	77.10	70.20	77.10
Al2O3	11.00	12.00	12.50	15.10	16.50	14.80	16.70	11.40	9.09	11.10
Fe2O3	2.28	1.01	1.52	10.50	11.10	10.80	11.20	1.94	10.60	2.73
K2O	3.67	4.85	4.85	2.00	0.58	0.11	0.80	6.71	2.65	4.98
Na2O	3.96	4.02	3.82	4.14	3.88	0.11	5.17	2.08	0.15	3.44
MgO	0.13	0.04	0.20	4.91	5.19	1.00	5.06	0.07	0.62	0.08
MnO	0.01	-	0.03	0.20	0.16	0.16	0.18	-	0.01	0.04
P2O5	0.02	0.02	0.03	0.41	0.49	0.36	0.47	0.02	0.11	-
CaO	0.25	0.05	0.55	6.32	6.87	15.80	3.58	0.06	0.16	0.30
TiO2	0.12	0.09	0.20	2.15	2.23	1.62	2.19	0.13	0.44	0.24
Ba	69.00	123.00	369.00	304.00	782.00	53.00	618.00	141.00	277.00	646.00
LOI	0.50	0.50	0.40	2.00	2.50	2.40	4.00	0.70	6.00	0.50
ASI	1.01	1.00	1.00	0.74	0.85	0.51	1.05	1.06	2.67	0.96
Ga/Al	3.50	3.29	2.72	1.99	1.88	2.83	1.65	2.83	2.03	3.55
Al	1.05	1.01	1.08	1.68	2.35	49.33	1.78	1.07	2.92	1.00
Cl	84.94	451.99	155.87	345.21	116.54	144.78	96.48	120.72	65.44	112.14
Nb	43.35	48.04	32.17	15.00	14.75	10.18	14.60	52.36	10.25	51.70
S	104.22	128.74	122.88	175.06	140.07	130.57	136.78	115.29	34834.91	266.57
Y	85.36	32.42	54.60	41.26	34.92	23.70	33.91	89.47	11.01	78.90
Zr	749.48	211.45	182.53	206.85	648.11	511.33	625.05	701.84	173.24	979.04
Bi	-	0.30	-	0.41	-	-	-	0.19	0.78	-
Cd	0.14	0.10	0.06	0.71	0.15	0.21	0.16	0.13	0.04	0.16
Co	0.35	0.37	1.36	35.02	35.23	5.28	39.41	0.17	26.27	1.59
Cr	16.00	16.00	9.00	99.00	54.00	44.00	55.00	6.00	41.00	7.00
Cs	0.56	1.54	2.24	1.06	0.80	0.15	1.90	0.90	4.06	0.85
Dy	15.14	5.44	10.95	8.14	7.40	5.19	6.95	15.78	2.20	17.27
Er	10.40	5.54	7.36	4.62	4.21	2.98	4.01	10.95	1.03	11.43
Eu	0.69	0.20	0.74	2.26	3.16	2.53	2.76	0.19	1.07	1.33

	3889	3894	3895	3896	3897	3898	3899	3900	4327	4331
Ga	26.35	26.97	23.22	20.59	21.25	28.68	18.87	22.10	12.63	26.96
Gd	11.59	1.99	8.23	8.47	7.90	5.66	7.60	9.42	3.33	13.96
Ho	3.35	1.46	2.37	1.63	1.49	1.05	1.41	3.51	0.39	3.65
In	0.15	0.07	0.06	0.15	0.08	0.07	0.08	0.08	0.03	0.16
La	35.80	4.71	17.00	27.34	25.71	19.55	27.04	3.77	29.16	55.33
Li	1.70	1.60	18.00	36.00	15.00	9.60	20.40	1.80	13.20	2.50
Lu	1.50	1.15	1.10	0.60	0.57	0.40	0.54	1.55	0.14	1.75
Mo	0.68	2.74	2.48	2.51	1.01	0.62	0.51	0.63	1.11	2.74
Nd	40.70	4.84	28.51	33.60	35.35	25.93	33.88	9.41	25.54	62.29
Ni	-	2.30	-	44.70	40.10	8.60	39.30	-	23.10	-
Pb	7.00	16.10	20.00	109.90	7.70	16.60	7.40	11.30	6.30	10.30
Pr	10.16	1.30	6.81	7.96	8.16	5.94	7.91	1.92	6.81	15.68
Rb	108.26	196.78	173.43	84.66	6.71	1.95	19.33	233.93	117.89	140.30
Sb	0.06	0.21	0.13	1.01	0.07	0.12	0.06	0.26	1.44	0.13
Sc	-	-	2.40	30.80	31.40	22.40	30.40	-	4.10	1.20
Sm	10.73	1.44	8.01	8.04	8.02	5.73	7.77	5.90	4.68	14.33
Sr	239.70	0.14	7.67	17.48	42.19	136.42	52.01	60.38	7.80	10.70
Ta	2.54	3.47	2.22	0.87	0.81	0.58	0.77	3.16	0.58	3.11
Tb	2.18	0.58	1.58	1.31	1.18	0.86	1.16	2.15	0.42	2.58
Ti	703.00	525.00	1222.00	13081.00	13263.00	9529.00	12828.00	716.00	2426.00	1217.00
Tl	0.49	0.95	0.87	0.49	0.04	0.01	0.11	1.31	0.94	0.74
Tm	1.54	1.01	1.14	0.64	0.58	0.41	0.56	1.64	0.15	1.74
U	6.42	5.09	5.05	1.55	1.11	0.89	0.93	8.72	1.91	6.59
W	0.36	1.68	0.46	3.90	0.26	0.17	0.20	1.81	4.95	0.78
Yb	10.12	7.52	7.63	4.03	3.77	2.68	3.65	10.76	0.92	11.70
Zn	30.00	37.00	52.00	260.00	111.00	22.00	126.00	25.00	20.00	38.00
Be	4.70	4.30	4.80	1.70	1.50	0.50	1.10	5.50	1.30	3.90
Ca	74.00	21.00	65.00	49.00	55.00	37.00	55.00	17.00	61.00	110.00
Cu	-	12.00	-	94.00	43.00	4.00	19.00	1.00	57.00	36.00
Hf	17.00	11.00	8.00	5.00	11.00	8.00	11.00	17.00	-	18.00
Nd	30.00	3.00	20.00	28.00	28.00	22.00	27.00	4.00	26.00	51.00
Sn	8.00	13.00	3.00	4.00	1.00	-	2.00	8.00	-	4.00
Th	18.00	19.00	18.00	5.00	2.00	2.00	2.00	23.00	7.00	20.00
V	12.00	9.00	15.00	255.00	244.00	240.00	187.00	17.00	48.00	5.00
F	N.D.	100.00	400.00	1000.00	400.00	300.00	500.00	100.00	N.D.	N.D.

	4332	4333	4334	4339	4340	4341	4342	4343	4344	4345
	2010	2010	2010	2010	2010	2010	2010	2010	2010	2010
	rhyolite	rhyolite	Ksp porphyry	Am-Pyx porphyry	Am-Pyx porphyry	Am-Pyx porphyry	Bt-granite	Pegmatite Vein	granitic dyke	rhyolite
	Ssf	Ssf	Ssm	Smg	Smg	Sp	Sm	Sdc	Sdc	Ssf
	outcrop	outcrop	outcrop	outcrop	outcrop	outcrop	outcrop	outcrop	outcrop	outcrop
	499290	499898	499097	496413	497672	486846	487587	486300	486311	486437
	5414534	5414185	5416725	5420024	5419403	5413219	5413328	5408745	5408745	5408654
SiO2	75.10	78.70	65.10	75.80	74.90	76.90	74.30	83.50	76.30	80.50
Al2O3	11.70	10.90	14.00	12.10	11.80	11.30	13.40	3.50	9.02	11.50
Fe2O3	1.16	0.78	5.16	4.78	3.08	1.74	1.60	5.07	6.60	1.48
K2O	2.62	3.76	4.10	4.00	4.86	4.38	5.24	0.40	4.40	4.28
Na2O	4.33	1.36	4.47	0.31	4.01	4.04	4.02	0.40	3.67	0.44
MgO	0.26	0.29	1.61	0.32	0.15	0.04	0.26	0.18	0.04	0.24
MnO	0.17	0.03	0.11	0.02	0.07	0.04	0.01	0.23	0.05	-
P2O5	-	-	0.30	0.02	0.03	-	0.03	0.04	0.02	-
CaO	2.32	0.12	1.65	0.05	0.34	0.06	0.49	3.77	0.14	0.06
TiO2	0.08	0.14	0.96	0.27	0.31	0.09	0.31	0.19	0.15	0.12
Ba	689.00	934.00	683.00	67.00	234.00	45.00	432.00	53.00	33.00	261.00
LOI	2.50	3.30	1.70	3.20	0.30	0.50	0.60	2.40	0.30	1.90
ASI	0.83	1.67	0.95	2.45	0.95	0.98	1.02	0.44	0.82	2.10
Ga/Al	1.65	2.04	1.92	3.40	3.05	3.64	2.29	7.35	5.20	2.48
Al	1.17	1.73	1.19	2.50	1.00	0.99	1.09	3.21	0.84	2.15
Cl	81.41	85.69	220.89	28.76	125.70	274.82	176.31	121.69	149.10	109.82
Nb	15.42	12.63	16.14	52.21	34.29	56.10	27.64	394.97	31.38	39.17
S	219.50	146.24	125.07	136.23	135.52	127.78	156.92	157.65	118.41	3217.76
Y	43.02	15.98	48.40	111.20	50.81	41.69	52.76	1812.64	32.60	58.70
Zr	143.48	105.20	490.24	980.85	607.12	348.29	286.93	6202.24	737.07	395.17
Bi	-	0.44	-	0.18	0.23	0.33	0.25	1.27	0.16	0.59
Cd	0.10	0.03	0.20	0.32	0.18	0.13	0.07	3.32	0.20	0.19
Co	0.81	0.31	8.82	1.34	1.07	0.48	2.02	0.95	0.46	0.81
Cr	10.00	6.00	11.00	5.00	9.00	4.00	6.00	7.00	6.00	15.00
Cs	0.95	1.26	0.17	1.09	0.56	1.14	0.69	0.22	0.38	1.38
Dy	7.91	1.98	8.67	18.48	10.21	11.28	9.84	354.00	6.45	10.21
Er	5.17	1.50	5.00	11.97	7.57	8.68	6.14	167.00	5.81	6.85
Eu	0.84	0.30	2.38	1.23	0.97	0.55	1.00	36.50	0.55	0.17



